Study on regional scale mass variation using GRACE satellite gravity data(Dissertation_全文)

AUTHOR(S):

Yamamoto, Keiko

Study on Regional Scale Mass Variation Using GRACE Satellite Gravity Data

Keiko Yamamoto

Abstract

The dedicated gravity mission GRACE (Gravity Recovery and Climate Experiment) launched in 2002 is the first satellite which provides temporal gravity field variation of the Earth with an unprecedented accuracy. GRACE is providing us monthly solutions of global gravity fields as a set of spherical harmonic coefficients, and several studies have already showed that GRACE has successfully revealed the seasonal varying signals in the spatial scale about 1000 km.

On the other hand, although it is known that GRACE can detect further small scale mass variation at least about several hundred km, such smaller spatial scale mass recovery has not been sufficiently studied. Thus, regional scale mass recovery from GRACE monthly gravity field solutions is discussed in this study. The seasonal landwater mass variation in the Indochina Peninsula and the interannual ice sheet mass change in Antarctica are picked up and studied.

In the Indochina Peninsula, regional scale mass variations of 4 major river basins, i.e., Salween, Chao Phraya, Irrawaddy and Mekong river basins, were estimated. The results show that GRACE detected at least the Mekong and Irrawaddy basin scale variations, while the detection of the mass variations associated with Salween and Chao Phraya river basins is still difficult. The comparison over the combined area of the 4 river basins shows fairly good agreement, although there remain small discrepancies quantitatively. Amplitudes of the annual signals from the GRACE solutions are 0.9-1.4 times larger than the one from the hydrological model, and the phases are delayed about 1 month compared with the model signal. The phase differences are probably due to improper treatments of the groundwater storage process in the hydrological model and this suggests that the GRACE data possibly give constraints to the model parameters. Further, it was proved that the obtained regional mass variation can be used for the separation of the local and the regional signal containing in-situ gravimetry data. Thus, regional mass variation estimated by GRACE data also contributes to discuss the local signal precisely.

For the ice sheet mass variation in Antarctica, the sources of the 3 areas with striking interannual mass trend was investigated. In Antarctica, it is well known that post glacial rebound (PGR) also causes large mass trend. Thus to discuss the mass sources by each regional mass trend area contributes to discuss the large (continental or sub-continental) scale ice sheet mass change more precisely. Besides of the GRACE data, other various models and observations were used for discussion. Among these 3 areas, the source of the positive mass trend in Enderby Land, East Antarctica, has not been well explained due to the uncertainties in the estimation of the surface ice sheet mass balance, the post glacial rebound (PGR) and the errors in the GRACE data processing. In this study, the GRACE mass trend was compared with the ones estimated from in-situ snow-stake measurements and the Ice Cloud and land Elevation Satellite (ICESat) data. The result shows that

the main part of the mass trend can be explained by the snow accumulation. Further, interannual mass trends in East, West, and the whole area of Antarctica were also estimated. The result shows that the Antarctic ice sheet mass is decreasing and the rate is large in West Antarctica. However, because of the large uncertainties of now available PGR models, the quantities of the decrease cannot be discussed precisely, at present.

Table of Contents

1. Introduction

Precise determination of the Earth's gravity field is very important mainly because 1) it gives a physical reference surface of the Earth, i.e. geoid, and 2) it provides the mass information of the Earth (e.g. Torge, 2001).

For the determination of the Earth's gravity field, conventional land, ship-borne and/or air-borne gravity measurements have been conducted for local to regional scale surveys. However, these measurements are quite time consuming and their spatial coverage are limited. Therefore it is practically impossible to cover the whole globe uniformly by these measurements.

Since the beginning of satellite era, analyses of satellite orbits have been greatly contribute to determine the global scale Earth's gravity field (e.g. Schwintzer *et al*., 1997). Because the Earth's gravitation affects all satellites revolving around the Earth, perturbations of their orbits reflect the gravity field of the Earth. The gravitational potential (geopotential) V observed by a satellite is represented by the spherical harmonic series as follows (Heiskanen and Moritz, 1967):

$$V(r,\theta,\lambda)=\frac{GM}{R}\sum_{l=0}^{\infty}\left(\frac{R}{r}\right)^{l+1}\sum_{m=0}^{l}(\overline{C}_{lm}\cos m\lambda+\overline{S}_{lm}\sin m\lambda)\overline{P}_{lm}(\sin\theta) \qquad , (1.1)$$

where G is the gravitational constant, M is the mass of the Earth, R is the Earth's equatorial radius, (r, θ, λ) are spherical coordinates, $\overline{C}_{lm}$ and $\overline{S}_{lm}$ are fully normalized spherical harmonic coefficients of degree l and order m, and $\overline{P}_{lm}(\cos\theta)$ is the fully normalized Legendre function. Determining the Earth's gravity field actually means determining the spherical harmonic coefficients $\overline{C}_{lm}$ and $\overline{S}_{lm}$, i.e. Stokes coefficients.

Although any satellite orbits give the gravity field information in principle, there are some practical limitations (European Space Agency, 1999). The first is the satellite altitude. Most of satellites are not designed for geodetic purposes, and their altitudes are generally high (for example, GPS satellites are flying at the altitude of about 20000 km). Because the signals of the Earth's gravity field are attenuated by the factor of $(R/r)^l$ as shown in Eq. (1.1), the orbit perturbation of a high altitude satellite reflects only long wavelength gravity field information. It is difficult to estimate higher degree terms from such a high altitude orbit. The second is the effects of non-gravitational forces which perturb satellite orbits, e.g. atmospheric drag, attraction of Sun, Moon and other planets, solar radiation pressure. If the effects are not appropriately estimated and corrected, the precise recovery of the Earth gravity field is impossible. The third is the precision of the orbit determinations. So far, the satellite orbits have been determined by the observations from the ground stations. The observations from the Earth surface are suffering mainly from atmospheric

influence. Further, the number of the stations is limited and their spatial distribution is not even to cover the Earth surface uniformly. Thus the highest degree of the Earth's gravity field coefficients determined by the satellite orbit analyses is at most about 50 (corresponding half wavelength spatial resolution of about 400 km). This does not satisfy the recent requirements of the precise geoid (gravity field) determination for the studies of geodesy, oceanography, meteorology, and other Earth sciences.

Under the circumstances, satellite gravity missions, which measure the Earth's gravity field dedicatedly, have been proposed. Currently, CHAMP (CHallenging Minisatellite Payload, launched in 2000, Reigber *et al*., 2002), GRACE (Gravity Recovery and Climate Experiment, launched in 2002, Tapley *et al*., 2004a) are under operation and GOCE (Gravity Field and Steady-State Ocean Circulation Explorer, Drinkwater *et al*., 2003) will be launched in 2007. The common concepts of these missions are 1) using low Earth orbit (LEO) satellites (the altitudes are about 250 to 600 km) to decrease the signal attenuation due to orbital altitudes, 2) using GPS for the satellite tracking (High-Low Satellite-to-Satellite Tracking, H-L SST), and 3) using on-board accelerometers or an equivalent system to correct the non-gravitational forces. CHAMP is an experimental mission and the gravity field determination is performed by the orbit analyses using the GPS tracking data (H-L SST). GRACE is a twin satellite mission and the gravity field is determined by precisely measured range and range rate data between the two satellites (Low-Low Satellite-to-Satellite Tracking, L-L SST). In GOCE mission, the gravity field is determined from the data of the on-board gravity gradiometer. Because GRACE measures the first derivative of the gravity field and GOCE the second derivative, GOCE, GRACE and CHAMP in this order reveal short wavelength gravity signals more efficiently (European Space Agency, 1999). Thus these 3 missions are complemented mutually.

The spatial wavelength which GRACE satellite measures corresponds to the typical spatial scale of the Earth's temporally variable geophysical phenomena, e.g. annual or interannual landwater and ocean variations, interannual ice sheet mass variation, post glacial rebound (PGR) or co-seismic mass change of large scale earthquake (National Research Council, 1997). Because most of temporal phenomena on the Earth accompany the mass movements, they can be detected as gravity changes. Thus, besides of the determination of the static gravity field, another important task of GRACE mission is to investigate such geophysical mass variation by providing monthly gravity field solutions. Using the monthly gravity field solutions, geopotential at the month is represented as

$$V(r,\theta,\lambda,t)=\frac{GM}{R}\sum_{l=0}^{\infty}\left(\frac{R}{r}\right)^{l+1}\sum_{m=0}^{l}(\overline{C}_{lm}(t)\cos m\lambda+\overline{S}_{lm}(t)\sin m\lambda)\overline{P}_{lm}(\sin\theta) \quad , (1.2)$$

where $V(r,\theta,\lambda,t)$, $\overline{C}_{lm}(t)$ and $\overline{S}_{lm}(t)$ are the geopotential and spherical harmonic coefficients of

the Earth at the month.

The surface mass density on the Earth is expressed as follows (Wahr et al., 1998):

$$\Delta\sigma(\theta,\lambda) = \frac{R\rho_E}{3}\sum_{l=0}^{\infty}\frac{2l+1}{1+k_l}\sum_{m=0}^{l}(\Delta\overline{C}_{lm}\cos m\lambda + \Delta\overline{S}_{lm}\sin m\lambda)\overline{P}_{lm}(\sin\theta) \quad , (1.3)$$

where $\Delta\sigma(\theta,\lambda)$ is the surface density on the Earth, ρ_E is the average of the Earth's density, k_l is load Love number of degree l, $\Delta\overline{C}_{lm}$ and $\Delta\overline{S}_{lm}$ are variable components of the spherical harmonic coefficients of the Earth's gravity field. $\Delta\overline{C}_{lm}$ and $\Delta\overline{S}_{lm}$ are obtained by subtracting the static components from each $\overline{C}_{lm}(t)$ or $\overline{S}_{lm}(t)$.

One of the main targets of GRACE mission is large scale water movement on and beneath the Earth's surface. The GRACE data have been widely used for the studies of, for example, landwater movements, ocean flow, ice sheet mass changes.

One of the most promising applications of GRACE data is monitoring landwater movements or terrestrial water storages. Wahr *et al*. (2004) and Chen *et al*. (2005a) reported that the GRACE data are well correlated with estimation from global landwater models at half wavelength of about 800 to 1000 km. For the basin scale mass recovery, Famiglietti (2004) reported that GRACE successfully detects landwater mass variations at spatial scale larger than about 1000 km, for example, Amazon, Mississippi, Ob, Ganges and Yangtze river basins. In these river basins, Amazon is the largest river basin in the world and its seasonal mass variation is very large. After the earlier results by Wahr *et al*. (2004) and Tapley *et al*. (2004b), the landwater mass variation in this area has been often picked up and used as a reference area, for example, to confirm availability of new methods. The recovery of mass variations over the ocean is more difficult than the one of landwater mass variations because of the small signal compared to land area and the relatively large error of the short-period ocean model used in the GRACE data processing (Kanzow, 2005). In spite of these deficiencies, it is reported that GRACE well recovers the several major ocean mass variations in the world (Chambers, 2004). For the study of ice sheet mass change, continental to sub-continental scale mass variation in Antarctica (Velicogna and Wahr, 2006a) and Greenland (Velicogna and Wahr, 2006b; Chen *et al*., 2006a), which are directly useful to estimate the global sea level change, were studied using GRACE data.

The studies mentioned above treat large spatial scale mass variations and the results contribute directly to understand global scale terrestrial water circulation. On the other hand, to study regional scale mass variation is also important. For example, global ocean circulation is closely related with basin scale water movement. Landwater mass variation occurs by each drainage area as a fundamental unit. Melting speeds of ice are different by each glacier. For the purpose of studying mechanisms of such phenomena in detail, GRACE is also useful because it is known that GRACE can treat regional scale mass variation at least about several hundred km. As a result, the result of the

regional scale mass variation will also contribute to improve the knowledge of global mass movement.

Further, the estimation of regional scale mass variation can be available for the study of local mass variations. The signal of the gravity measurement on land includes both of the local short wavelength gravity variation, which is mainly reflects the effects of human activities in urban area, and the regional or global long wavelength variation, which is mainly caused by hydrological or other geophysical sources. Only by the in situ measurements, these two signals cannot be separated precisely. By subtracting GRACE regional signal from the ground observed value, more precise discussion of the local signal will be possible.

Thus, in this study, the regional scale mass recovery using GRACE monthly gravity field solution is discussed. The outline of GRACE mission and the current status of the data sets are overviewed firstly. Several error sources which degrade GRACE solutions are discussed. After that, regional mass variations is recovered and discussed. The seasonal landwater mass variation in the Indochina Peninsula and the interannual ice sheet mass change in Antarctica are picked up in this study.

In the Indochina Peninsula, precise gravimetry on land combining with GPS observation is planned near future for the purpose of detecting the groundwater decrease caused by the rapid urbanization (Research Institute for Humanity and Nature, 2005). Therefore, it is discussed whether the regional scale mass variation from GRACE data can useful for the correction to remove regional signal from the local observed data.

On the other hand, in Antarctica, the melting of ice sheet has attracted special attention. However, the mass change is caused not only by ice sheet mass change but by other sources, e.g. PGR. Thus, for more precise recovery of ice sheet mass change, the regional mass variations of each trend area are discussed. It is useful to estimate more precise global sea level change, as a result.

Finally, the regional mass recovery from GRACE data is discussed on the basis of these results.

2. GRACE Mission

2.1. Gravity field determination by GRACE

2.1.1 Principle of GRACE gravity field measurement

In GRACE mission, the Earth's gravity field is measured by the twin LEO satellites (Tapley *et al*., 2004a). The initial altitudes of the satellites are about 500 km. They are about 220 km apart on the same orbital plane and the one satellite chases the other one. The change in distance between the two satellites is measured precisely by the microwave ranging system, and it reflects the fluctuations of the Earth's gravity field. Highly accurate accelerometers are placed at the center of mass of the satellites to measure non-gravitational force. The GPS receivers are equipped on the satellites for the determination of the precise locations of the satellites in orbit.

By the GRACE observation, the range (distance between the two satellites), the range rate, and the range acceleration are obtained Because the range acceleration is related with Stokes coefficients ($\overline{C}_{lm}$ and $\overline{S}_{lm}$) as shown in follows, the Earth's gravity field is determined by GRACE observation. The details are stated in Thomas (1999), and only the outline is stated in this section.

Range acceleration is represented with range vector between the two satellites by

$$\ddot{R} = \ddot{\mathbf{R}} \cdot \frac{\mathbf{R}}{R} + \dot{\mathbf{R}} \cdot \left(\frac{\dot{\mathbf{R}}}{R} - \frac{\dot{R}}{R} \frac{\mathbf{R}}{R} \right) \equiv \ddot{R}_g + \ddot{R}_c \quad , (2.1)$$

where

$$\mathbf{R} = \mathbf{x}_q - \mathbf{x}_p \quad , (2.2)$$

is the range vector and $\mathbf{x}_p$ and $\mathbf{x}_q$ is the vectors from the Earth's center to GRACE satellites p (the forward satellite) and q (the backward satellite), $\dot{\mathbf{R}}$ and $\ddot{\mathbf{R}}$ is the vectors of the range rate and the range acceleration, respectively, and R, $\dot{R}$ and $\ddot{R}$ are the scalars of the range, the range rate and the range acceleration, respectively. The second term in Eq. (2.1) represents the range acceleration caused by the centrifugal force. Gravitation induced range acceleration is represented by the first term in Eq. (2.1), i.e.

$$\ddot{R}_g = \ddot{\mathbf{R}} \cdot \frac{\mathbf{R}}{R} \quad . (2.3)$$

$\ddot{R}_g$ is related with the Stokes coefficients $\overline{C}_{lm}$ and $\overline{S}_{lm}$ as follows.

$$\frac{\partial \ddot{R}_g}{d\overline{C}_{lmj}} = (\tilde{\mathbf{a}}_{C_{lmj,q}} - \tilde{\mathbf{a}}_{C_{lmj,p}}) \cdot \frac{\mathbf{R}}{R} \quad , (2.4)$$

where

$$\tilde{\mathbf{a}}_{\overline{C}_{lmj,x}} = \frac{\partial \tilde{V}_{\overline{C}_{lmj,x}}}{dr_x}\hat{\mathbf{u}}_r + \frac{1}{r_x}\frac{\partial \tilde{V}_{\overline{C}_{lmj,x}}}{d\theta_x}\hat{\mathbf{u}}_\theta + \frac{1}{r_x \cos\theta_x}\frac{\partial \tilde{V}_{\overline{C}_{lmj,x}}}{d\lambda_x}\hat{\mathbf{u}}_\lambda \quad , (2.5)$$

$$\tilde{V}_{\overline{C}_{lmj,x}} = \frac{GM}{R}\left(\frac{R}{r_x}\right)^{l+1} \overline{P}_{lm}(\sin\theta) T(m\lambda_x) \quad , (2.6)$$

$\overline{C}_{lmj}$ is $\overline{C}_{lm}$ for j=1 and $\overline{S}_{lm}$ for j=2, x means for satellite x (p and q), $(\hat{\mathbf{u}}_r, \hat{\mathbf{u}}_\theta, \hat{\mathbf{u}}_\lambda)$ is a point-specific unit vector in the direction of increasing $(r_p, \theta_p, \lambda_p)$, and $T(m\lambda_x)$ is $\cos(m\lambda_x)$ for j=1 and $\sin(m\lambda_x)$ for j=2. Using Eq. (2.4), Stokes coefficients of the Earth's gravity field ($\overline{C}_{lm}$ and $\overline{S}_{lm}$) can be derived by the least squares method.

2.1.2. GRACE data processing

In GRACE mission, the observed data is received, processed to a static or a monthly gravity field solution, archived in the system and distributed to users. The outline of the data processing in this section is stated in Bettadpur (2006a). Fig. 2.1 summarizes the flow chart of GRACE science data system (GRACE SDS). This processing is performed at 3 centers: Jet Propulsion Laboratory (JPL), The University of Texas Center for Space Research (UTCSR) and GeoForshungsZentrum Potsdam (GFZ). In the GRACE mission, all science data sets and housekeeping data of the satellites are generally collected on-board continuously. These data from the satellites are down linked at the ground stations as the telemetry data. The telemetry data is separated to the science data and the housekeeping data and stored by each satellite as a rolling archive at the GRACE Raw Data Center (RDC). These data are called GRACE Level-0 data products. After that, Level-1A data is made from Level-0 data by applying the sensor calibration in order to convert the binary encoded data to the engineering units. The ambiguity is also resolved and the time is tagged to the respective satellite receiver clock time at this stage. Further, the quality control flags are added. Finally the data is reformatted for the next stage of the data processing.

Next, Level-1B processing is performed. The data are correctly time-tagged and down sampled. The information of GPS ground segment data by IERS/IGS is obtained and used in the processing. The ancillary data and other data needed for further processing is also included.

Using Level-1B products, Level-2 data processing which is the final stage to derive the gravity field solutions is performed. Ancillary geophysical data, for example, atmospheric pressure model

and ocean model for de-aliasing, is acquired and used to the processing.

The processing from Level-0 to Level-1B is common with the 3 data centers. Level-2 processing is performed by each data centers with different algorism. UTCSR is routinely produced the Level-2 data sets, while JPL and GFZ data sets are produced for the verification of the UTCSR data. The verification is important because the GRACE data is new type data and has not been treated previously. For general users, the available data sets are Level-1B and Level 2 data, which are archived and released from each data center.

2.1.3. GRACE Level-2 gravity field solutions

An accurate estimation of the static and time-variable gravity field of the Earth is the main task of the GRACE mission. About an estimation of the GRACE Level-2 gravity field solution, the details are stated in Bettadpur (2006b) and summarized it in this section. In the real gravity field estimation, the infinite series of harmonics in Eq. (1.1) are practically truncated at the maximum degree $l_{\max}$. The Earth's geopoteintal (gravity field) at time t is expressed by Stokes coefficients of degree l and order m at time t, i.e. $\overline{C}_{lm}(t)$ and $\overline{S}_{lm}(t)$. The GRACE Level-2 gravity field solution is provided as data set of Stokes coefficients at each time period.

In Level-2 processing, the geopotential (Stokes coefficients) is estimated by updating a priori best-known geopotentail model (Background Model). The Background Model is also parameterized as spherical harmonic coefficients. It is represented by each coefficient, for example, as follows:

$$G(t) = G_0 + G'(t - t_0) + \delta G^{st}(t) + \delta G^{ot}(t) + \delta G^{pt}(t) + \delta G^{a+o}(t) \qquad . (2.7)$$

where G_0 is a priori best knowledge of the geopotetial. The second term is the secular variation and the following terms are the solid tide, the ocean tide, the pole tide and a combination of atmospheric and oceanic non-tidal variability. The terms appeared in Eq. (2.7) are not all components used in the Level-2 processing. The complete list of the models used in the actual processing is shown in the Level-2 gravity field user handbook released by each data center (e.g. Bettadpur 2003, Flechtner 2003, or. Watkins 2003). The difference between the background model and the true gravity field of the earth includes the information of geophysical phenomena and static geopotential components which is not estimated in a priori prediction besides of the estimation error of each model used in the Background Model. The difference is calculated by each sampling time along the orbit. The update with respect to the Background Model is determined from the difference data collected through the some time period by least squares method. All data in the time period is not necessarily used in the determination. Thus the new gravity field is derived by adding the update to the Background Model.

The estimated gravity field solution does not have a single epoch. It is the average of the gravity field throughout the time period. In case it is necessary to associate with the single epoch, the mid-point of the time period may be adopted.

Basically, static and monthly gravity field solutions are estimated by the same approach shown in above, but the time period used for the estimation is different. Long period (more than several months or years) data is used for the estimation of static gravity field, while about 1 month data for monthly gravity field.

2.2. Current status of the released GRACE data sets

2.2.1. Static gravity field solutions

The Earth's static gravity field was largely improved after the GRACE launch. As shown in Fig. 2.2, even in the preliminary GRACE satellite model, the errors significantly decrease compared with the pre-CHAMP satellite model and CHAMP model, especially in medium to long wavelength. Table 2.1 summarized the now available global gravity field models including the GRACE results. EIGEN-GL04C (Förste *et al*., 2006), which is one of the latest models, was made by the combination of GRACE and LAGEOS (Laser Geodynamics Satellites) mission plus 0.5 x 0.5 degrees surface data of gravimetry and altimetry. The comparisons the GRACE geoid with the geoid heights determined point-wise by GPS positioning and GPS leveling show the improvement of the precision of the EIGEN-GL04C model compared to EGM96 model (Lemoine *et al*, 1998), which is combination model of pre-CHAMP satellite and surface data (Table 2.2).

Table 2.1. Global gravity field models including GRACE data for the calculations. (International Centre for Global Earth Model, 2006)

Model	Year	Degree	Data	Citation
ITG-Grace02s	2006	170	S(GRACE)	Mayer-Gürr *et al*., 2006
EIGEN-GL04S1	2006	150	S(GRACE,LAGEOS)	Förste *et al*., 2006
EIGEN-GL04C	2006	360	S(GRACE,LAGEOS), G, A	Förste *et al*., 2006
EIGEN-CG03C	2005	360	S(CHAMP, GRACE), G, A	Förste *et al*., 2005
GGM02C	2004	200	S(GRACE), G, A	Tapley *et al*., 2005
GGM02S	2004	160	S(GRACE)	Tapley *et al*., 2005
EIGEN-CG01C	2004	360	S(CHAMP, GRACE), G, A	Reigber *et al*., 2006
EIGEN-GRACE02S	2004	150	S(GRACE)	Reigber *et al*., 2005
GGM01C	2003	200	TEG4, S(GRACE)	UTCSR, 2003
GGM01S	2003	120	S(GRACE)	Tapley *et al*., 2003
EIGEN-GRACE01S	2003	140	S(GRACE)	Reigber *et al*., 2003

(Data: S=Satellite Tracking Data, G = Gravity Data, A = Altimetry Data)

Table 2.2. Root mean square (rms) about mean of GPS-levelling minus gravity field model derived geoid heights [cm] (number of points in brackets), (GeoForschungsZentrum, Potsdam, 2006).

Gravity Model	USA (6169)	Canada (1930)	Europe (186)	Germany (675)
EIGEN-GL04C	43.5	31.1	34.0	18.1
EGM96	46.5	37.3	44.6	27.6

2.2.2. Monthly gravity field solutions

Table 2.3 shows the versions of GRACE monthly gravity field solutions released by now. Release 1 (RL01) of UTCSR (Bettadpur, 2003), RL01 of JPL (Watkins, 2003) and RL01 of GFZ (Flechtner, 2003) are the first released versions of each data center. After the release of the minor update version RL02 of GFZ (Flechtner, 2005a), 3 major update versions; RL02 of UTCSR (Bettadpur, 2005), RL02 of JPL (Watkins, 2005) and RL03 of GFZ (Flechtner, 2005b) were released. In the new versions, some of the error sources were investigated and corrected or improved, for example, using the new Background Model including the recent GRACE results, the new short-period ocean model and the latest ocean tide model. After the comparison with the previous solutions and the geophysical models by each data center, the versions of RL01 of UTCSR, RL02 of JPL and RL03 of GFZ have been continuously released for public at present. As reviewed in Ch. 1, the Earth's geophysical mass movements can be successfully recovered from these gravity field solutions.

Table 2.3. Versions of GRACE Level 2 monthly gravity field solutions.

Center	Version	Time Span (Number of Released Data Sets)
UTCSR	Release 01	All months from Apr/May in 2002 to Sep in 2006 except Jun, Jul in 2002 and Jun in 2003. (50 data sets)
	Release 02*	All months from Feb in 2003 to Apr in 2005 except Jul to Oct in 2004. (22 data sets)
JPL	Release 01	All months from Apr/May in 2002 to Mar in 2005 except Jun, Jul in 2002, Jan, Jun in 2003, Jan in 2004. (28 data sets)
	Release 02	All months from Jan in 2003 to Nov in 2005 except Jun in 2003, Jul to Oct in 2004. (30 data sets)
GFZ	Release 01	Apr/May, Aug, Nov in 2002, Mar, Apr/May, Jul, Aug, Oct, Nov in 2003. (9 data sets)
	Release 02	All months from Feb in 2003 to Jul in 2004 except Jun in 2003, Jan in 2004. (16 data sets)
	Release 03	All months from Feb in 2003 to Sep in 2006 except Jun in 2003, Jan in 2004. (41 data sets)

* released for science team only

However, in contrast with the static gravity solutions, GRACE monthly gravity solutions have not fully achieved the mission performance predicted before launch yet. As shown in Fig. 2.3, the degree amplitude of the calibrated standard deviation of the GRACE monthly gravity solutions, which is the approximate estimation of the GRACE error, is at least about order of 1 as large as the error predicted before the satellite launch.

The GRACCE error, which includes the satellite measurement error and errors from other sources, increases at the high degree though the Earth's gravity field signal is gradually decrease. To suppress the higher degree error and to see the lower degree signal more clearly, the spatial filter is usually applied to the GRACE monthly solutions. The globally normalized Gaussian filter (Wahr *et al*., 1998) is most frequently used for the purpose.

$$\Delta\sigma(\theta,\lambda)=\frac{R\rho_E}{3}\sum_{l=0}^{L}\frac{2l+1}{1+k_l}W_l\sum_{m=0}^{l}(\Delta\overline{C}_{lm}\cos m\lambda+\Delta\overline{S}_{lm}\sin m\lambda)\overline{P}_{lm}(\sin\theta) \quad . (2.8)$$

Fig. 2.4 shows the non-filtered and the Gaussian filtered variable components of GRACE monthly gravity solutions in spatial domain. As the correlation length of the filter is long, the error is decrease, but the signal information of the higher degree is also lost. Wahr *et al*. (2004) and Chen *et al*.

(2005a) compared the Gaussian filtered GRACE data with the global landwater model and the ocean model, and reported that about 800 to 1000 km Gaussian smoothing radius is effective to detect the terrestrial water signal.

The remarkable feature of the GRACE error is the north-southward spatial pattern called striping, which are related to the near-polar orbit ground tracks of the GRACE satellites. When the isotropic filter like Eq. (2.8) is used, the relative large correlation length filter should be applied to suppress the striping. Some filtering or smoothing methods to decrease the striping error has been proposed by now. For example, Han *et al*. (2005) developed the non-isotropic filter, which has different correlation length between degree and order. Swenson and Wahr (2006) developed the correlated-error removing filter by investigating the parity of the error GRACE coefficients. Applying such de-striping method, the signal to noise rate is improved and relatively small correlation length (about 400 to 600 km) can be applicable.

2.3. Several main error sources of GRACE monthly gravity field solutions

2.3.1. Difference of the data sets of 3 data centers

As mentioned in Sec. 2.2, the 3 data centers of UTCSR, JPL and GFZ calculate the monthly gravity field solutions. Although the GRACE data is commonly processed from Level-0 to Level-1B processing, the Level-2 data is calculated with the different algorisms. The back ground static gravity models and other models for correction are different by each data center. As a result, the calculated solutions are something different by the 3 data centers. Currently the 3 data sets have a consensus in the point of detecting the geophysical signal variations both in the ocean and the land area. However, about the amplitude of the signals, the 3 data sets are different as shown in Fig. 2.5 and Fig. 2.6.

The land area has relatively large landwater signals and smaller errors compared with the ocean area. The GRACE observation detects the landwater signals, which includes not only the surface but the ground water, well. However, because most of the now released global landwater models does not sufficiently express the groundwater components, and because the model's precision is different by each river basins, it is difficult to conclude which of the amplitudes of the 3 data center solutions represents the true landwater signal well. Thus, the difference of the amplitude becomes the uncertainty of the GRACE data at present.

In the ocean area, the error is relatively large because of the small signals. Chambers (2006) investigated the difference of the data sets released by 3 data centers in the ocean area. They compared the 3 data center data sets with the steric components removed TOPEX/Poseidon data and reported that the average of the 3 data sets shows best correspondence with the estimated ocean signal.

2.3.2. C_{20} coefficients

GRACE observed the Earth's gravity field by L-L SST method, which corresponds to measure the difference of first derivatives of the geopotential over a long baseline. In L-L SST method, the long wavelength components are not well determined. Especially, the C_{20} coefficient, which is the lowest zonal component of the GRACE solution, has larger error compared with the other coefficients. It is reported that the error is largely improved in the new versions of data sets of UTCSR RL02, JPL RL02 and GFZ RL03. However, in spite of the improvement, the C_{20} values of the 3 data sets are very different as shown in Fig. 2.7 and it implies that the errors are still large.

Generally, users estimate mass variation with excluding C_{20} components or replace to the solutions determined by SLR observation, which has smaller error than the GRACE one. Chen *et al*. (2005b) reported that the replacement of the degree 2 values to those of EOP/SLR improved the estimation results in several large river basins and fairly good agreements with the landwater model were obtained. The list of the value of the C_{20} components corresponding to the GRACE mission time period has been released from UTCSR for the purpose (Cheng and Ries, 2006).

2.3.3. Aliasing of short period mass variations

Because GRACE Level 2 monthly gravity field solutions represents one month average of the gravity field, the rapid variable components within one month cannot be recovered in the data. However, if they are neglected, they corrupt the monthly solutions through aliasing. The short-time period variations of ocean tides, non-tidal ocean, and atmosphere mainly bring such aliasing error and the models for de-aliasing are used in the GRACE data processing (Flechtner, 2005c). Although the short-time period landwater component also brings the aliasing, the effect is small compared with the GRACE errors and therefore not estimated in the processing. If the de-alias model are not sufficiently represent the true variations, the mismodeling also gives the error to the GRACE solutions.

The short-period atmosphere variation gives the largest effect for the aliasing. Han *et al*. (2004) assumed the difference between the surface pressure data of European Centre for Medium-Range Weather Forecast (ECMWF) and National Centers for Environmental Prediction (NCEP) as atmospheric modeling error and estimated the aliasing effect by simulation. The result shows that the errors in the recovered coefficients less than degree 20 are large enough to corrupt GRACE monthly gravity field solutions. Further, the errors comes from the mismodeling of atmosphere above degree 30 are larger than GRACE measurement error over all degrees. Thus the atmospheric estimation error degrades the all degrees performance of GRACE monthly solutions. They stated that it introduces 30 % more error with respect to GRACE satellite measurement error.

The short-period ocean mass variation is about order of 1 smaller than that of atmosphere, but still larger than GRACE measurement error. In the ocean area, there are no numerical models covering

from short period to long period variations, at present. The de-aliasing is performed with a short-period ocean model. Thus the ocean area of the GRACE monthly gravity field represents the ocean mass variation of the period longer than one month if the de-aliasing is performed perfectly. In the preliminary versions of GRACE monthly solutions (UTCSR RL01, JPL RL01, GFZ RL01 and RL02), the Pacanowski, Ponte, Hirose and Ali (PPHA, Ponte, 1993; Hirose *et al*., 2001) barotropic ocean model, which is only forced by wind and pressure, is used for the de-aliasing model. However, the obtained GRACE monthly solution over the ocean area overestimates the mass variation compared with in situ ocean bottom pressure data and a long period ocean model (Estimating the Circulations and Climate of the Ocean (ECCO) general circulation model, Stammer *et al*., 2003) (Kanzow *et al*., 2005). Kanzow *et al*. (2005) pointed out that the PPHA model does not well represent the oceanic variation at periods shorter than 1 day and longer than 2 weeks and need improvement. In the new GRACE solutions (JPL RL02 and GFZ RL03), the short-period ocean model for de-aliasing is replaced to the Ocean Model for Circulation and Tides (OMCT) baroclinic model (Wolff *et al*., 1996; Drijfhout *et al*., 1996; Thomas, 2002). The output of the OMCT model accounts for the effects of the thermohaline, the wind- and pressure-driven baroclinic circulations, the impact of loading, and the self-attraction of the water column. By using the OMCT model, the GRACE monthly solution over the ocean area is largely improved and confirmed to detect several major mass variations of the ocean (Chambers, 2006). However, it is reported that now used OMCT model for the de-aliasing brings a slope on the GRACE monthly solution because of its improper treatment of freshwater run-off and the mass conservation (Bettadpur *et al*., 2006). The slope is small over the ocean, but large over the land. The error will be improved in the next versions of GRACE solutions, but as a transitory treatment, the data sets for the correction of the slope (GAB and GAC products) are also released by each data center.

The aliasing effect caused by errors of short-period tide models was investigated by Knudsen (2003), Han *et al*. (2004) and Wunsch *et al*. (2005). The aliasing effect of each tide constituent shows the specific aliasing frequency (apparent frequency) determined by the frequency of each tide constituent and the sampling rate from satellite. Table 2.4 shows the aliasing frequencies which effect on GRACE solutions estimated by Knudsen (2003). Semidiurnal components give alias effect with the frequency of 13.6, 162.2, 9.1 and 1460 day for M_2, S_2, N_2 and K_2, respectively. Therefore, these errors bring a problem for the estimation of seasonal or interannual signals. On the other hand, the alias period of diurnal constituents are within 1 day, but they bring the modulation of the amplitude and also effects on the seasonal or interannual mass variation estimated by GRACE. Globally, M_2, K_1, O_1 causes no problems for GRACE monthly solution because of their small spatial scale. The error at less than degree 30, where most of the (one month or longer) ocean and landwater signal power lies, is small compared to the GRACE measurement error. The effects of N_2, P_1 and Q_1 are also small. Only the S_2 and K_2 gives a problem because of the long alias periods and the large

relative magnitude with respect to the original amplitudes of the constituents. Because tide models have a large error outside of the maximum latitude of TOPEX/Poseidon orbit (>±66º), the error of the tide de-aliasing in GRACE solutions are large near the polar areas. In the new version GRACE solutions (UTCSR RL02, JPL RL02, GFZ RL03), which use the new tide model (FES2005), the effect becomes relatively smaller than that in the preliminary models, in which older tide models (CSR4.0 or FES2002) are used.

Table 2.4. Tidal and the preliminary alias frequencies, modulation of amplitudes and relative magnitudes for major 8 tidal components (Knudsen 2003).

Constituent	Frequency [day]	Alias [day]	Modulation [day]	Relative Magnitude
M_2	0.1575	13.6	-	0.10
S_2	0.5000	162.2	-	0.94
N_2	0.5274	9.1	-	0.08
K_2	0.4986	1460	-	1.00
K_1	0.9973	0.9969	2920	0.01
O_1	1.0758	0.9969	13.6	0.01
P_1	1.0028	0.9969	9.1	0.01
Q_1	1.1195	0.9969	9.1	0.01

On the other hand, although the long period ocean tide is removed by the model, the error magnitude and the effect on the GRACE monthly solution is not sufficiently known at present. In UTCSR RL01, the effect of the long period ocean tide, Sa and Ssa above degree 10 are not corrected. The effects are corrected in this study using NAO99L long period ocean tide model (Takanezawa *et al*., 2002), though they are very small and almost negligible.

2.3.4. Effect of orbit decay

Because the GRACE satellites are not maintained to keep the same orbit during the mission's lifetime due to thruster fuel limitation (Case *et al*., 2004), the orbit gradually decays from an initial altitude. This causes temporal variation of the ground track of the satellite. For the gravity field solutions, globally uniform ground tracks is preferred, but large gaps in the ground tracks appear at a some specific orbit altitude. Large gaps are compensated by using relatively long period data. Therefore it does not effect in case of the static gravity field recovery using some months or years of data. However, in case of monthly a gravity field recovery, a relatively short period data is used and the variation of ground tracks affects the precision of the gravity-field solutions. The effect on the monthly gravity field has not been investigated well and thus Yamamoto *et al*. (2005) studied the impact of satellite's ground-track variation on a monthly gravity field recovery by simulation.

The outline of the simulation procedure is as follows. Using the simulated orbit of GRACE satellite (the change of the satellite altitude of the simulated orbit is shown in Figure 2.8), geopotential value along the orbit was calculated from the known spherical harmonic coefficients and the 'observational' value was synthesized by adding the stochastic error to the geopotential value. Next, the spherical harmonic coefficients were recovered from 4-week observational data using least squares method. Then, recovered coefficients were compared to the original ones and estimated the recovery precision of the gravity field. Geoid height errors were calculated from the difference between the recovered and 'true' spherical harmonic coefficients by calculating the global standard deviation at each time period (Figure 2.9).

As shown in Figure 2.9, the error levels of the recovered geoid were large in some periods. In order to discuss the relation between satellite ground track and recovery precision of the gravity field, spatial distribution of observational point at each period was transformed to spherical harmonic coefficients. Although the recovery of the gravity field was up to degree 30 to simplify the simulation, the cut off degree of this spherical harmonic transformation was set to degree 180 so that the spectrum express sufficiently small periodic pattern of ground track. From the derived spherical harmonic coefficients, the amplitude of degree l and order m,

$$s_{lm} = \sqrt{\overline{C}_{lm}^{\,2} + \overline{S}_{lm}^{\,2}} \qquad , (2.9)$$

was calculated for each l and m. As an example, the original observational point distribution (Figure 2.10 (a)) and the derived amplitude of each l and m (Figure 2.10 (b)) of the period 108 are shown. Large amplitude coefficients are concentrated at several specific orders of m. To see the feature of the order of direction more clearly, an order amplitude was introduced as follows and calculated by each period;

$$\sigma_m = \sqrt{\sum_{l=m}^{L} (\overline{C}_{lm}^{\,2} + \overline{S}_{lm}^{\,2})} \qquad , (2.10)$$

where σ_m is the order amplitude of each order m and L is the cut off degree, that is, 180 in our simulation. Figure 2.10 (c) shows the order amplitude spectrum of the period 108. Generally, the large peak of order m in Figure 2.10 (c) represents the fact that sampling points concentrate at the specific cycle which divide equator with $2m$ nodes. However, if m is not a prime number, the $2m$ nodal cycles per n times (n is an integer number) revolution of the Earth also appear at the spectrum in the order m. Considering the effect, I estimated the actual ground-track separation N and

corresponding order of k for all original orders m of the containing cycles of each period. Power spectra of the same order k were added each other. Each order (k) peak is maintained throughout some time periods. The orders (k) whose largest amplitudes (square root of power spectrum) are above 1.0 (except order (k) 0 and 180) are listed in Figure 2.11. Llarge specific cycle peaks which gave large ground track separations appeared as the orbit decayed (Figure 2.11). Some ground track separations are too large to precisely determine gravity field up to degree/order 30 as shown in Figure 2.9. Such peaks correspond to the short-period repeating orbital cycles. For example, the large peak of the period 108 corresponds to the repeating cycles of 31 cycles per 2 sidereal days. Although such specific cycle observation is useful to check or calibrate the corresponding specific degree/order of the derived spherical harmonic solutions (Klokočník, *et al*., 2003), it is disadvantageous for global gravity field recovery.

The decay rate of the altitude in the real GRACE mission may not be the same in this simulation. Therefore, the length of period which gives large ground-track separation may also be different in our simulation, but such a period will appear because the order of cycles contained in each period are determined mainly by the orbital altitude. From our simulation, ground tracks of around period 19, 56, 107, 142 and 156, which correspond to the altitude (mean semimajor axis minus the mean equatorial radius of the Earth) 473, 448, 399, 350, and 337 km, respectively, give insufficient spatial resolutions even for the gravity field recovery up to degree/order 30. When these solutions are used for detecting temporally changing geophysical phenomena, especially the phenomena near the detection limit, the precise estimation of the signal cannot be expected because the information used for updating at such periods does not have a sufficient high quality.

In the real GRACE mission, the data from August to November in 2004 corresponds to the period of 61 cycles per 4 day. Wagner *et al*. (2006) shows that the ideal gravity field resolution in September 2004 was only about 30 x 30 from linear perturbation theory. UTCSR calculated and released the monthly solutions (RL01) in the period is in the same way of other time periods, while JPL solutions (RL02) is not released in the period. GFZ is released the solution calculated with constraint field (RL03, GK2 solution) besides of the solution of routine analysis (RL03).

2.3.5. Effect of ocean pole tide

The variations in the geocentric position of the earth's rotation axis (polar motion) cause the deformation of the Earth. It effects not only on the solid Earth, but on the ocean. Thus, the ocean mass is redistributed periodically by the polar motion and mainly affects on C_{21} and S_{21} values. The effect of the ocean pole tide is corrected in the new versions of the GRACE monthly solutions (UTCSR RL02, JPL RL02 and GFZ RL03), but not in the first version (UTCSR RL01, JPL RL01, GFZ RL01 and RL02). In this study, the effect are estimated by the method of Wahr (1985) using IERS polar motion values when the first version data is used, though the effect is small and almost

negligible compared to the geophysical land or ocean signal.

2.4. Summary

The outline of the GRACE mission and the current status of the solutions were reviewed in this chapter. The static gravity field solution of the Earth is largely improved by GRACE mission and some precise gravity field models including the GRACE results are available now. On the other hand, the GRACE monthly gravity field solutions have not fully achieved the precision predicted before launch, yet. For the recovery of the geophysical signal, the spatial filter is usually applied to decrease the higher degree errors. Although the globally normalized isotropic Gaussian filter is popularly used for the purpose, non-isotropic or correlated-error removing filters have been developed to decrease the striping error of the GRACE solution. The filtered GRACE data is corresponds to the global ocean and landwater model in the correlation length several hundred to 1000 km. Several main error sources which degrade the GRACE monthly solution were reviewed. Most of them are caused from the gravity measurement method of GRACE satellite (C_{20} error, effect of orbit decay) or by the GRACE data processing of the data centers (data difference between the released data centers, aliasing error) and difficult to correct for users though some correction methods are suggested by the data centers. But for a few sources (ocean pole tide, effect of tidal error), the error can be estimated or corrected using models or other data sets.

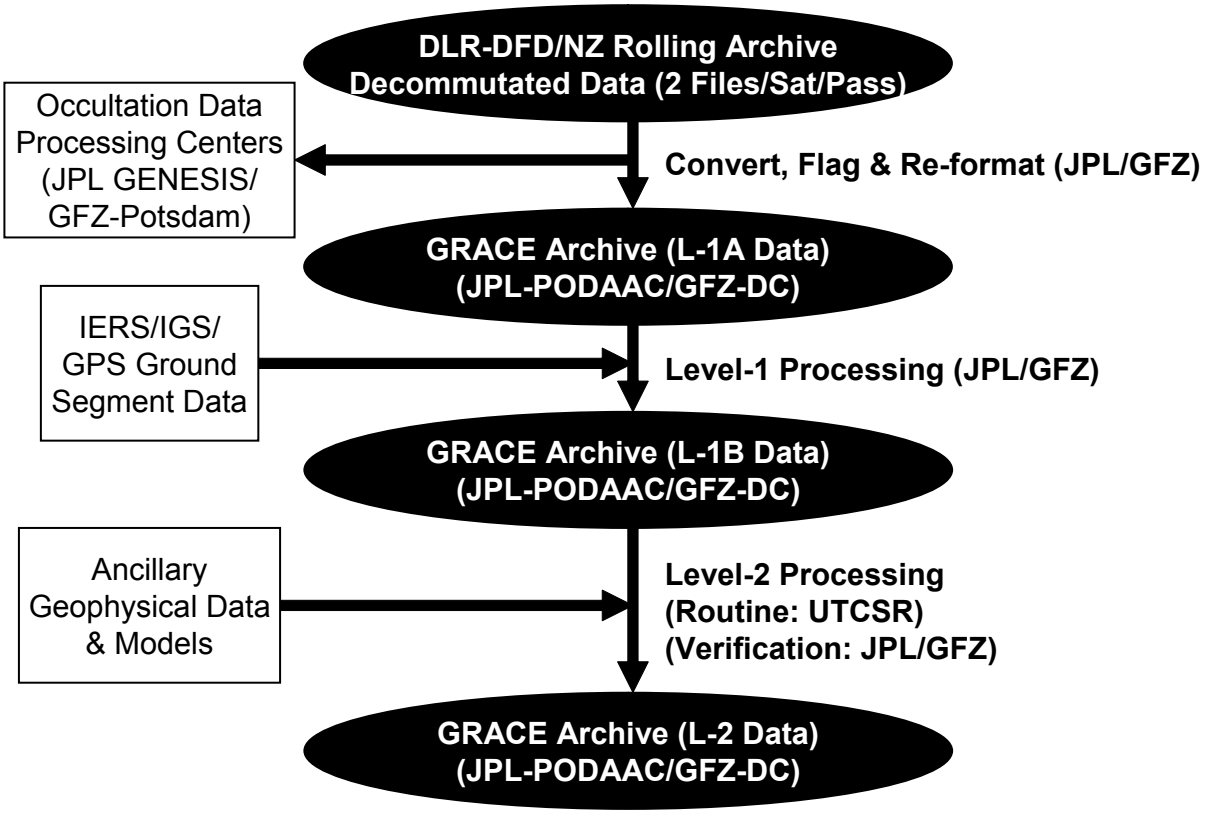

Fig. 2.1. Flow chart of GRACE science data system (Bettadpur, 2006a).

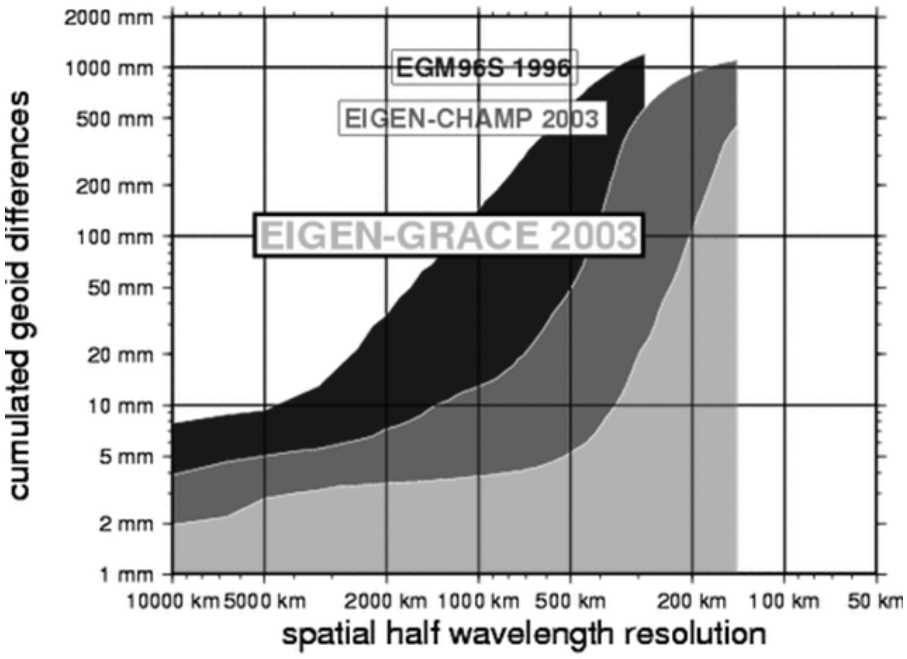

Fig. 2.2. Cumulated geoid differences EGM96S, EIGEN-CHAMP02S and EIGEN-GRACE01S vs. resolution (GeoForschungsZentrum, Potsdam, 2003).

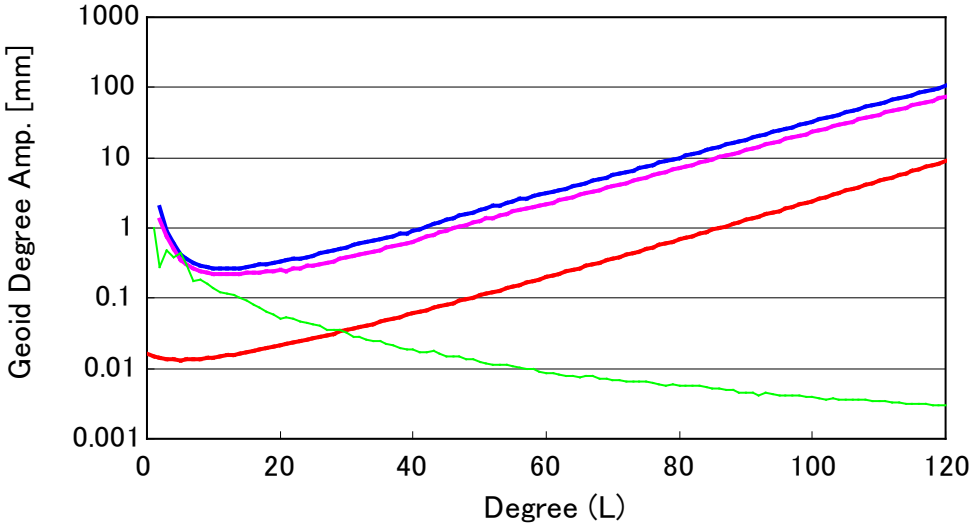

Fig. 2.3. Geoid degree amplitudes of calibrated standard deviations for UTCSR RL01 solutions (Blue: year 2002, Magenta: year 2003 to 2006). Geoid degree amplitudes of GRACE error predicted before launch (Red) and of the landwater model (Green) also shown.

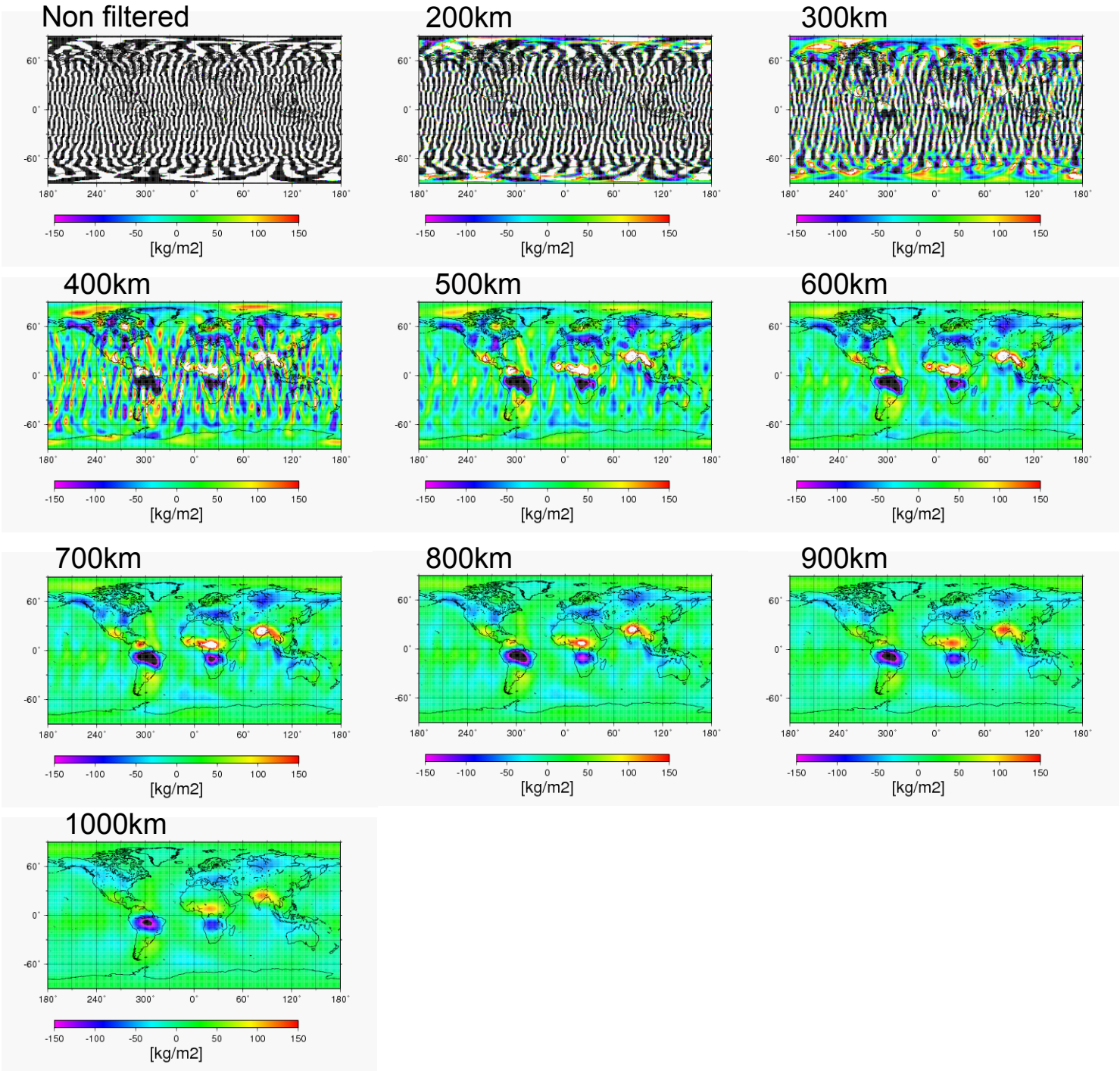

Fig. 2.4. Examples of the non-filtered and Gaussian filtered variable components of GRACE monthly gravity solutions in spatial domain.

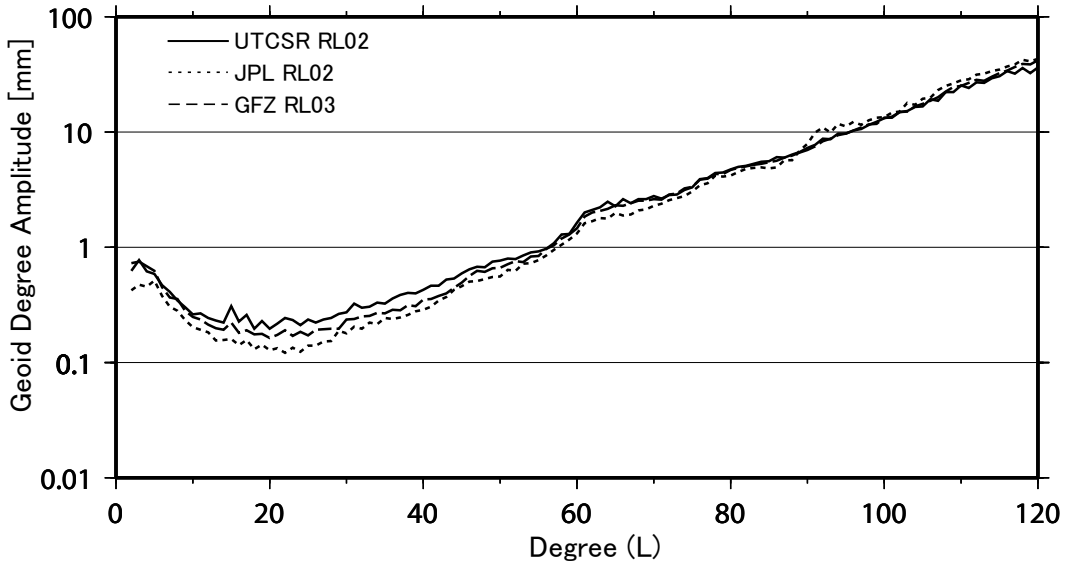

Fig. 2.5. Degree amplitudes of the variable components of UTCSR RL02, JPL RL02 and GFZ RL03 data sets. The variable components are derived by subtracting temporal averages from the original GRACE data.

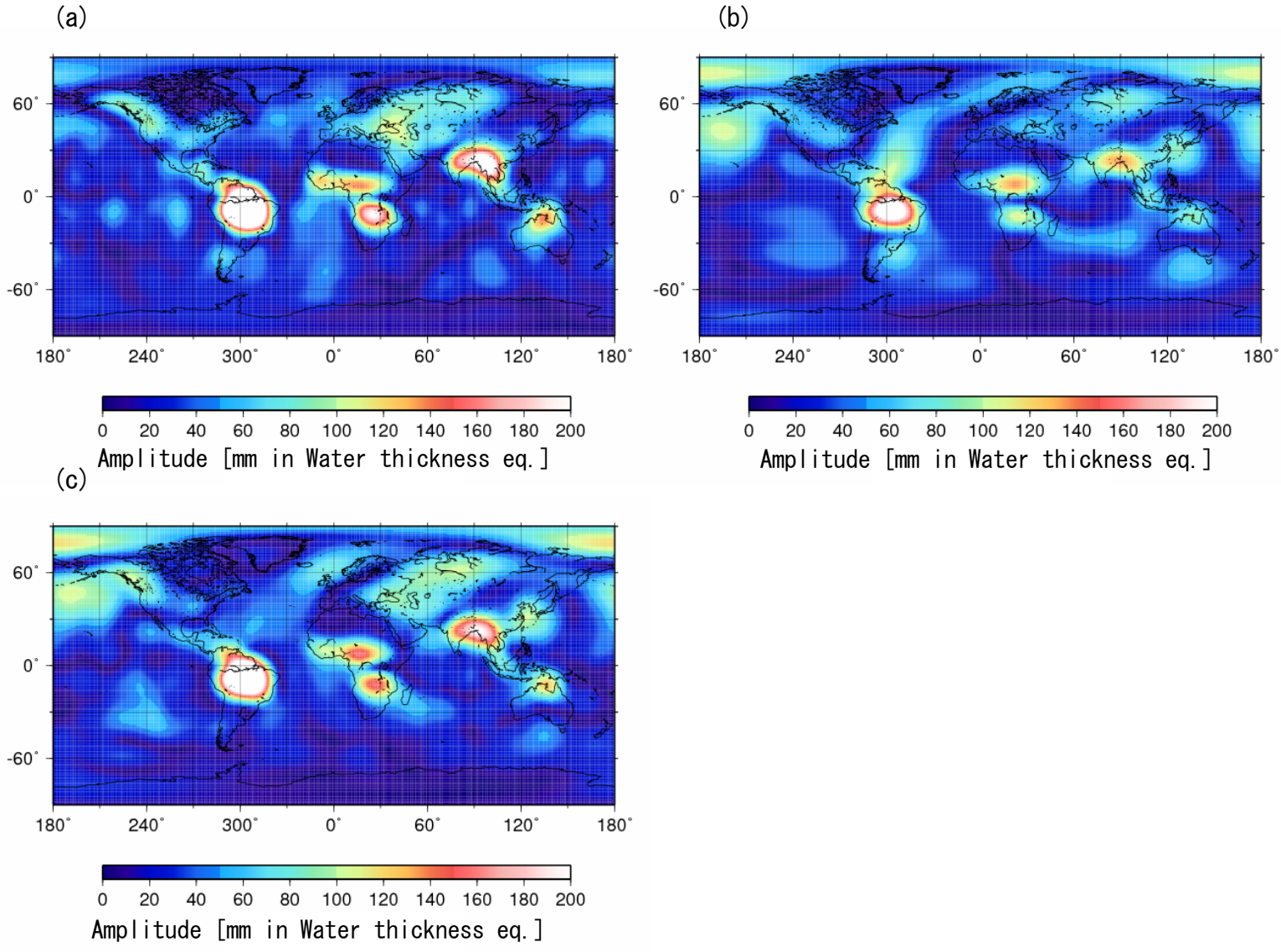

Fig. 2.6. Amplitude of annual components of UTCSR RL02 (a), JPL RL02 (b) and GFZ RL03 (c) data sets. The unit is water thickness equivalent.

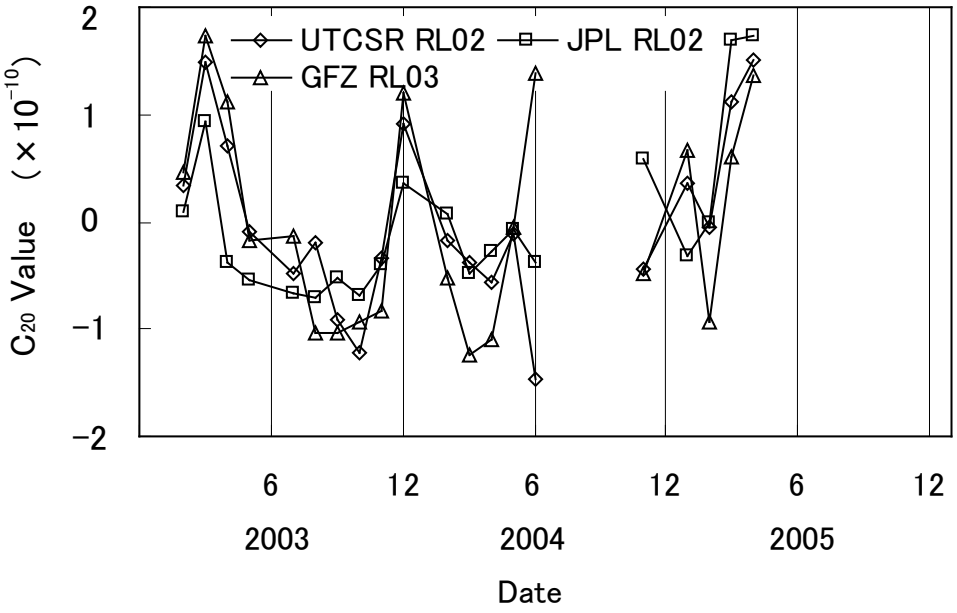

Fig. 2.7. Variable components of the C20 values of the UTCSR RL01, JPL RL02 and GFZ RL03 data sets over the 20 common time period.

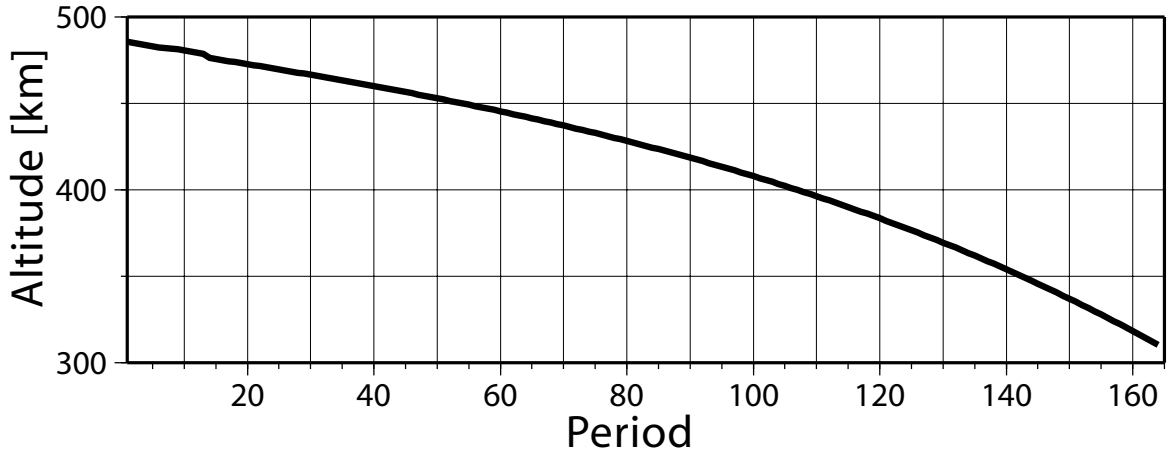

Fig. 2.8. Temporal decay of the simulated mean orbit altitude. The simulated orbit was divided into periods of 4 weeks, and the period numbers of 4 weeks are shown at the x-axis of the graph.

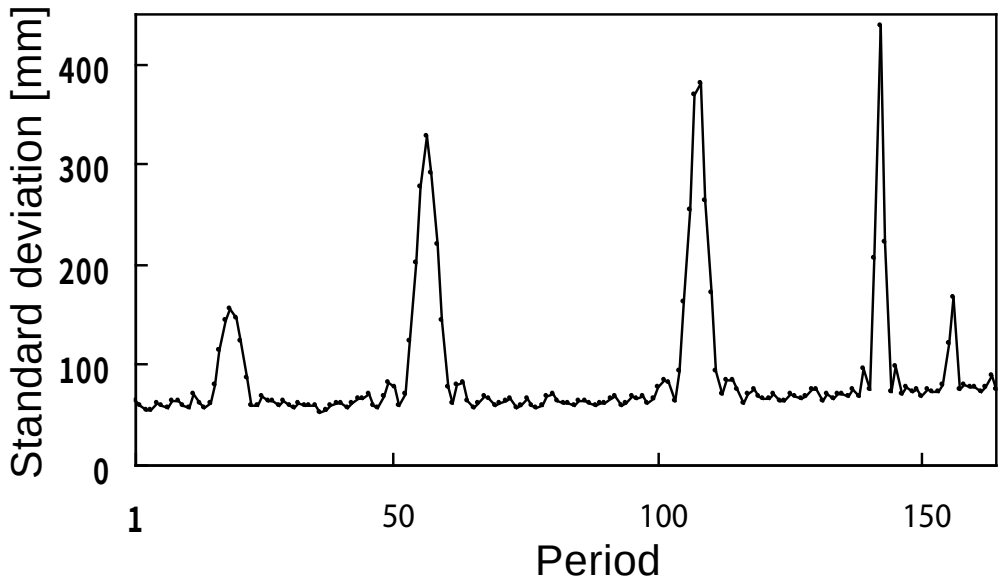

Fig. 2.9. Global standard deviations of the geoid height error calculated from the difference of recovered and true (original) spherical harmonic coefficients at each time period. The simulated orbit was divided to periods of 4 weeks, and the period numbers of 4 weeks are shown at the x-axis of the graph.

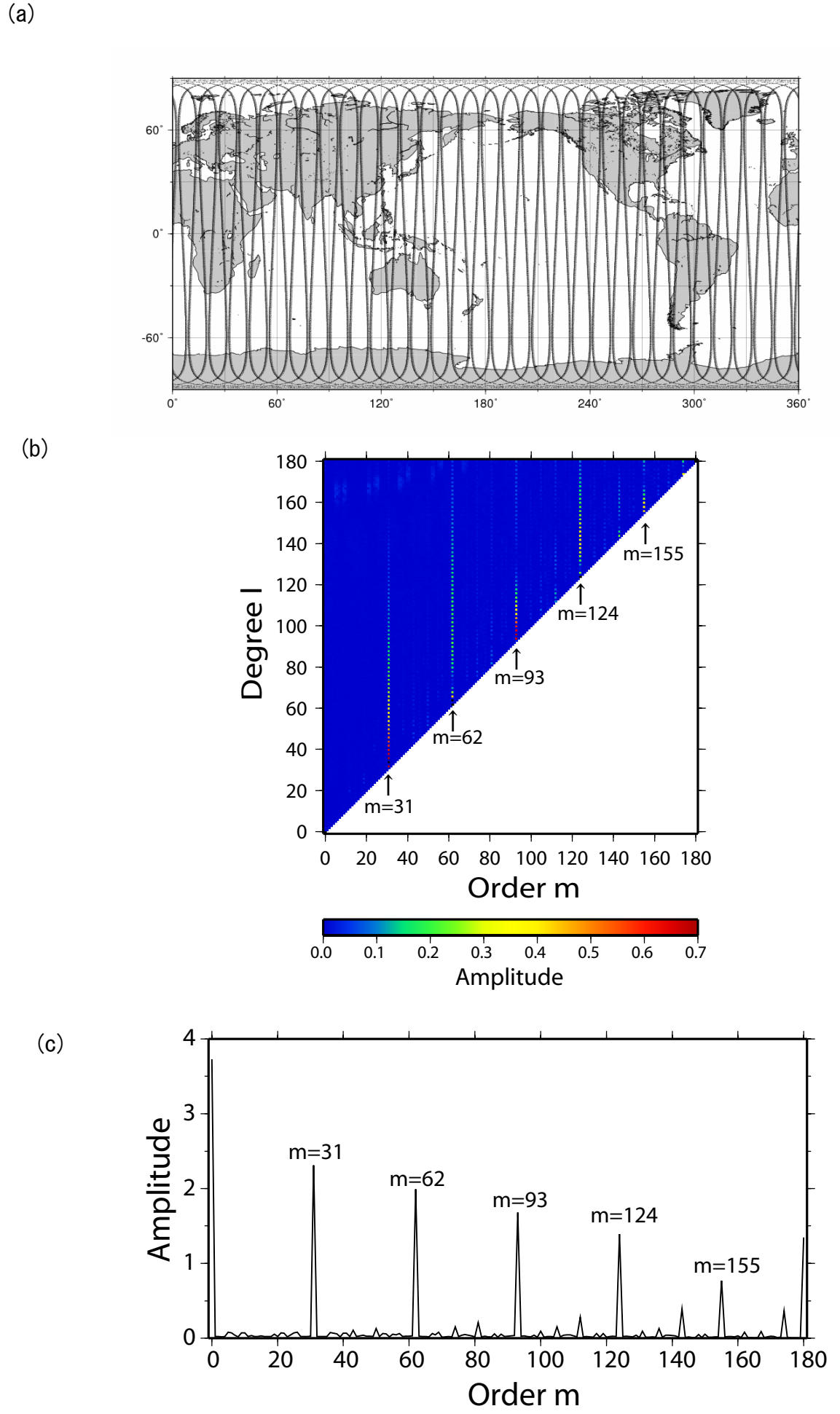

Fig. 2.10. (a) Spatial distributions of observational points of period 108. (b) Amplitude of the each l and m (Eq. (2.3)) derived from fully normalized spherical harmonic transformation of (a). (c) Order amplitude spectrum (Eq. (2.4)) derived from fully normalized spherical harmonic transformation of (a).

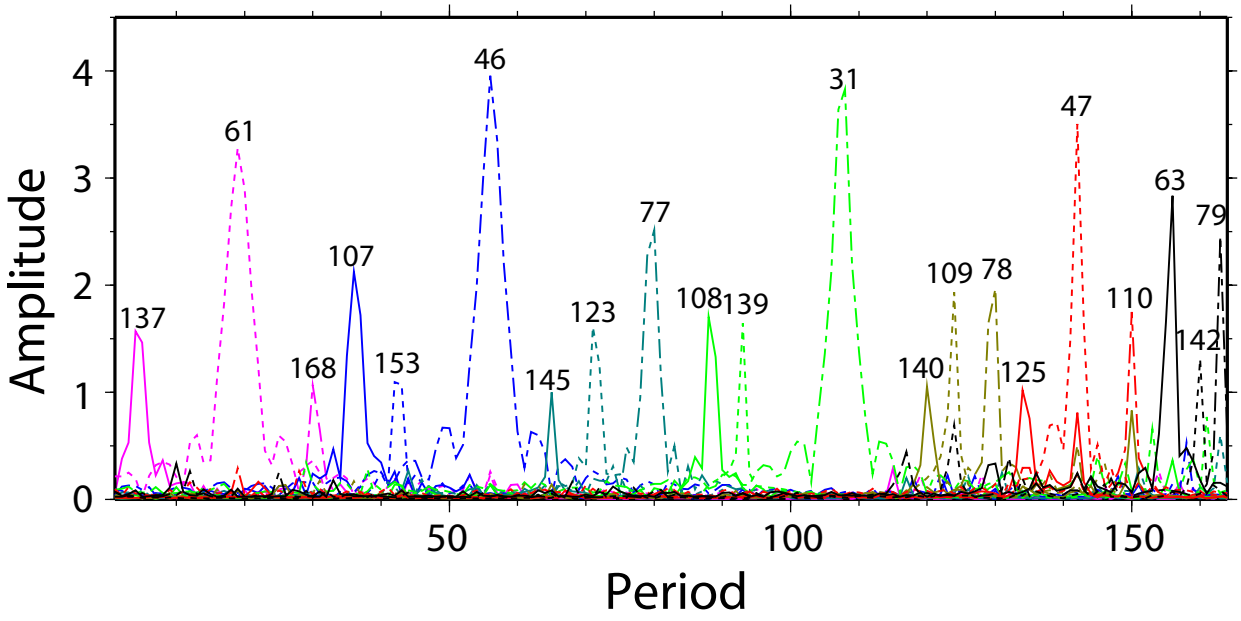

Fig. 2.11. Amplitude (square root of power spectrum) of each order peak contained in order amplitude spectra of spatial distributions of observational points at each period. The simulated orbit was divided into periods of 4 weeks, and the period numbers of 4 weeks are shown at the x-axis of the graph. The orders of cycles which give same ground-track separations are combined to one order by adding the power spectra. Numbers above the graph represent the corresponding order (k) of the order amplitude spectra. Only orders whose maximum amplitudes are above 1.0 (except order 0 and 180) are shown.

3. Landwater Mass Variation in the Indochina Peninsula

3.1. Introduction

In this chapter, the regional scale mass recovery from GRACE monthly gravity field solutions is performed and discussed in the Indochina Peninsula (Yamamoto *et al*., 2006a). The Indochina Peninsula is located in the area of Southeast Asian monsoon system, which plays an important role in the global energy and water cycle of climate system. In this area, it is generally believed that the monsoon wind shifts from northeast in winter to southeast in summer. The dry condition is caused by the winter monsoon while the wet and rainy situation by the summer monsoon in most of land areas. As a result, the magnitude of seasonal and interannual variation of landwater is quite large (Yasunari *et al*., 2003). Thus it is expected that the mass variation is sufficiently recovered from GRACE data. Further, near future, precise gravimetry on land combining with GPS observation is planned at Bangkok, Thailand for the purpose of detecting the landwater decrease caused by the rapid urbanization (Research Institute for Humanity and Nature, 2005). Regional scale mass variation recovered from GRACE data is expected to use for the correction to remove seasonal signal from the local observed data. More details are stated and discussed in Sec. 3.4.

Practically, the mass variations associated with the 4 major river basins in the Indochina Peninsula, i.e., Mekong, Irrawaddy, Salween and Chao Phraya river basins, were attempted to recover to investigate the applicability of the GRACE data. Fig. 3.1 shows the location of these river basins. The combined area of these 4 basins is 1,750,000 km^2 which is probably large enough for GRACE to recover the mass variations, while the square measures of Mekong, Irrawaddy, Salween and Chao Phraya river basins are 814,000, 425,000, 330,000, and 178,000 km^2, respectively. Bangkok is located in the downstream of Chao Phraya river basin.

To know the approximate regional mass variation caused by landwater, numerical model data set is useful. Japan Meteorological Agency (JMA) Simple Biosphere (SiB) model (Sellers *et al*., 1986; Sato *et al*., 1989), produces the components of soil moisture and snow storage, and improved recently for the seasonal forecasts and climate simulations (Tokuhiro, 2000; Nakaegawa and Sugi, 2001). Global River flow for TRIP (GRiveT) model (Hosaka *et al*., 2006; Nohara *et al*., 2006) produces the river water storage. These models are used for checking the recovered mass variation from GRACE monthly solutions. On the other hand, in these models, the groundwater variation is not sufficiently considered as well as most of other landwater models because of the difficulty of the observation of groundwater. Because the landwater variation detectable by GRACE is a total sum of the surface and ground water storage, it will be useful to give the constraint to the landwater model and, as a result, to the groundwater estimation. Thus, the results of comparison between the GRACE mass recovery and the model estimation are also discussed in this study.

Besides of the scientific interest, one of the purposes in this chapter is to confirm the availability

of the method of regional mass recovery developed by Swenson *et al*. (2003). The determination of the parameters in this method is also discussed. Another purpose is to confirm whether the new versions of GRACE monthly solutions (UTCSR RL02, JPL RL02 and GFZ RL03), are useful in the regional mass recovery. The results from the 3 versions of the new data sets are compared. The approximate limited basin size which the GRACE solutions can detect with reliable precision are investigated. The mass variation in the Indochina Peninsula is suitable for these purposes because the seasonal signal is large and the spatial scales of the river basins are small, but not too small for the GRACE mass recovery.

3.2. Method

3.2.1. Data sets

The new versions of GRACE Level 2 monthly gravity field solutions, i.e. UTCSR RL02, JPL RL02 and GFZ RL03 data sets, up to full degree and order 120 are used in this study. The data periods are summarized in Table 3.1. The numbers of data sets are 22 (UTCSR RL02), 27 (JPL RL02) and 27 (GFZ RL03). In JPL RL02 and GFZ RL03, the slopes caused from insufficient mass conservation of the ocean de-aliasing model (see Sec. 2.3.3.) are reported. However, our main target in this section is the seasonal mass variation in this area and the slope is relatively small and safe to be neglected compared to the large seasonal variation. Variable components of the gravity field solutions were calculated by subtracting the average value over the whole periods from the monthly solutions.

Table 3.1. The newly released GRACE Level 2 (near) monthly gravity field solutions of UTCSR RL02, JPL RL02 and GFZ RL03 used in this chapter.

Year	Jan	Feb	Mar	Apr	May	Jun	Jul	Aug	Sep	Oct	Nov	Dec
2003		○	○	○	○		○	○	○	○	○	○
	●	●	●	●	●		●	●	●	●	●	●
		◎	◎	◎	◎		◎	◎	◎	◎	◎	◎
2004	○	○	○	○	○	○					○	○
	●	●	●	●	●	●					●	●
		◎	◎	◎	◎	◎					◎	
2005	○	○	○	○								
	●	●	●	●	●	●	●	●				
	◎	◎	◎	◎	◎	◎	◎	◎	◎	◎	◎	

○: UTCSR RL02, ●: JPL RL02, ◎: GFZ RL03

For comparison and verification of the estimated mass variations, the combined mass variation

model that consisted of following ocean and landwater models were employed: (1) the ocean bottom pressure data of ECCO (Estimating the Circulation and Climate of the Ocean) – JPL Ocean Data Assimilation Project model of Kalman filter run with data assimilated with respect to the control mean (kf049f; Fukumori *et al*., 1999); (2) the landwater model of JMA-SiB and GRiveT, mentioned in Sec. 3.1. The landwater model takes into consideration the variations in snow storage, soil moisture (down to 1 m from the surface) and river storage, while the groundwater storage process is only considered insufficiently. The combined model data were averaged over time corresponding to the GRACE solution periods (nearly monthly), and variable components were calculated by subtracting the average of the whole period. The components of C_{00}, C_{10}, C_{11} and S_{11} were removed from the model coefficients for consistency with the GRACE data.

3.2.2. Recovery of the regional mass variations

For the recovery of regional mass variations, Swenson and Wahr (2002) developed a method in which they designed a regional spatial filter so as to minimize both the satellite measurement error and the leakage error (unwanted signals from nearby regions). Swenson *et al*. (2003) revised the method to optimize it for signals expected in actual GRACE data. The modified method of Swenson *et al*. (2003) is used in this study.

The surface mass variability over the region $\Delta\sigma_{region}$ was approximated by the following equations:

$$\Delta\sigma_{region} = \sum_{l=0}^{l\max}\sum_{m=0}^{l} \frac{1}{\Omega_{region}} \frac{a\rho_E}{3} \frac{(2l+1)}{(1+k_l)} (W_{lm}^{C}\Delta\overline{C}_{lm} + W_{lm}^{S}\Delta\overline{S}_{lm}) \quad , (3.1)$$

where Ω_{region} is the angular area of the region, a is the equatorial radius, ρ_E is the average density of the Earth, k_l is the load Love number of degree l, $W_{lm}{}^{C}$ and $W_{lm}{}^{S}$ are the designed filter coefficients, $\Delta\overline{C}_{lm}$ and $\Delta\overline{S}_{lm}$ are fully normalized Stokes coefficients of degree l and order m, and l_{max} is the truncated degree of the spherical harmonics.

$W_{lm}{}^{C}$ and $W_{lm}{}^{S}$ are obtained by the following equation

$$\begin{Bmatrix} W_{lm}^{C} \\ W_{lm}^{S} \end{Bmatrix} = \left[1 + \frac{2(2l+1)B_l^2}{\sigma_0^2 G_l (1+k_l)^2} \left(\frac{a\rho_E}{3} \right)^2 \right]^{-1} \begin{Bmatrix} \vartheta_{lm}^{C} \\ \vartheta_{lm}^{S} \end{Bmatrix} \quad , (3.2)$$

where B_l is degree amplitudes of the satellite measurement errors, $\sigma_0{}^2$ is the local signal variance, G_l is the Legendre coefficients of a covariance function and $\vartheta_{lm}{}^{C}$ and $\vartheta_{lm}{}^{S}$ are the spherical harmonic coefficients of the regional template, i.e., 1 inside and 0 outside the area concerned.

To suppress the higher degrees errors effectively, the Gaussian covariance function

$$G(\gamma, d) = \exp\left[\frac{-(1-\cos\gamma)\ln 2}{(1-\cos(d/a))}\right] \quad , (3.3)$$

was employed as the covariance function, where γ is angular distance and d is correlation length.

For the optimal design of the regional filter, B_l and d should be fixed in advance, and σ_0^2 is determined so as to minimize the sum of the satellite measurement errors and the leakage errors iteratively. Finally the amplitude degradation was corrected by multiplying a factor which was given as the ratio between non-filtered and filtered model data.

To determine the B_l values, the error degree amplitudes of the GRACE measurements have to be known. As an approximation of the error degree amplitudes, Wahr *et al*. (2004) employed 1.1-fold as large as the residual signals which were obtained by removing constant and annual components. The same approximation was adopted to evaluate the error degree amplitudes. Fig. 3.2 shows the estimated error degree amplitudes of the three data sets.

Using a hydrological model, Swenson *et al*. (2003) investigated the d dependence of the recovered signal and reported that the optimal d value was between 200 and 800 km in most cases. This range of spatial scale is consistent with the correlation length of typical soil moisture variations. Chen *et al*. (2005a) reported that GRACE results corresponded well to landwater model estimations across the world when the Gaussian filter with d = 800 km was applied. However, this d value is not always best for the regional mass recovery, because the spatial features of the signal are different in each area. In this study, to find an appropriate d value, the degree amplitude of a hydrological model inside the area was compared with the filtered GRACE data by applying Eq. (3.2) to the Stokes coefficients. Fig. 3.3 shows the degree amplitudes of filtered (corresponding to different d values from 200 to 1000 km) and non-filtered GRACE data (JPL RL02) together with the hydrological model degree amplitudes for the combined area of 4 rivers. Note that almost the same result was obtained even if UTCSR RL02 or GFZ RL03 data was employed. Although a smaller d value is beneficial for detecting fine spatial scale mass variations, it suffers from measurement errors at higher degrees. Contrary, a larger d value can suppress the higher degree errors, but it loses spatial resolution; further, widespread leakage errors prevent accurate mass estimation. Weighing the trade-off, 600 km was selected as the d value from Fig. 3.3. We used the same d value throughout this section for all the test areas because the correlation length of landwater signals and the GRACE measurement errors should be almost the same in the neighboring areas. As an example, Fig. 3.4 shows the designed filter for the combined area of 4 rivers.

After applying the filters, surface mass variations were calculated using Eq. (3.1). Because degree 0 and degree 1 terms were not included in the GRACE monthly products, these terms were omitted

in the calculation.

3.2.3. Error estimations

The satellite measurement errors, which are shown as the error bars in the following figures, were calculated by the following equation:

$$\Delta\varepsilon_{region} = \frac{1}{\Omega_{region}} \sqrt{\sum_{l=0}^{l\max} \left(\frac{a\rho_E}{3} \frac{(2l+1)}{(1+k_l)} \right)^2 \sum_{m=0}^{l} \left[(W_{lm}^C \Delta\overline{C}_{lm(error)})^2 + (W_{lm}^S \Delta\overline{S}_{lm(error)})^2 \right]} \quad . (3.4)$$

Here, the same regional filters were applied to the GRACE error coefficients.

The leakage errors were estimated as follows. Firstly the Stokes coefficients associated with the leakage effects was calculated using Eq. (3.5) by integrating $\Delta\sigma(\theta,\lambda)$ only outside the area concerned

$$\begin{Bmatrix} \Delta\overline{C}_{lm} \\ \Delta\overline{S}_{lm} \end{Bmatrix} = \frac{3(1+k_l)}{4\pi a\rho_E (2l+1)} \iint \Delta\sigma(\theta,\lambda) \overline{P}_{lm}(\cos\theta) \begin{Bmatrix} \cos(m\lambda) \\ \sin(m\lambda) \end{Bmatrix} \sin\theta d\theta d\lambda \quad , (3.5)$$

where $\Delta\sigma(\theta,\lambda)$ is the surface density at colatitude θ and longitude λ, $\overline{P}_{lm}(\cos\theta)$ is the fully normalized Legendre function of degree *l* and order *m*. The leakage effects were then estimated by applying the same filter designed in Sec. 3.2.2 to the derived Stokes coefficients. Finally the effects were subtracted from the GRACE gravity solutions. There may be two candidates for the input data of $\Delta\sigma(\theta,\lambda)$ in Eq. (3.5): one is calculated from model values and the other from GRACE data. As discussed in the following sections, both cases were tested and ultimately choose to use the GRACE data in this study. Note that to suppress the large errors of higher degree coefficients which may cause an inaccurate estimation of the leakage errors, the globally normalized Gaussian filter (Wahr *et al*., 1998) with the same *d* value was applied to the original GRACE data.

3.3. Results and discussion

Although most parts of following discussions are based on the JPL RL02 results, the results obtained by the other data sets are essentially the same. The comparisons between the 3 data sets are discussed in Sec. 3.3.4.

3.3.1. Spatial size limitation of mass recovery from GRACE monthly solutions

Fig. 3.5 shows the estimated mass variations from GRACE. The model values, which are the regional averages of the gird values, are also shown in Fig. 3.5.

The GRACE estimations of the combined area of the 4 river basins (Fig. 3.5(a)) and the Mekong

river basin (Fig. 3.5(b)) are in good agreement with the model values. The estimated values for the Irrawaddy river basin (Fig. 3.5 (c)) basically agree with the model values, although the GRACE estimation in Fig. 3.5 (c) appears to be slightly noiser compared with Fig. 3.5 (a) and (b).

Because the widths of Salween and Chao Phraya river basins are smaller than the correlation length *d* of 600 km, a smaller *d* might be preferable for these areas if the measurement errors were small enough. However, as shown in Fig. 3.5 (d) and (e), the errors were larger than the derived mass variations, and the results appear to be unrealistic. If the smaller *d* values were used, the errors became much larger due to higher degree errors.

In addition to the size of the basin, its shape is another important factor for the precise mass recovery. The error distribution of the GRACE monthly gravity field solutions is not isotropic, but strongly correlated with the satellite track, i.e., the north-south direction ("striping error", mentioned in Sec. 2.2.2.). The striping error is more serious for the extremely north-south-oriented basins like Salween than for the isotropic or east-west-oriented basins. This is another reason why the mass recovery in the Salween and Chao Phraya river basins are quite difficult.

In the following discussion, only the result on the combined area of the 4 rivers is referred, but the same discussions are basically valid for the cases of the Mekong and Irrawaddy river basins.

3.3.2 Leakage effect

As previously discussed, there are two choices of surface mass densities for the estimation of the leakage effect. Fig. 3.6 shows a comparison of these in which it is apparent that there are slight differences between two estimations in both amplitude and phase. One of the reasons for the amplitude difference may be the influence of the global filter applied to the GRACE data. However, at present, further discussions on the amplitudes are quite difficult due to the uncertainties of the model amplitude and the GRACE measurement errors.

On the other hand, it is true that the present landwater model has a problem in treating the groundwater storage and that it causes the error in phases. Because most of leakage errors come from the adjacent area where large groundwater signals are expected, the model error is more serious for the final results. Therefore, in this study, finally the GRACE data was ultimately employed for estimating the leakage effects. Kanzow *et al*. (2005) reported that GRACE errors in the ocean area and on the land area are different. Therefore the leakage effects were estimated from the ocean area and the land area separately. Fig. 3.7 shows the results. In this figure, the estimations using model data are also plotted for the comparison. Compared with the old versions data sets, which have larger errors in the ocean than on land (Kanzow *et al*., 2005), the short period ocean model is updated in the newly released data sets as mentioned in Sec. 2.3.3. However, because the ocean effect is very small as shown in Fig. 3.7 (a), the improvement does not affect our mass estimation and the errors due to the ocean models can be completely negligible in this area. As shown in Fig. 3.7 (b), the

leakage effect of the landwater is larger than the one of the ocean. The difference between the results using the GRACE data and the model data is small, and it can be safely neglected.

3.3.3 Effect of C_{20}

As stated in Sec. 2.3.2., the C_{20} value cannot be well determined by L-L SST method. Therefore most of the previous studies excluded the C_{20} value in the estimation of mass variations (e.g. Wahr *et al*., 2004). In the newly released data sets, the ocean pole tide has already corrected. It has also been announced that the accuracies of the C_{20} values have been dramatically improved. To confirm the improvement of the C_{20} values, the C_{20} contributions were calculated separately. Fig. 3.8 (a) shows the results. The seasonal variation of the C_{20} contributions is slightly different from the total mass variation; in fact, the C_{20} values of the 3 data sets still have relatively large differences of about 10-mm equivalent water thickness at most (the data are not shown). However, as shown in Fig. 3.8 (b), the influence of C_{20} on the final result is small with respect to the total signal and there is no positive reason to exclude the C_{20} values. Therefore I decided to include these values in the estimations.

3.3.4 Comparison of the results of the 3 new version data sets

Fig. 3.9 shows the derived mass variation in the combined area of the 4 rivers based on the 3 new data sets. A common feature to all 3 data sets is a good agreement with the model in 2003 and the first half of 2004. Large discrepancies, especially in UTCSR RL02 and GFZ RL03, are seen in November 2004, just after the GRACE data gap from July to October 2004 when the solutions are unstable because of the repeat orbit of the GRACE satellites (Wagner *et al*., 2006 and Yamamoto *et al*., 2005). In this period, the resolution of the GRACE monthly field is significantly degraded to only about degree 30 (Wagner *et al*., 2006). It is suspected that there may be a GRACE data error after the data gap period.

In any case, all 3 results show clear seasonal mass variations even though slight differences exist, especially in the amplitudes. The amplitude of the estimated mass variation is large and is in the order of UTCSR RL02, GFZ RL03, and JPL RL02. This corresponds to the order of the degree powers of the variable components as shown in Fig. 2.5 and mentioned in Sec. 2.3.1. Although it cannot be concluded which data set is the most preferable and/or reliable at present, Fig. 3.9 shows that the best agreement between JPL RL02 and the model can be seen in this area.

3.3.5 Annual variations

Annual signals of the estimated mass variations were calculated for both GRACE and the model data sets and compared with each other. The signal fittings were conducted for two cases: one in

which all the data were used and one in which the data of November 2004 was excluded. The results are summarized in Table 3.2.

Table 3.2. The annual amplitudes and the phases lags (+: delay) of the derived mass variations relative to those estimated from the model data. Two cases of using all data and excluding the data of November 2004 are shown.

	All Data		Excluding Nov. 2004	
	Amplitude	Phase lag [day]	Amplitude	Phase lag [day]
UTCSR RL02	1.37	+29.5	1.32	+26.7
JPL RL02	0.92	+27.4	0.94	+26.7
GFZ RL03	1.18	+24.4	1.15	+20.8

Due to several uncertainties, as previously mentionedm we dare not discuss the amplitudes here. On the other hand, the phases of all 3 GRACE results commonly show a delay of about 1 month or less compared to the model. Chen *et al* (2005b) compared the mass variation derived from GRACE data to the GLDAS landwater model (Rodell *et al*., 2004) in several large river basins and also pointed out the phase delay in the GRACE data. They considered that one of the possible reasons for this delay is the influence of groundwater flow, which is not considered in the GLDAS model. In our cases, the same reason can be considered because the phase lag of the groundwater storage is not considered in either the SiB or GRiveT model.

3.4. Future application for the correction of in situ gravimetry

In the Indochina Peninsula, the population density is generally high, and securing water resources in this region is very important. It is especially serious around the cities in the development stage of urbanization, where transformation of water resources between groundwater and surface water is occurring rapidly (Global Water System Project, 2005). Thus the project to assess the effects of human activities on the subsurface environment in Asian cities has started (Human Impacts on Urban Subsurface Environment (HIUSE) project, Research Institute for Humanity and Nature, 2005). In this project, the precise in-situ gravity measurements combined with GPS and groundwater level measurements for monitoring local or urban scale groundwater variations at urbanized cities in East Asia is planned to be conducted. Because the effects of groundwater variations are one of the largest sources which cause the local temporal gravity changes, precise gravimetry on land should be a powerful technique to monitor the groundwater variations. In this project, Bangkok in Thailand is selected as one of the research targets. Bangkok is located at the downstream region of Chao Phraya river basin and the large seasonal mass variation is expected as discussed in this chapter. These

variations may cause gravity changes on the Earth's surface and such influence, at least conceptually, should be removed from the in-situ gravity measurement data for the purpose to detect local or urban scale gravity variation.

From the results in Sec. 3.3, it is confirmed that the GRACE data surely detected the regional mass variation over the combined area of the 4 rivers including Chao Phraya. To investigate the effect of the magnitude of regional mass variation on the ground gravity measurement, the GRACE gravity field solution is converted to the terrestrial gravity variations, which corresponds to the ground observation, by the following equation.

$$\Delta g_G(\theta,\lambda) = \frac{GM}{R^2}\sum_{l=0}^{l\max}\left[\frac{1/2+(n+1)k_l' - 2h_l'}{1+k_l'}\right]\sum_{m=0}^{l}[\Delta C_{lm}\cos m\lambda + \Delta S_{lm}\sin m\lambda]P_{lm}(\sin\theta) \qquad (3.6)$$

The estimation is performed at the location of Bangkok (13.45°N and 100.32°E) using the 1000-km (globally normalized) Gaussian filtered GRACE solution (Fig. 3.10). The result shows that the about ± 2 to 4 μGal of 1000 km scale regional mass variation effects on the ground gravity measurement on Bangkok. On the other hand, the change of the infinite water table of sub meter corresponds about a few 10 μGal. Although the gravity change of the seasonal mass variation is smaller than the value, but should not be neglected for the precise estimation. I believe that the GRACE data is useful for the purpose.

3.5. Conclusion

It is confirmed that the new versions of GRACE Level 2 data sets should be useful to detect at least Mekong and Irrawaddy river basin-scale mass variations. The relatively large-scale mass variation of the combined area of the 4 rivers, of which spatial scale is larger than 1000km, shows a fairly good agreement with the numerical model. However it is still difficult to reveal the mass variations in the spatial scale of the Salween basin or Chao Phraya basin. This is mainly because the insufficient spatial resolution of the current GRACE data sets, but another important issue is the non-isotropic feature of the GRACE errors. The north-southward signal is difficult to recover by the 'striping error' though there may be some space for improving this feature by introducing de-striping techniques as mentioned in 2.2.2.

With respect to the comparison based on the data from the 3 different data sets, the obtained amplitudes are slightly different from each other. Although JPL RL02 shows the best agreement with the model, it is still difficult to conclude which data set is the most reliable because of the insufficient reliability of the model itself. On the other hand, the phases of the estimated mass variations of all 3 data sets commonly show a 20- to 30-day delay compared to the model. A possible reason is the groundwater behavior which is not properly treated in the model. This suggests that

GRACE can provide useful information to improve the hydrological model.

As a future plan, a new technique of precise in situ gravity measurements combined with GPS positioning will be performed for monitoring the groundwater changes in Bangkok. To obtain more accurate local groundwater variation, GRACE data will be useful for the correction of the background variations due to larger scale landwater. More reliable discussion for the groundwater variation can be possible by combining the GRACE data and in-situ measurements. It is also expected that the in-situ measurements give a constraint to investigate the discrepancies between the GRACE solutions and the hydrological model previously described.

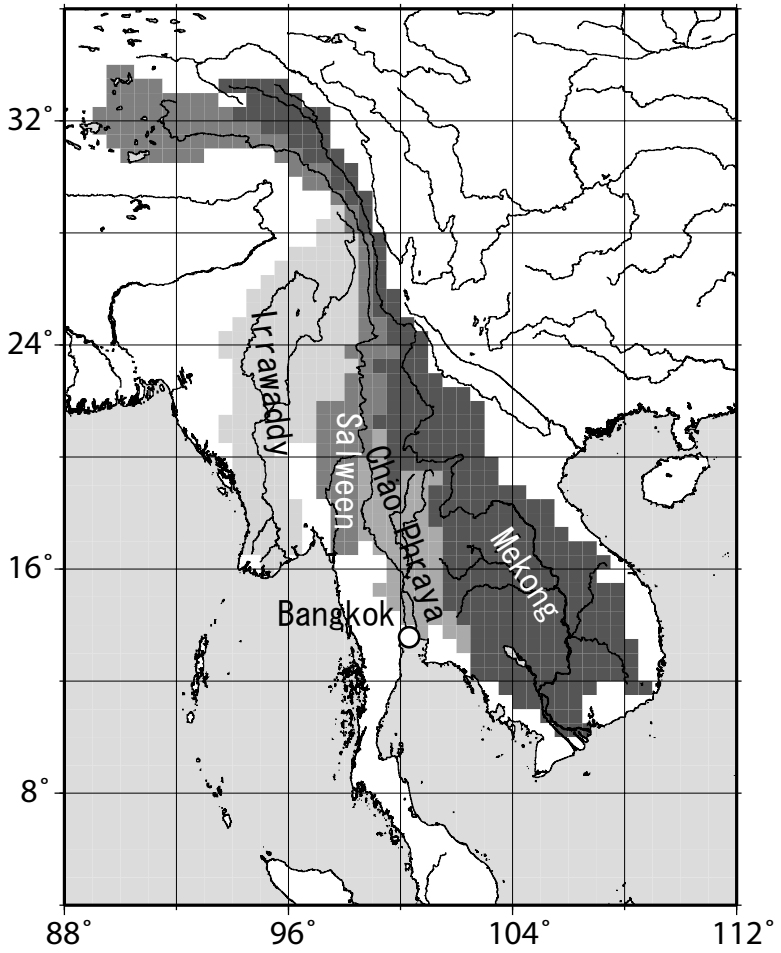

Fig. 3.1. Locations of the drainage areas of Mekong, Irrawaddy, Salween and Chao Phraya river basins.

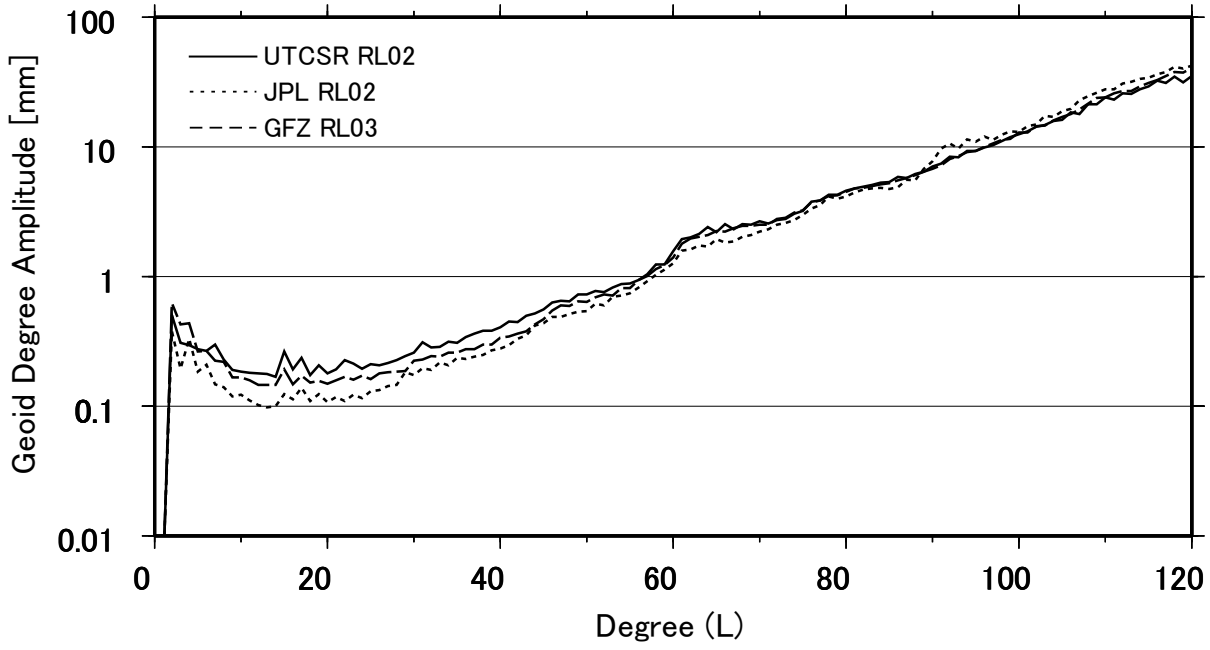

Fig. 3.2. Degree amplitudes of the estimated error of UTCSR RL02, JPL RL02 and GFZ RL03 data sets.

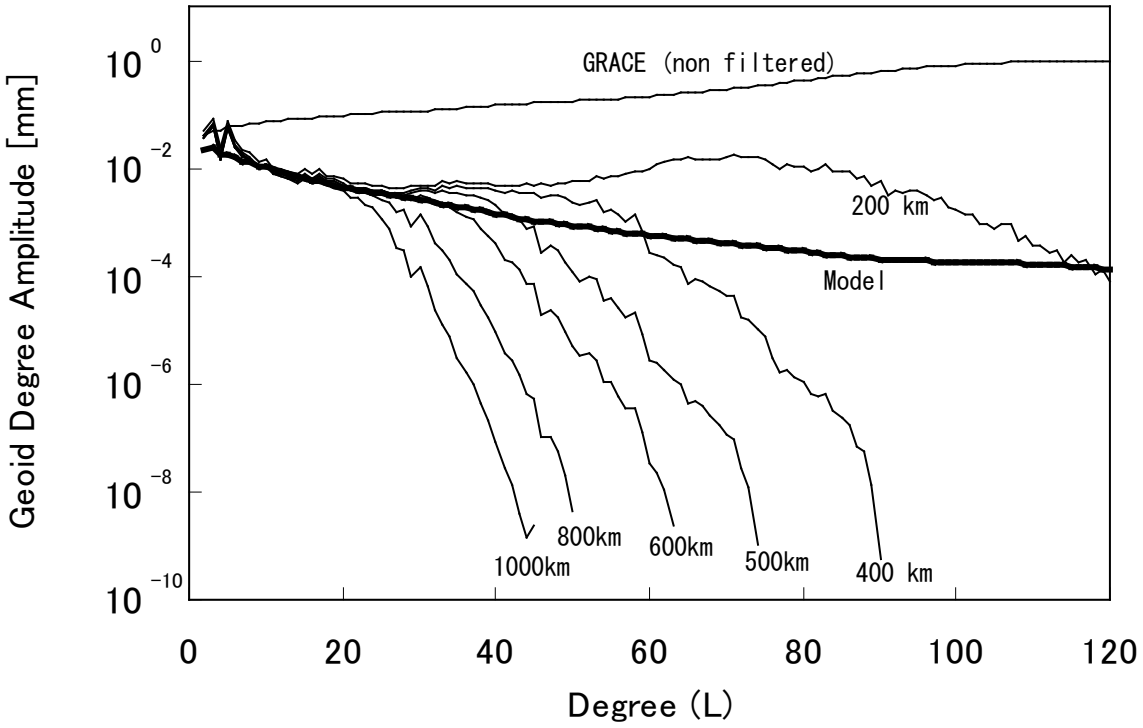

Fig. 3.3. Degree amplitudes for the combined area of 4 rivers calculated from the filtered GRACE data with different correlation lengths (from 200km to 1000km). Degree amplitudes of non-filtered GRACE data and the landwater model are also shown.

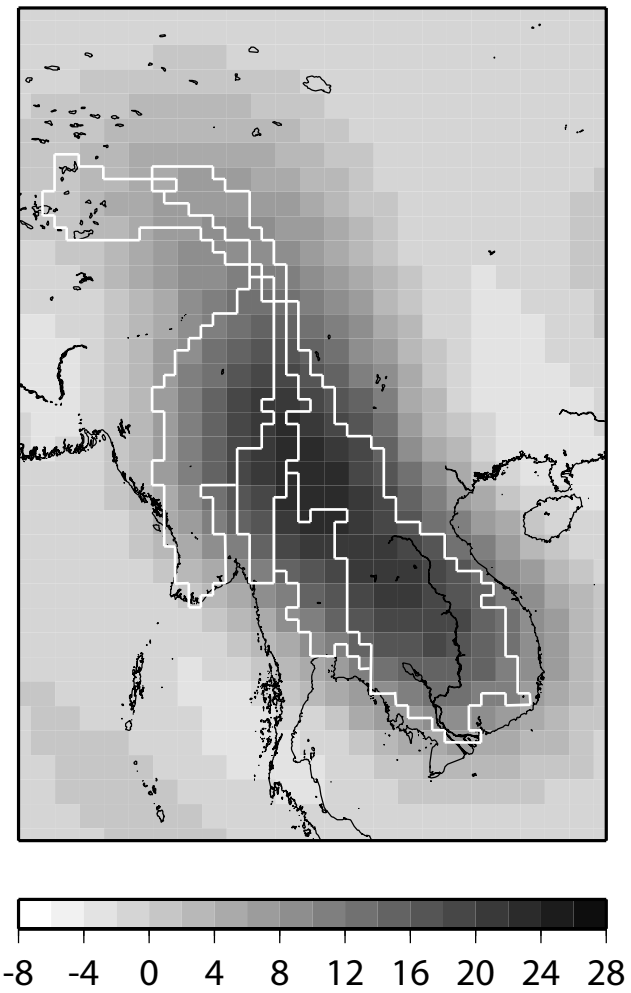

Fig. 3.4. An optimal filter for the JPL RL02 data sets designed for the combined area of Mekong, Irrawaddy, Salween and Chao Phraya river basins. The white lines show the boundaries of the drainage areas.

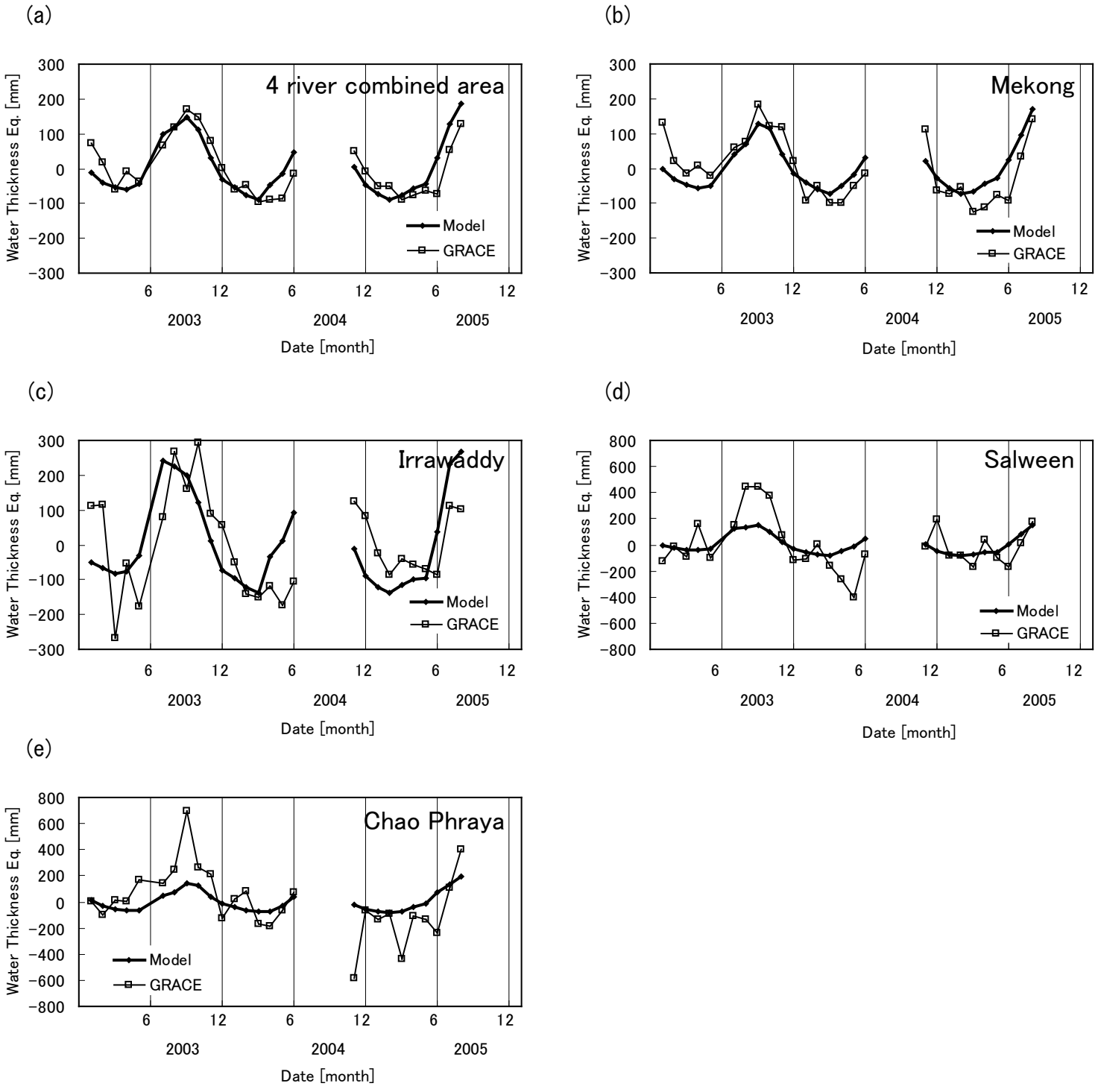

Fig. 3.5. Estimated mass variations for: (a) the combined area of 4 rivers, and the (b) Mekong, (c) Irrawaddy, (d) Salween, and (e) Chao Phraya river basins. The JPL RL 02 data set and correlation length d = 600 km are used. The mass variations estimated from the model are also shown. Note that the vertical scales of (d) and (e) are different from the others.

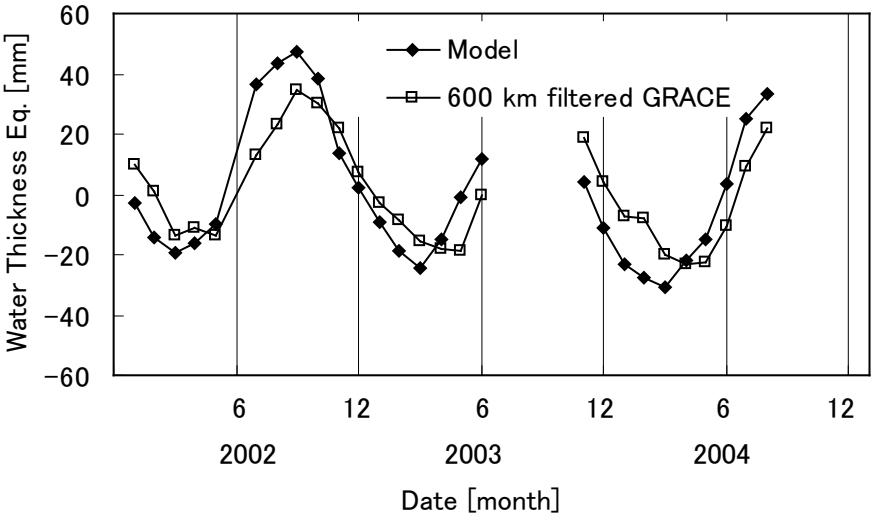

Fig. 3.6. Comparison of the leakage estimations. For the estimations, the model and the 600-km global filtered GRACE data are employed as the surface mass distributions.

(a)

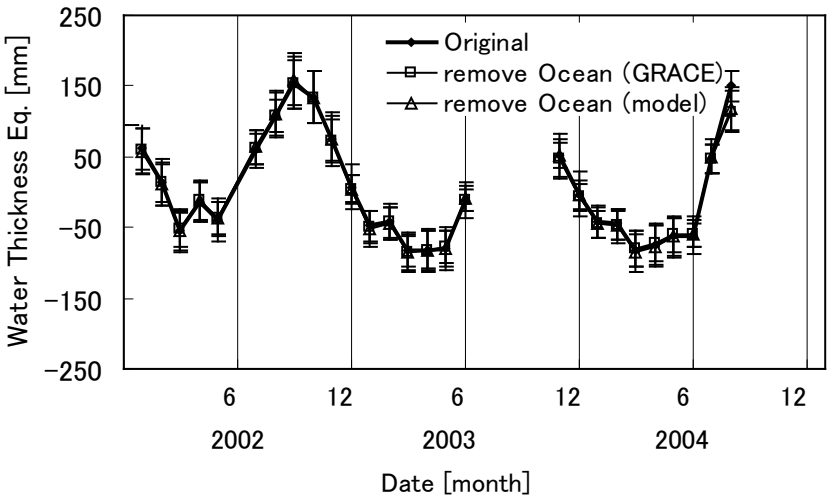

(b)

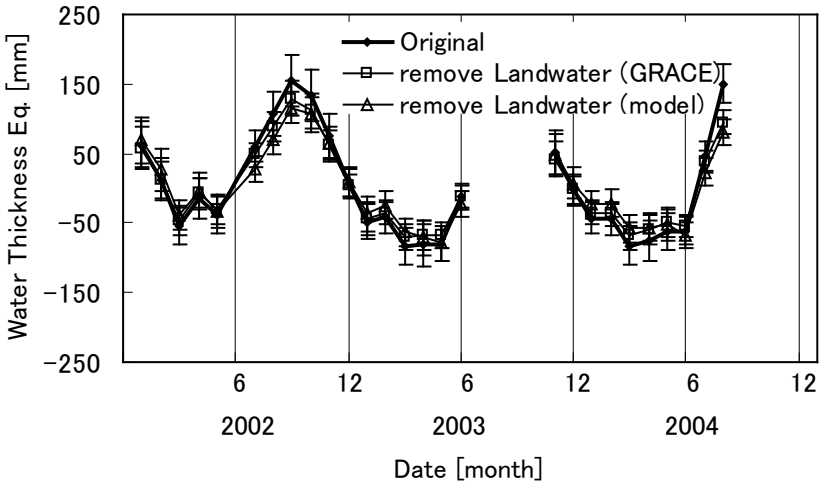

Fig. 3.7. Comparison of the mass variations before and after corrections. (a) The leakage influence of the ocean, and (b) the leakage infuluence of the landwater. The leakage influence is estimated using the GRACE data and the model data.

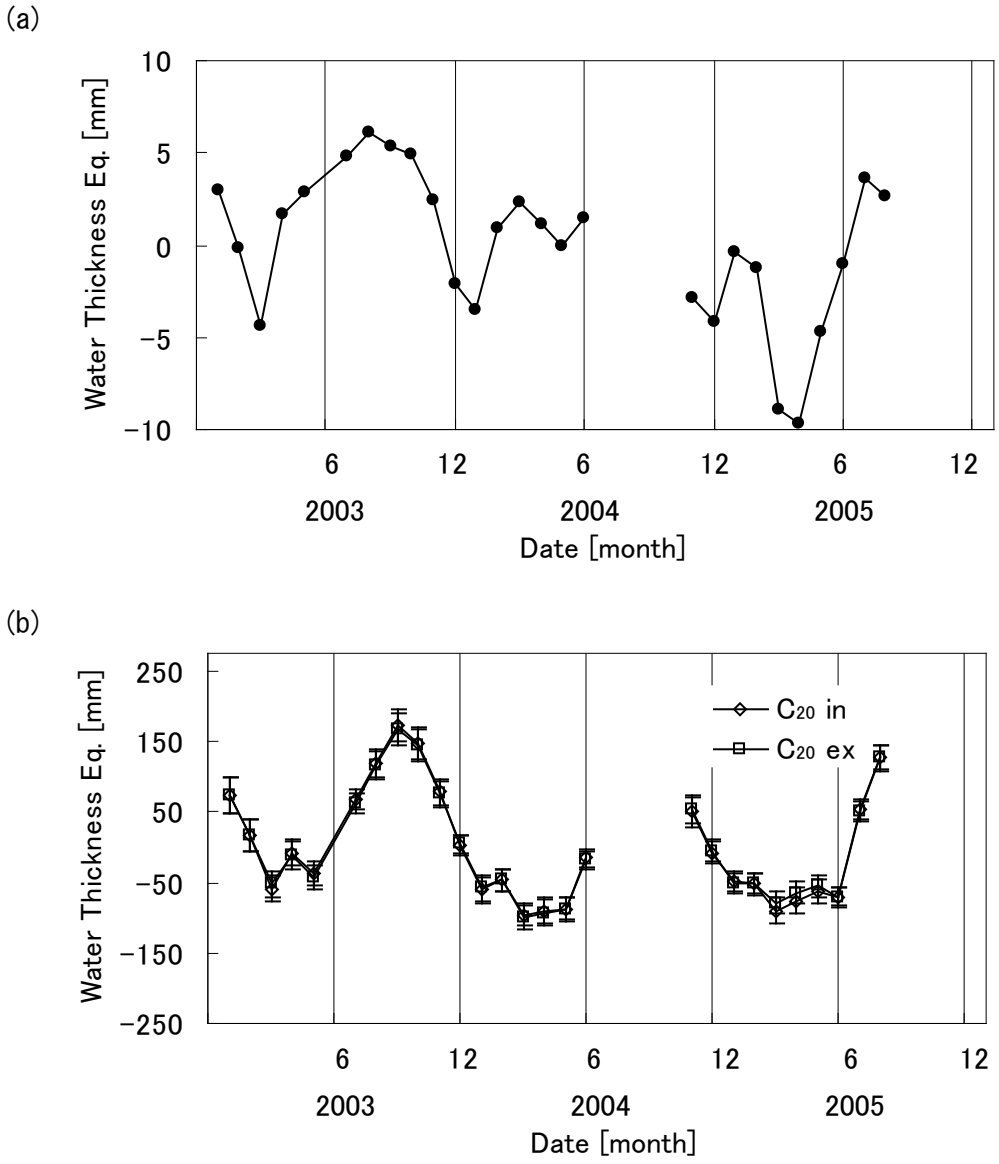

Fig. 3.8. (a) Contribution of the C20 value to the mass variations in the combined area of the 4 rivers. (b) Estimated total mass variations, including and excluding the C20 value.

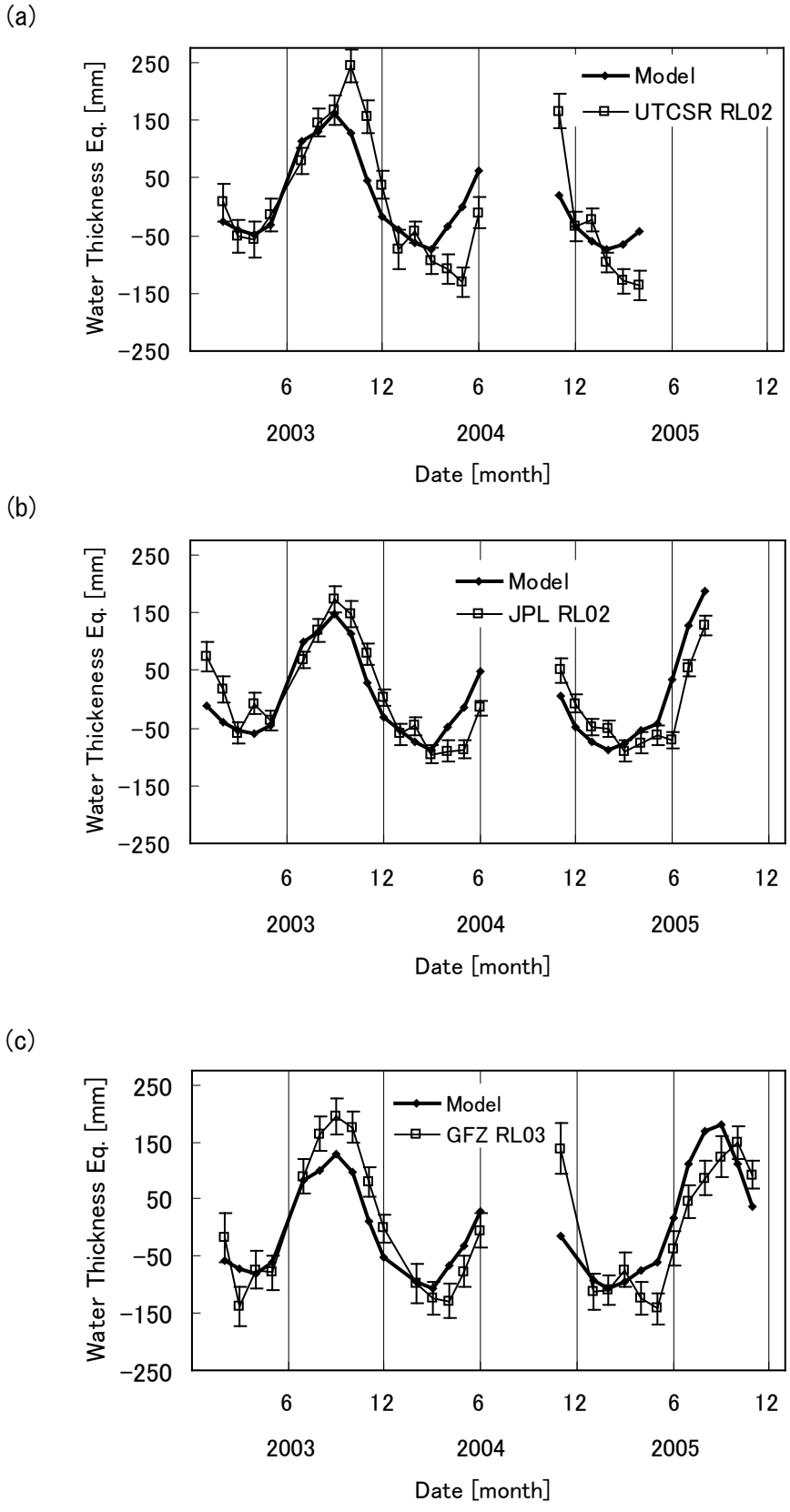

Fig. 3.9. Mass variations in the combined ara of the 4 rivers recovered by the (a)UTCSR RL02, (b) JPL RL02, and (c) GFZ RL03 data sets. The estimated variations by the model are also shown in the figures.

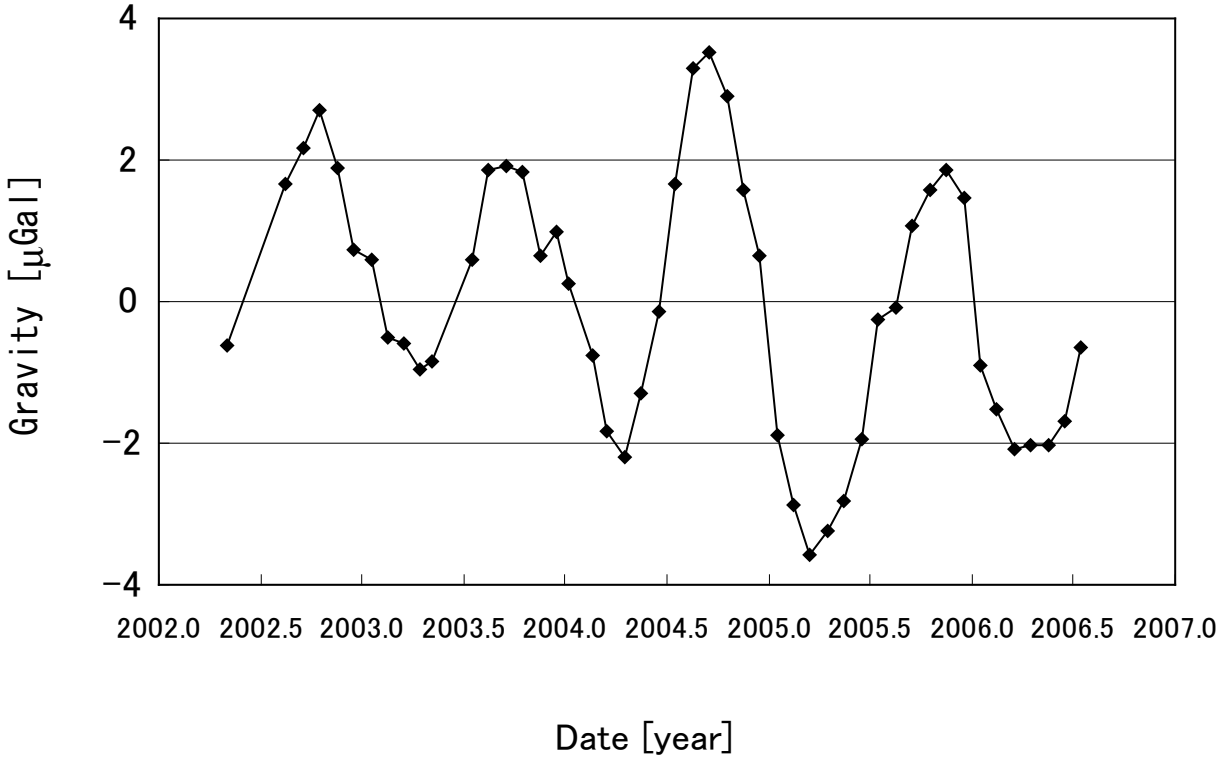

Fig. 3.10. Terrestrial gravity variations in Bangkok derived from 1000 km filtered GRACE monthly gravity solutions (UTCSR RL01).

4. Antarctic Ice Sheet Mass Variation

4.1. Introduction

Using the regional mass recovery method confirmed in Ch. 3, the regional and continental scale interannual ice sheet mass change in Antarctica is discussed in this chapter. To study the interannual ice sheet mass changes in Antarctica and Greenland are important for the studies of global climate change because these ice sheets holds 33 million of ice, which equivalent to raise sea level by almost 70 m. Thus even if changes of these ice sheet masses are small, it gives a significant effect on the global water mass balance and the sea level change (Church *et al*., 2001).

Conventionally, ice sheet mass balance have been estimated by the mass budget method, which calculate the net accumulations minus losses in each small regions or measuring the elevation change over the time period with satellite and/or air-borne altimetry. However, the mass balance method is difficult to determine the large scale ice sheet mass balance because of the large uncertainties of the estimation of the accumulations and losses, while the reliable results can be derived for small regions by combining GPS and InSAR data. On the other hand, the altimetry method gives elevation change over the large area, but need to consider the compaction effect, which needs to convert elevation to mass. Further, the elevation change is difficult to estimate on large topographic undulation area.

The Greenland ice sheet is easy to access and the ice sheet area is small compared to the Antarctic ice sheet. Thus, for the Greenland ice sheet, many of ground observations have been performed. The understanding of the mass balance has been further advanced since 1990's by technical advances in remote sensing (laser and radar altimetry, InSAR and GPS) (Rignot and Thomas, 2002).

On the other hand, although the Antarctic ice sheet is the largest water reservoir, which holds about 90 % of the fresh water on the Earth, it has not been investigated well, yet. Compared with the Greenland ice sheet, the Antarctic ice sheet is far larger and therefore it is difficult to cover over the continental area by ground observations. Further, most of remote sensing satellites do not cover the whole area of Antarctica up to high latitude. Thus the accurate estimation of ice sheet mass balance have been limited in some regions in West Antarctica, where ground observations are concentrated, and low latitude and small slope regions, where satellite altimetry data is available with reliable precision.

Since the GRACE launch, another method to estimate ice sheet mass balance, i.e. monitoring the mass variation of the ice sheet mass with the gravity measurement, has been available. One of the advantages to use the GRACE data for the study of ice sheet mass balance is to know the relatively large scale (e.g. continental scale) mass variation directly, which is difficult to determine by far. Large scale mass balance information is directly useful to estimate the contribution for global scale sea level change. Because the GRACE satellite covers high latitude area due to the near-polar orbit,

the data is available for Antarctic area. Thus, the continental or sub-continental scale interannual ice sheet mass variation was estimated with the GRACE data not only for Greenland (Velicogna and Wahr, 2005; Chen *et al*., 2006a; Velicogna and Wahr, 2006b), but also for Antarctica (Velicogna and Wahr, 2006a).

However, there is a problem to determine ice sheet mass variation by the GRACE data. Because the observed mass variation by GRACE is the radial integration on and beneath the Earth, the source of the mass variation cannot be distinguished by GRACE data only. To derive the ice sheet mass component, other sources of mass change should be estimated and removed from the GRACE estimation. For example, it is well known that the post glacial rebound (PGR) also causes large mass trend besides of the ice sheet variation. In Greenland, other satellite or ground observed data is helpful to determine ice sheet mass components but such data is limited in Antarctica. Therefore, to derive the interannual ice sheet mass trend in Antarctica, Velicogna and Wahr (2006a) used the latest PGR model IJ05 (Ivins and James, 2005) and ICE5G (Peltier, 2004) for the estimation of total PGR mass trend in the test area (East, West and the whole area of Antarctica) , and subtracted it from the GRACE estimation. However, the uncertainty of the PGR model is very large even in such the latest model and the difference between the several PGR models is also large. If the PGR model is inaccurate, such simple subtraction of the PGR model trends from GRACE trend may give large errors to the ice sheet estimation.

To avoid the estimation error caused by the mismodeling of PGR, and to derive more reliable ice sheet mass trend, the comparison of the spatial patterns and the signal magnitudes of the regional mass trend of the GRACE data with the ones determined by other methods or models is very important in Antarctica as well as in Greenland. Thus, in this chapter, the sources of the regional GRACE interannual mass trends in Antarctica are discussed. As a precedential work, Chen *et al*. (2006b) investigated the spatial distribution of Antarctic mass trend derived after subtracting IJ05 PGR model and determined the rate of the two prominent mass trends of West and East Antarctica. They compared the results with the recent surface mass balance estimations of Antarctica based on satellite altimetry, InSAR and GPS data. However, they did not discuss the sources of each trend in detail. In this study, after the discussion of regional mass trends in Antarctica, how the estimation of the trend of the continental scale ice sheet mass variation changes as a result with the change of the regional one is also discussed.

4.2. Data sets

4.2.1. GRACE monthly gravity field solutions

For the purpose of estimation of the interannual mass trend, to use long time period data sets is preferable. Although several versions of the GRACE monthly solutions are released, the data sets released throughout long time period are limited. In this study, UTCSR RL01, JPL RL02 and GFZ

RL03 are used. Table 4.1 summarizes the data sets used in the estimation.

Table 4.1. Time spans of GRACE Level 2 (near) monthly gravity field solutions used in this chapter.

Year	Jan	Feb	Mar	Apr	May	Jun	Jul	Aug	Sep	Oct	Nov	Dec
2002				○				○	○	○	○	○
2003	○	○	○	○	○		○	○	○	○	○	○
	●	●	●	●	●		●	●	●	●	●	●
		◎	◎	◎	◎		◎	◎	◎	◎	◎	◎
2004	○	○	○	○	○	○	○	○	○	○	○	○
	●	●	●	●	●	●					●	●
		◎	◎	◎	◎	◎	◎	◎	◎	◎	◎	◎
2005	○	○	○	○	○	○	○	○	○	○	○	○
	●	●	●	●	●	●	●	●	●	●	●	
	◎	◎	◎	◎	◎	◎	◎	◎	◎	◎	◎	
2006	○	○	○	○	○							
	◎	◎	◎	◎	◎							

○: UTCSR RL01, ●: JPL RL02, ◎: GFZ RL03

For the JPL RL02 and GFZ RL03, the GAB solutions (the monthly average of the oceanic variability time series used for de-aliasing) are added on the basis of the guidline for the trend estimation of these data sets (Bettadpur *et al*., 2006). For GFZ RL03 solutions, GK2 solutions (constrained solutions) are available from August to November in 2004, when the data corruption by orbit decay (see Sec. 2.3.4) was occurred, and the solutions are used. The C_{20} components were replaced to Satellite Laser Ranging (SLR) solutions (Cheng and Ries, 2006). The data sets are truncated at degree and order 70 in this study because the use of the coefficients after degree/order 70 shows the increase of the noise and no significant improvement of the signal. The average of all data solutions was subtracted from each of data set to derive the variable components over the period.

The discussion is mainly performed using the UTCSR RL01's result because of the longest time period and no slope problem caused by ocean de-aliasing model (see Sec. 2.3.3), though the results of the other data sets also discussed for the comparison.

4.2.2. ICESat data

Ice Cloud and land Elevation Satellite (ICESat) (Zwally *et al*., 2002) launched in 2003 is laser altimetry satellite and gives us the information of elevation change. The observed area covers Antarctic area. GLAS/ICESat L2 Antarctic and Greenland Ice Sheet Altimetry Data (GLA12) Release 26 are now available in the several time periods of 2003 to 2005 (Zwally *et al*., 2006). Although the 4 time period data sets are now available, the Release 26 version of the two data sets of the same season and on the same repeat orbit are used in this study; October 1st to November 18th in 2003 and October 21st to November 23rd in 2005, for the purpose of minimizing the estimation error of topographic undulation and the effect of seasonal change. The instrument corrections, atmospheric delays and tides have been applied for the released data. For each time period, the elevation with respect to DEM was averaged by 30'' x 30" grid. The trend of the elevation change was calculated from the difference between the 2 time period grid data.

4.2.3. JARE snow accumulation data along the traverse route

Snow accumulation along the routes of inland traverses has been observed for more than 30 years by Japan Antarctic Research Expedition (JARE) with snow stakes. Snow stakes are placed along the traverse routes on the ice sheet at intervals of 0.5 to 5 km. Surface mass balance is obtained by multiplying the elevation change of the snow by snow density of each observed point (Motoyama, personal communication). The snow density along the traverse route has also been measured by JARE for a long time though it is not measured so frequently as snow stake measurement. The density used for the conversion to the mass is empirically estimated value on the basis of the observations. The data of 1993 to 2001 and 2003 to 2005, which are before and overlapping the GRACE mission period was used in this study.

4.2.4. Model data

The model data sets of PGR and landwater were also used for the comparison. As the PGR models, the 7 ice models (ARC3+ANT4, ARC3+ANT3, ICE-3G, ARC3+HB, ARC3+D91, ARC3+ANT5 and ARC3+ANT6) in Nakada *et al*. (2000) were used. They calculated the rate of change of the surface gravities (dg/dt) and the vertical crustal velocities (dh/dt) on the solid surface for these ice models. Gravity change at the surface depends both on the vertical change of the distance from the center of mass of the Earth and the change of the density distribution. On the other hand, GRACE can detect only the latter. Therefore, for the comparison with GRACE result, I assumed the free-air gradient to the vertical change of the distance and calculated the rates of the change of surface mass density (dσ/dt) by the following equation:

$$2\pi G d\sigma / dt + \beta dh / dt = dg / dt \quad , (4.1)$$

where G is gravitational constant and β = –0.3086 [μGal/mm] is free-air gradient. The original estimation of dg/dt, dh/dt and the obtained dσ/dt are shown in Figure 4.1.

As a snow (landwater) model, the combined model of the Japan Meteorological Agency SiB and GRiveT models used in Ch. 3 was used again. This model contains Antarctica. However, note that the model does not include the runoff (and the basal discharge) in Antarctic region. Nevertheless it is still useful because it is independent to ICESat results and gives the prediction of the landwater mass variation overlapping GRACE mission after ERA 40 (ECMWF 40 years Reanalysis, 1957 - 2002) and because most of landwater models (e.g. GLDAS, Rodell *et al*., 2004, or LaD, Milly and Shmakin, 2002) are not include Antarctic area. The degree 0 and 1 components were removed from the model for the consistency with the GRACE data.

In Fig. 4.2, the spatial patterns of the interannual mass trends of the landwater model and the ICESat data are compared. Both of the figures are mainly represents the snow accumulation, but the data are mutually independent. Nevertheless, one of the interesting things is that these data look relatively similar for the spatial pattern of the location of the negative and positive interannual trend. On the other hand, for the amplitude of each trend, the difference is large. In principle, the ICESat result is probably provides more reliable information because it is the observed value. However, the ICESat result does not cover the Antarctica uniformly and does not show sufficiently available pattern over Filchner-Ronne Ice Shelf and Pine Glacier area (the locations are shown in Fig. 4.3 (d)) discussed in this study. Therefore, the landwater model was also used in these areas as supplemental information.

4.3. Regional mass trend

4.3.1. Estimation of regional GRACE mass trend in Antarctica

To estimate the spatial distribution of the interannual mass trend in Antarctica roughly, the globally normalized Gaussian filter (Wahr *et al*., 1998) was firstly applied to the GRACE data sets. Fig. 4.3 shows the 600 km Gaussian filtered interannual mass trend after fitting and removing annual and constant components. Although some differences are observed between the 3 data sets, the following 3 trends are prominent and also shown commonly: 1) the northwest positive trend around Filchner-Ronne Ice Shelves (FRIS), 2) the southwest negative trend around Pine Island Glacier (PIG), and 3) the northeast positive trend around Enderby Land (EL).

For these 3 areas, the regional Gaussian filter (Swenson *et al*., 2003) used in Ch. 3 was applied to discuss each trend more detail. This filter cannot estimate the spatial pattern of the mass variation like the global Gaussian filter of Wahr *et al*. (1998), but can obtain the signal amplitude in the test area more strictly by estimating and correcting the signal degradation and the leakage effect caused by filtering. As the correlation length of the filter, the value of 600 km was adopted. The estimated region is shown in Fig. 4.3 (d). The signal degradation by the filtering was corrected by multiplying

the scaling factor following Veliconga *et al*. (2005). The detail of the method of the mass recovery was stated and discussed in Sec. 3 and is not stated here again. In the following sections, the mass variations in each trend area are discussed, respectively.

4.3.2. Filchner-Ronne Ice Shelves

Fig. 4.4 shows the recovered mass variation over the FRIS by UTCSR RL01. The estimated mass trend is shown in Table 4.2 with the ones by JPL RL02 and GFZ RL03. The estimated mass trend in this area by UTCSR RL01 are above 100 mm/yr in equivalent water thickness, and about 25 and 20 % smaller estimations are derived by JPL RL02 and, GFZ RL03, respectively.

Table 4.2. Estimated interannual mass trend over Filchner-Ronne Ice Shelves by GRACE monthly gravity solutions.

Data Sets	Interannual Mass Trend
UTCSR RL01	110.5
JPL RL02	76.1
GFZ RL03	80.2

(Unit is mm/yr in equivalent water thickness)

I attempted to express the mass trend in this area by assuming that it is from the sum of the following 6 sources, as shown in Fig. 4.5: 1) aliasing error of ocean tide model, 2) uplift by PGR, 3) precipitation and evapotranspiration, 4) inflow from the neighboring glaciers, 5) outflow from the ice sheet front and 6) inflow and outflow from the base of ice shelf.

The large periodic signal in Fig. 4.4 is caused by the aliasing of the ocean tide in this area because CSR4.0 ocean tide model used in UTCSR RL01 for de-aliasing is not estimated the ocean tide of this area. The effect on the GRACE mass trend was investigated by simulating the GRACE along orbit observation of the tide in this area. As a 'true' tide, circum Antarctic regional tide model CADA00.10 (Padman *et al*., 2002), which shows best correspondence with in situ observed data (King and Padman, 2005) was used. As a result of simulation, the effect on the interannual mass trend is small (only -2.2 mm/yr) for the time span of UTCSR RL01 data used in this study though it gives serious effect for the seasonal mass variation as shown in Fig. 4.6. In JPL RL02 and GFZ RL03, new ocean tide model FES2004, which includes the model over the FRIS area, is used and the de-aliasing error is relatively smaller than in UTCSR RL01 and considered to safe to be neglected.

The predicted PGR uplifts are shown in Table 4.3. In this area, relatively large PGR trend is predicted. However, even after removing PGR effect using the ICE-3G model, which gives maximum uplift, the positive trend still remains. In Chen *et al*. (2006b), the surface mass trend in this area were not discussed because in their estimation, the mass trend around here is deleted by

subtracting PGR uplift. In my estimation, the PGR uplift is insufficient to explain the total uplift.

Table 4.3. Predicted interannual mass trend caused by PGR over Filchner-Ronne Ice Shelves.

Ice Model	Interannual Mass Trend
ICE-3G	42.0
ARC3+HB	38.6
ARC3+D91	37.8
ARC3+ANT3	34.6
ARC3+ANT4	29.8
ARC3+ANT5	17.3
ARC3+ANT6	13.1

(Unit is mm/yr in equivalent water thickness)

The residual mass trend should be expressed by surface mass balance (Table 4.4). The estimated values are from 34.1 to 94.5 mm/yr. The difference is caused by the different estimations of the GRACE solutions and ice models are used for the estimation.

Table 4.4. Estimated interannual surface mass trend over Filchner-Ronne Ice Shelves

GRACE Data Sets	Interannual Mass Trend
UTCSR RL01	65.6 to 94.5
JPL RL02	34.1 to 63.0
GFZ RL03	38.2 to 67.1

(Unit is mm/yr in equivalent water thickness)

The approximate inflow from the neighboring glaciers is estimated to 442 mm/yr with flux gate-mass balance method combined new 1 km DEM (Joughin and Bamber, 2005). The outflow from the ice sheet front was estimated to -502 mm/yr by Joughin and Padman (2003). I could not find the estimation of inflow and outflow from the base of the ice shelf because these values are difficult to observe directly and therefore estimated by assuming the total inflow and outflow are balanced on the ice sheet, by far. However, the assumption of the balance may not necessarily true in the short time span. The total sum of the surface mass balance derived from the values of previous works (without the basal inflow and outflow) becomes -27.4 mm/yr. It looks very different with the surface mass estimation by GRACE data (Table 4.4). However, note that the previous estimations of the inflow from the neighboring glaciers and the outflow from the ice sheet front are order of 1 larger than the other estimations and the value using these results probably contains large error. Compared with such previous results, the result of GRACE is meaningful because it gives the order

of 1 precise constraint.

I think that the main contributor of the obtained surface mass trend is probably snow because the spatial pattern of the GRACE mass trend around Antarctic Peninsula to FRIS is similar with the one of the ICESat result, which cannot use only partially, and the landwater model. The estimation of the snow accumulation by the landwater model is 36.6 mm/yr, but the amplitude model is not so reliable, as discussed in Sec. 4.3.4. Although the pattern also looks like the some PGR uplift model, the magnitude of the trend is subtracted in Table 4.4.

4.3.3. Pine Glacier

In this area, large negative mass trend is observed by GRACE (Fig. 4.7 and Table 4.5), and it is agreeable with Chen *et al*. (2006b).The predicted PGR uplift is 20 mm/yr at maximum (Table 4.6) and the estimated surface mass trend after removing the effect of PGR uplift is -172.4 to -104.9 mm/yr (Table 4.7). Large negative trend is also reported by Davis *et al*., 2005, in which the result of the radar altimetry data of European Remote-Sensing Satellite-1 (ERS-1) and ERS-2 from 1992 to the beginning of 2003 are shown. When the observed elevation change by ERS-1 and ERS-2 is assumed to be caused by the basal ice melting (the ice density is ~ 900 kgm^{-3}), the rate becomes about -160 to -140 mm/yr, which is agreeable with the GRACE results. In case that the snow accumulation by the landwater model (40.8 mm/yr) is assumed, the components of melting becomes about -210 to -140 mm/yr, which implies very fast melting is occurred though the amplitude of the landwater model is again not so reliable (see Sec. 4.3.4). Actually, in PIG and other glaciers discharging directly into the Amunsen Sea, large scale melting from the glacier base is reported (e.g. Rignot and Jacobs, 2002) and it is concluded that it is the main source of the mass decrease in this area.

Table 4.5. Estimated interannual mass trend around Pine Glacier by GRACE monthly gravity solutions.

Data Sets	Interannual Mass Trend
UTCSR RL01	-151.57
JPL RL02	-106.6
GFZ RL03	-108.4

(Unit is mm/yr in equivalent water thickness)

Table 4.6. Predicted interannual mass trend caused by PGR around Pine Glacier.

Ice Model	Interannual Mass Trend
ICE-3G	14.0
ARC3+HB	10.8
ARC3+D91	20.9
ARC3+ANT3	13.6
ARC3+ANT4	11.2
ARC3+ANT5	11.9
ARC3+ANT6	3.5

(Unit is mm/yr in equivalent water thickness)

Table 4.7. Estimated interannual surface mass trend around Pine Glacier

GRACE Data Sets	Interannual Mass Trend
UTCSR RL01	-172.4 to -155.0
JPL RL02	-127.5 to -110.1
GFZ RL03	-129.3 to -104.9

(Unit is mm/yr in equivalent water thickness)

4.3.4. Enderby Land

The mass trend in Enderby Land is discussed in Yamamoto *et al*. (2006b). Chen *et al*. (2006b) pointed that the large positive interannual mass trend in this area was not consistent with the ones estimated from neither the recent surface mass balance nor the latest ice model. They suggested that unquantified snow accumulation or, more likely, unmodelled PGR would be the source of the trend, but in fact, the trend has not been well interpreted yet.

For more detail evaluation of the trend, following the boundaries given by Davis *et al*. (2005), I divided the area into 3 major basins as shown in Fig. 4.8 and estimated the mass variations (Fig. 4.9 and Table 4.8).

Table 4.8. Estimated interannual mass trend over Enderby Land by GRACE monthly gravity solutions. The division of the areas of A, B and C is shown in Fig. 4.7.

Data Sets	Interannual Mass Trend		
	Area A	Area B	Area C
UTCSR RL01	106.1	162.2	14.6
JPL RL02	54.6	87.8	-15.8
GFZ RL03	71.1	93.5	71.2

(Unit is mm/yr in equivalent water thickness)

Table 4.9. Predicted interannual mass trend caused by PGR over Enderby Land. The division of the areas of A, B and C is shown in Fig. 4.7.

Ice Model	Interannual Mass Trend		
	Area A	Area B	Area C
ICE-3G	5.59	20.4	10.7
ARC3+HB	-15.4	-5.1	1.81
ARC3+D91	5.25	15.3	5.35
ARC3+ANT3	6.63	9.69	3.34
ARC3+ANT4	3.95	4.00	3.75
ARC3+ANT5	7.78	4.26	1.72
ARC3+ANT6	3.75	3.86	2.22

(Unit is mm/yr in equivalent water thickness)

Table 4.8 shows that the large mass trends are observed in Area A and Area B, but they can not be explained by the model estimations of PGR (Table 4.9). Further, the landwater model cannot explain the trend, either. The landwater mass trend predictions are 9, 6, and 2.3 mm/yr in equivalent water thickness for area A, B and C, respectively.

Thus, I considered that the model estimation of the PGR or the landwater model (or the both) is not accurate in this area. Therefore, I firstly checked the accuracy of these models.

In Antarctica, several continuous GPS sites exist as a part of a monitoring network of the International GNSS Service (IGS) and the 2 stations, i.e. Syowa (SYOG, 69.0070S, 39.5837E) and Mawson (MAW1, 67.6048S, 62.8707E) are located in Enderby Land (Fig. 4.10 (a)). Ohzono *et al*. (2006) analysed these GPS data and shows that the vertical uplifts from 1998 to 2004 are 1.37±0.21 and 1.29±0.13 mm/yr for SYOG and MAW1, respectively (Fig. 4.10 (b)). The results correspond to the small vertical velocities (about 1 to 4 mm/yr) predicted by several ice models (Nakada *et al*., 2000). It means that the error of PGR estimation is small at least on the points of SYOG (in Area A) and MAW1 (in Area B).

On the other hand, the value of the landwater model is probably inaccurate in Antarctica compared to the one of the low or medium latitude. Besides of the unconsidering of the runoff from the surface as mentioned in Sec. 4.2.4, there is some problems on the forcing data of the model. The landwater model is forced with the global atmospheric analysis (GANAL) and the snow depth analysis (SDA). It is confirmed that the quality of these input data is almost comparable to the one of ERA40. However, in Antarctica, these data contain large errors because of the difficulty of the quality control and the output is not validated by the ground observation. Therefore, it is dangerous to discuss the amplitude of the signal from only the result of the landwater model, at present.

For the snow observation, as previously described, there are in-situ snow-stakes measurements along JARE traverse route in Area A. Fig. 4.11 (a) shows the mass trend estimated from the snow-stake data for the period from 2003 to 2005, and the same trend for the different periods. The spatial variations of the trend for the period of 2003-2005 are also shown in Fig. 4.11 (b). Note that the trend values are the averages for every 0.5° along latitude and the snow densities employed for the height to mass conversion are also plotted in Fig. 4.11 (a).

Fig. 4.11 (a) shows that the mass trend increases toward the coastal area and this tendency is quite similar at least for last 10 years. This is consistent with the GRACE mass trend in Fig. 4.9. For the interannual mass trend and the spatial distribution along this JARE traverse route have been studied in detail by many researchers. The surface mass trend before year 1993 also shows the similar spatial pattern (National Institute of Polar Research, 1997). Basically, the snow accumulation near the coastal area was larger than the inland area mainly due to the water vapor from the ocean (Furukawa *et al*., 1996). The coastal area is called accumulation zone. The surface mass trend is positive every year though the amplitude shows relatively large variation because of the high sensitivity for the climate. The surface mass around 70S is very small. It is caused by katabatic wind. On the slope of the ice sheet in Antarctica, katabatic winds are formed by the gravitational force of cold air massed, and generate drifting snow throughout the year. Thus in the strong katabatic-wind zone, the accumulation is small. In inland zone, the yearly variation of the snow accumulation is small and as a result, the rate of the surface mass increase is almost constant. It is considered that such difference of the spatial pattern mainly depends on the distance from the coastline and the topography (elevation and undulation). In Area A, the distance from the coast and the topography change roughly correspond to the change of latitude. Thus I assumed that the longitudinal distribution of the route is almost similar as the route over Area A. Although the trend values measured by the snow stakes vary from 50 mm/yr to 200 mm/yr, under the assumption, the average over the traverse route, which almost covers Area A in latitude, becomes 78.6 mm/yr. This value shows a good agreement with the GRACE trend in Area A (see Table 4.8).

Fig. 4.11 (c) shows the mass trend estimated from ICESat data. For the conversion from height to mass changes, the average snow density of 377 kgm^{-3} along the JARE traverse routes (Nishio, 1978) was used. The mass trends derived from the snow stake measurements (Fig. 4.11 (b)) are also superimposed on Fig. 4.11 (c). They show similar spatial pattern as the ICESat data. The average mass trends in Area A, Area B and Area C are 33 mm/yr, 36 mm/yr and 26 mm/yr, respectively. The values in Area A and Area B are smaller than the trend estimated from the snow stake measurements. This is mainly due to the sparse satellite ground tracks near the coast area and the difficulty of the estimation of topographic large undulation area with ICESat. Hence, if the data coverage is successfully taken into account, the mass trend is probably consistent with the GRACE trend. In Area C, on the other hand, ICESat gave a larger mass trend than the GRACE trend. Besides of the

same reasons mentioned above, another considerable reason of the reasons may be the snow density employed for the conversion. We employed the average value over JARE traverse routes, but it may be slightly large for the inland area. I think there is a place for improvement in the ICESat data processing, but it is very difficult at present. This is for future work.

On the other hand, as Chen *et al*. (2006b) pointed out, Rignot and Thomas (2002) reported that the surface mass estimated by satellite altimetry, InSAR and GPS data in this area is almost balanced, which is not consistent with GRACE results. Davis *et al*. (2005) estimated the Antarctic surface elevation change of 1992 to the beginning of 2003 from the radar altimetry data of European Remote-Sensing Satellite-1 (ERS-1) and ERS-2. Although the result shows the positive trend of about 40 to 80 mm/yr in the area B, the mass trend derived by multiplying the density of firn (~350 kg/m^3) becomes very small (14 to 27 mm/yr) and does not agree with the GRACE trend, either.

One of the most likely possibility is that the estimation error of these works. In conventional mass balance method, the outflow is usually measured in the small area. The coastal results in Davis *et al*. (2005) probably have large uncertainties compared to the inland area because of the difficulty of the detection of the coastal elevation change by the altimetry.

Another considerable reason is that the difference of mass balance estimation method. Rignot and Thomas (2002) estimated the outflow by the ice thickness deduced from hydrostatic equilibrium which is calculated from the surface elevation near the grounding line and a conversion factor taking account of different seawater and ice densities. On the other hand, GRACE mass balance is estimated in the defined drainage divisions. If the outflow estimation of the conventional method is estimated outside the division, it is not detect by such method. The situation is quite different in PIG and other glaciers discharging to the Amunsen Sea, where large spatial scale basal ice melting is occurred not only across the coastline but beneath the drainage area estimated with GRACE data.

One of the methods to confirm whether the GRACE mass trend is mainly comes from surface mass increase or PGR trend is to investigate the yearly change of the GRACE trend. If the mass trend is mainly caused by PGR uplift, the rate of mass trend is constant. As shown in Fig. 4.12, the yearly change of the snow-stick mass trend shows that the rate of 2004 trend is larger than that of 2003, and the 2004 trend is further larger than that of 2004. Around the Syowa station (located in area A), the large scale ice sheet melting caused by high temperature is observed from the last of 2003 to the beginning of 2004 (Yamagishi, 2006). The increase of the snow accumulation in 2005 is probably caused by the increase of the precipitable water. Our GRACE estimation also shows the large mass trend in 2005 (Fig. 4.9 (a)) and it looks relatively agreeable with the snow-stake data (Fig. 4.12).

Thus I conclude that the most part of the GRACE mass trend in this area can be explained by snow accumulation though it does not mean that I exclude the possibility that the trend of PGR is superposed to the surface mass trend. Because the PGR models have relatively poor constraints in

this area, the discussion is difficult at present.

4.4 Continental scale mass trend

Fig. 4.13 shows the GRACE mass variation in East, West, and the whole area of Antarctica. Because these GRACE mass trends are regarded as the sum of the surface mass balance and the PGR uplift, the PGR effect should be subtracted to derive the surface ice sheet mass variation. As summarized in Table 4.10, the mass trends derived from GRACE data are almost zero, in all of the 3 area estimations. On the other hand, the magnitudes of the model estimations of PGR uplift are relatively different from each other as shown in Table 4.11; some (e.g. ICE-3G) are about one order larger than GRACE estimations, but others (e.g. ARC3+ANT6) are comparable level. In Table 4.11, the PGR estimation using the latest ice model IJ05 is also shown. The model is not publicly released, but the prediction of East, West and the whole area of Antarctica is estimated by Velicogna (2005). Thus, the quantitative estimation of ice sheet mass variation is largely depends on the PGR model used as shown in Table 4.12. Because the PGR estimation has a large uncertainty, it is difficult which estimation is best at present.

Table 4.10. Estimated interannual mass trend over East, West and the whole area of Antarctica by GRACE monthly gravity solutions.

Data Sets	Interannual Mass Trend		
	East	West	Total
UTCSR RL01	2.67	3.82	2.03
JPL RL02	-3.38	1.14	-1.76
GFZ RL03	2.28	4.38	1.99

(Unit is mm/yr in equivalent water thickness)

Table 4.11. Predicted interannual mass trend caused by PGR over East, West and the whole area of Antarctica. The estimation for IJ05 is based on Velicogna (2005).

Ice Model	Interannual Mass Trend		
	East	West	Total
ICE-3G	9.06	34.1	15.7
ARC3+HB	0.308	20.2	5.48
ARC3+D91	6.90	25.6	11.9
ARC3+ANT3	7.09	21.6	10.9
ARC3+ANT4	6.34	18.1	9.37
ARC3+ANT5	5.29	10.5	6.62
ARC3+ANT6	1.66	5.4	2.71
IJ05	19.0	41.0	23.5

(Unit is mm/yr in equivalent water thickness)

Table 4.12. Estimated interannual surface mass trend over East, West and the whole area of Antarctica.

Data Sets	Interannual Mass Trend		
	East	West	Total
UTCSR RL01	-16.3 to 1.01	-37.1 to -1.58	-21.5 to -0.68
JPL RL02	-22.4 to -5.04	-39.9 to -4.26	-25.3 to -4.47
GFZ RL03	-16.7 to 0.62	-36.6 to -1.02	-21.5 to -0.72

(Unit is mm/yr in equivalent water thickness)

Table 4.13 shows the comparison the surface mass trend estimation in this study used IJ05 model with the previous studies of Antarctic ice sheet mass variation. In the previous works, they commonly used the latest ice model, IJ05. Thus, the values in Table 4.7 are derived by nearly the same estimation of PGR model. My estimation shows some difference with the other estimations. The estimation error caused from the data span used for the estimation. The difference between this study and Ramillien *et al*. (2006) or Chen *et al*. (2006b) is probably caused by the difference of the estimation method. On the other hand, the method of Velicogna (2006) is almost the same as this study. One of the possibilities for the reason of the difference is the difference of the definition of the border of the West and East Antarctica. Another considerable reason is the difference of the treatment of the leakage error. In Velicogna, the effect of the ocean leakage is estimated and removed, but the leakage over the Antarctica is not estimated. In this study, the effect of the leakage over the Antarctic continent is also estimated and removed as well as the one over the ocean. In fact, the result of the whole area of Antarctica is relatively similar.

Table 4.13. Comparison the surface mass trend estimation in this study with the previous studies over East, West and the whole area of Antarctica. The IJ05 ice model is commonly used for PGR estimation.

	Interannual Mass Trend		
	East	West	Total
This study (UTCSR RL01)	-16.3	-37.1	-21.5
This study (JPL RL02)	-22.4	-39.9	-25.3
This study (GFZ RL03)	-16.7	-36.6	-21.5
Velicogna and Wahr (2006a)	0	-68.6	-19.6
Ramillien *et al*. (2006)	11.3	-49.6	-5.17
Chen *et al*. (2006b)	13.5	-45.9	-2.45

(Unit is mm/yr in equivalent water thickness)

4.5 Conclusion

Regional and continental scale interannual ice sheet mass trend is investigated in this chapter. The reasional mass trend over FRIS is explained using the PGR and the landwater model. The negative trend around PIG is caused from large scale basal ice melting beneath the region. The main part of the positive mass trend in Enderby Land can be explained by snow accumulation data observed on ground though the possibility that the trend of PGR is superposed to the surface mass trend cannot be excluded because of the poor constraints in this area. The continental scale ice sheet mass decreases, but for the quantitative discussion, to estimate the PGR trend precisely is very important. Besides of waiting the development of more precise PGR models, to use GRACE results for the PGR estimation is another approach.

In principle, the PGR trend is derived by subtracting the ICESat mass trend from the GRACE trend of the same time period because the elevation change of PGR is only the order of mm and safe to be neglected. However, at present, the released time period of ICESat is limited and the difference between the 3 versions of GRACE data is relatively large. Further, the estimation of the ice sheet elevation change in the topographic undulation area is difficult in ICESat data processing. Therefore, in this study, I did not estimate the PGR trend by the approach. However, near future, it will be enable by using the longer time period data of both the GRACE and ICESat data, decrease of the uncertainties of GRACE data and the improvement of the method.

(a)

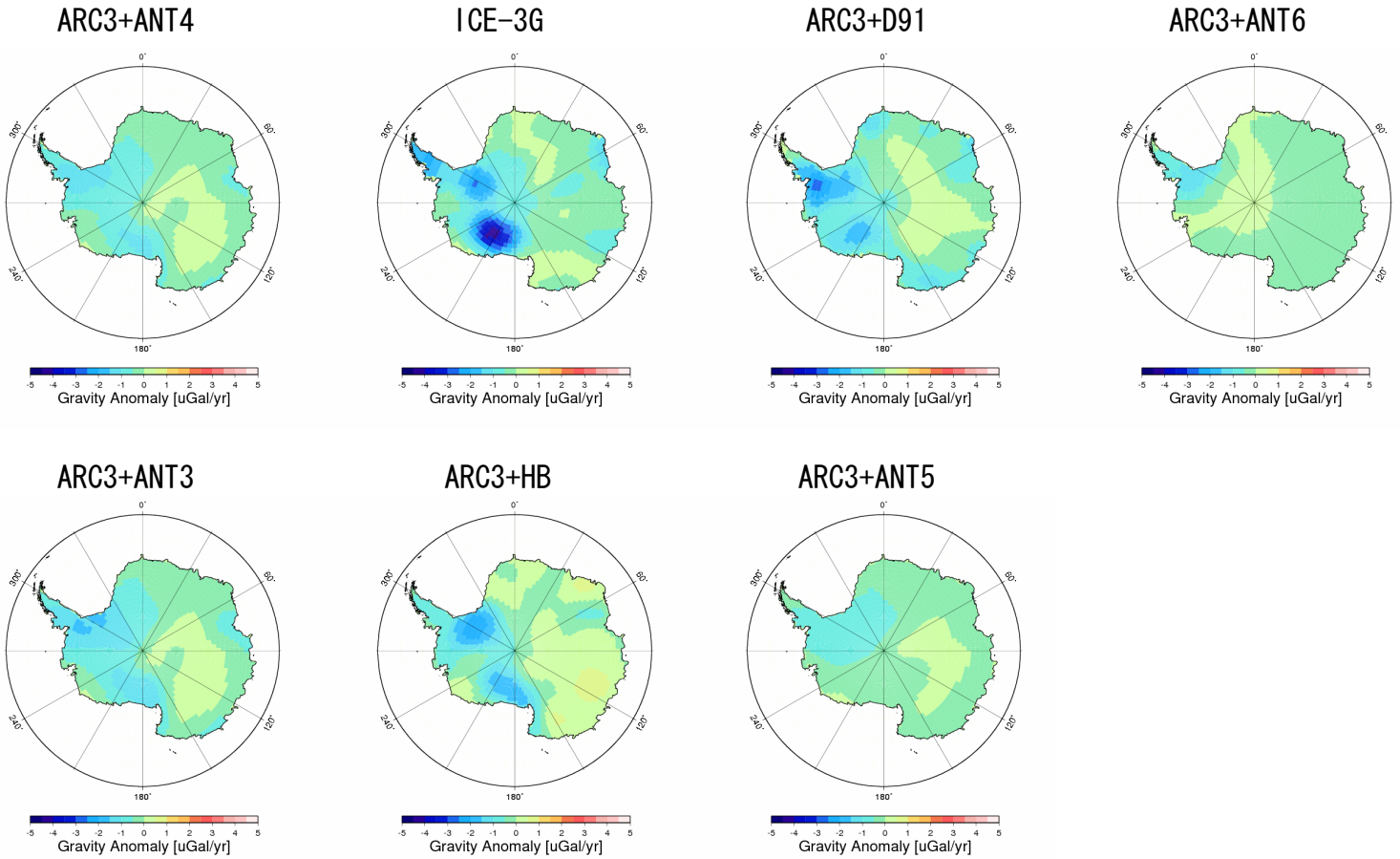
ARC3+ANT4
ICE-3G
ARC3+D91
ARC3+ANT6
ARC3+ANT3
ARC3+HB
ARC3+ANT5
Gravity Anomaly [uGal/yr]

(b)

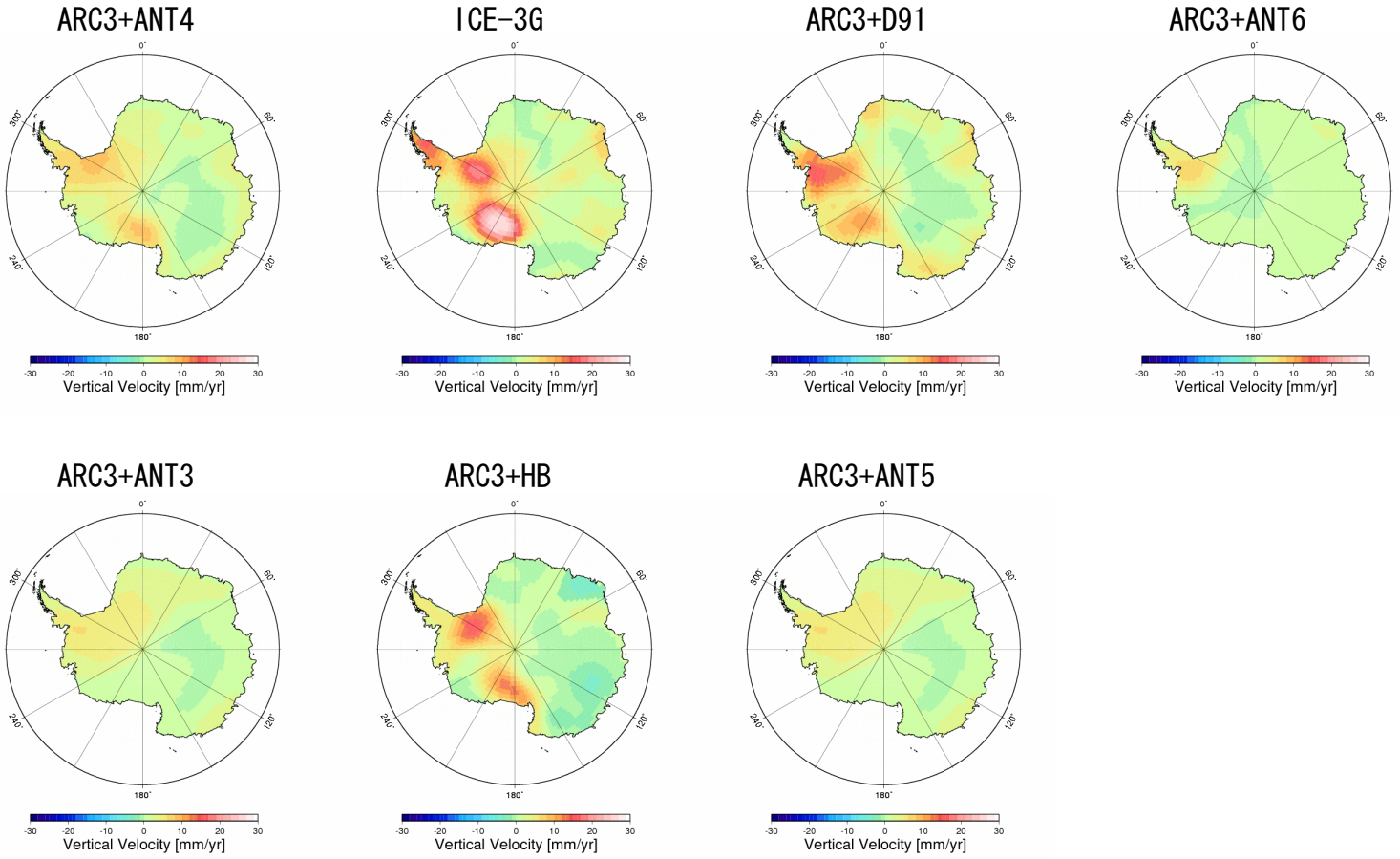
ARC3+ANT4
ICE-3G
ARC3+D91
ARC3+ANT6
ARC3+ANT3
ARC3+HB
ARC3+ANT5
Vertical Velocity [mm/yr]

(c)

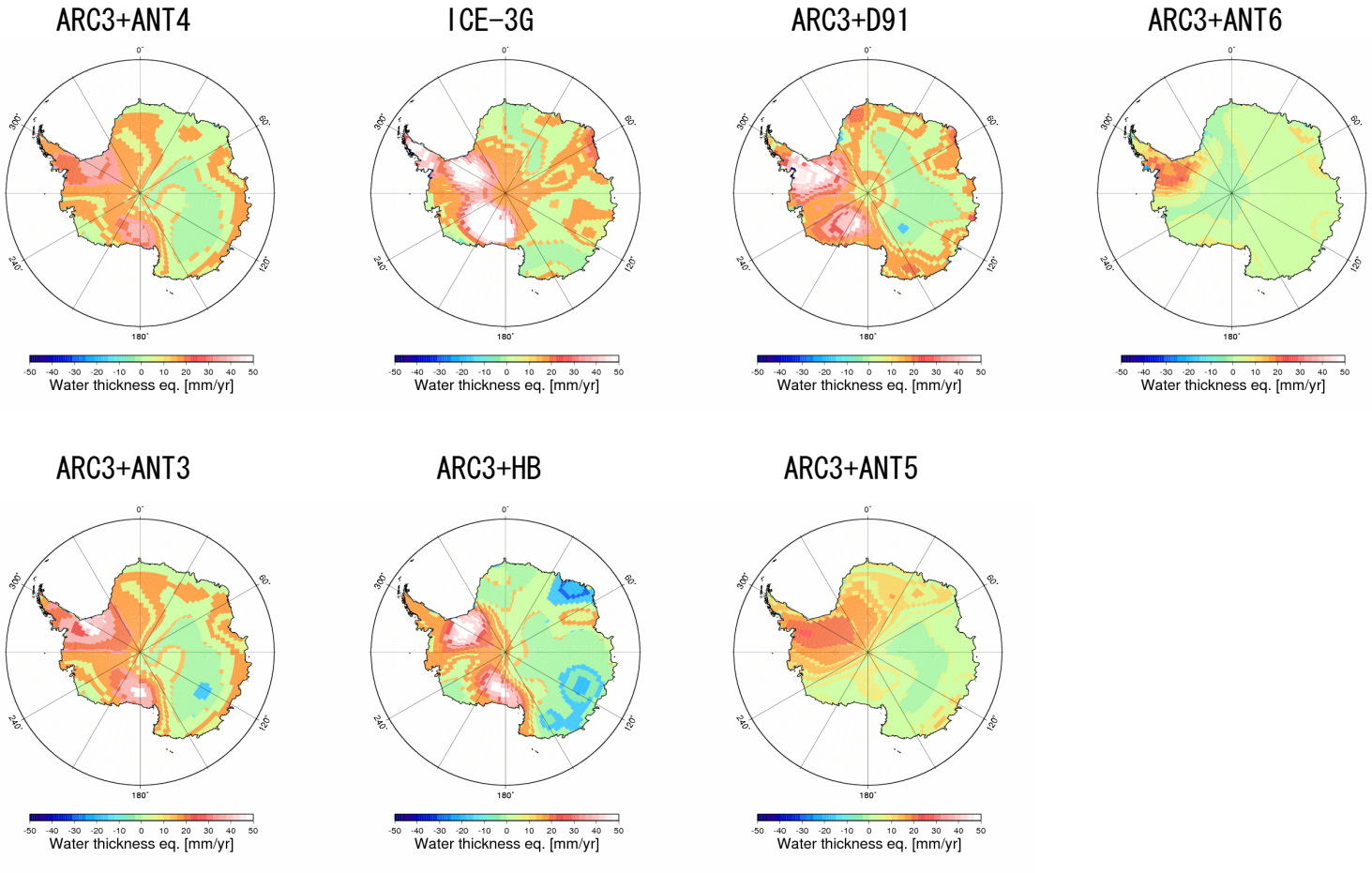

Fig. 4.1. The rates of change of the surface gravities (a), the vertical crustal velocities (b) predicted by ice models (Nakada et al., 2000). (c) is the rates of change of the surface mass density calculated from (a) and (b). More details are stated in Sec. 4.2.4.

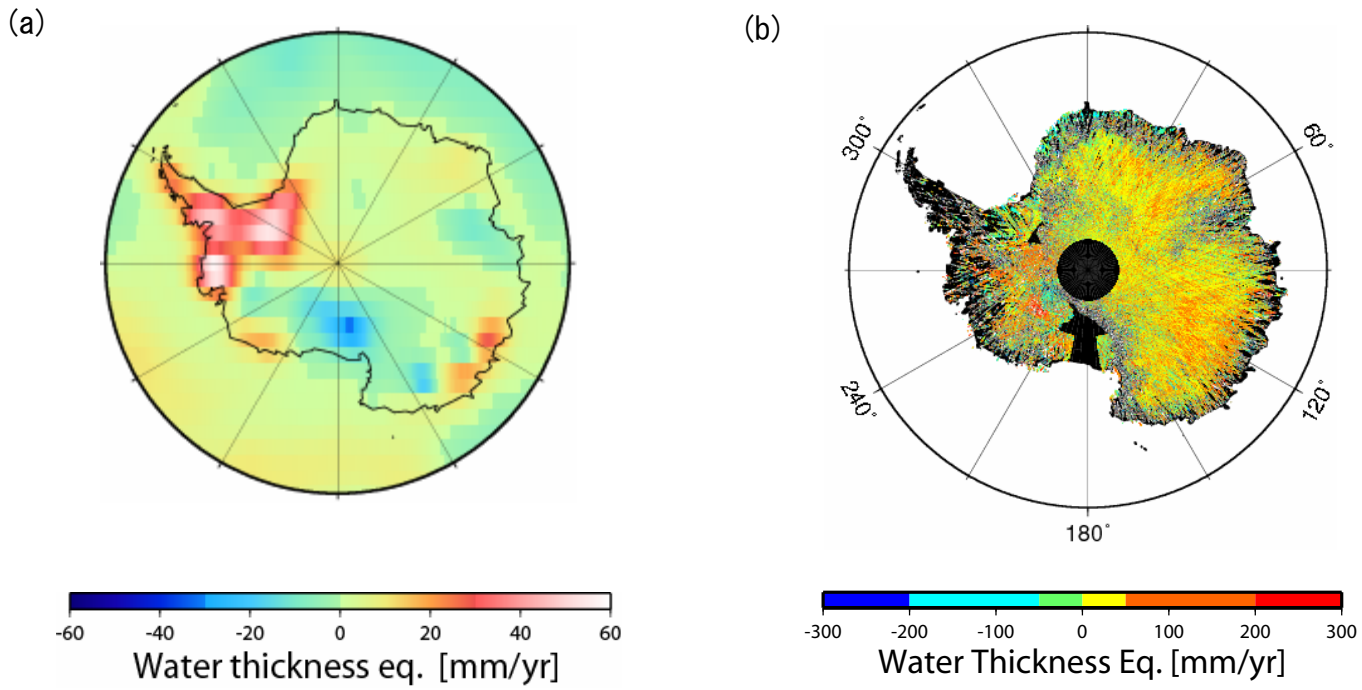

Fig. 4.2. Spatial patterns of the interannual mass trend obtained by the landwater model (a) and ICESat data (b). ICESat elevation change is converted to the mass trend by multiplying the density of firn (350 kgm-3).

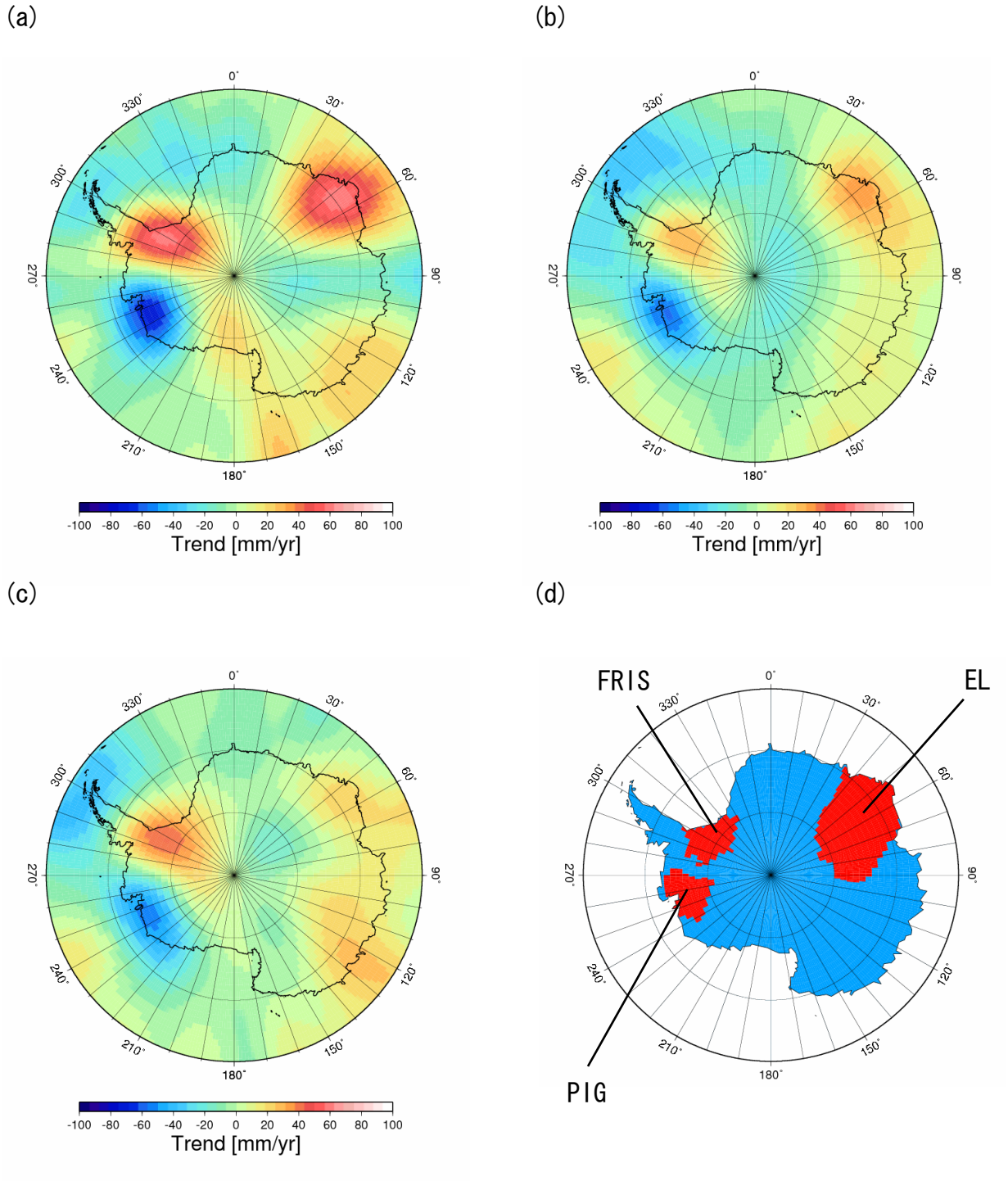

Fig. 4.3. The interannual mass trend in Antarctica estimated by the 600 km filtered UTCSR RL01 (a), JPL RL02 (b) and GFZ RL03 (c) GRACE data. (d) Locations of FRIS, PIG and EL discussed in Sec. 4.3.

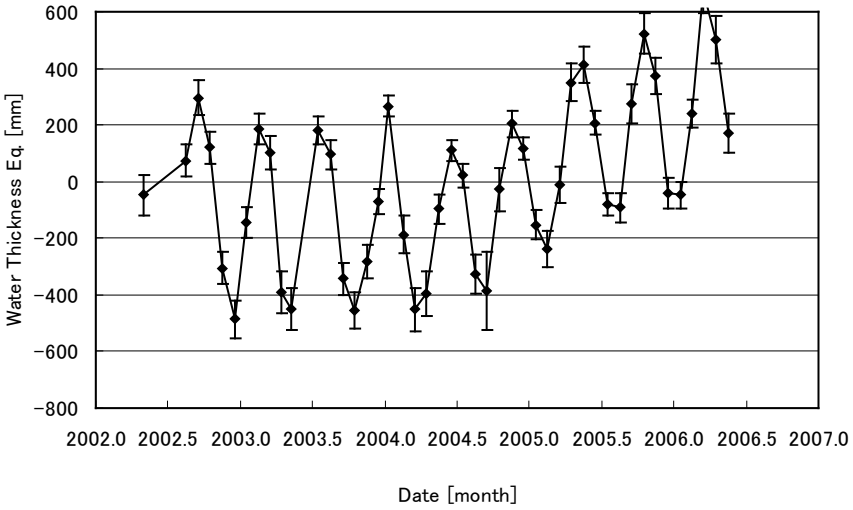

Fig. 4.4. Recovered mass variation over the FRIS by UTCSR RL01.

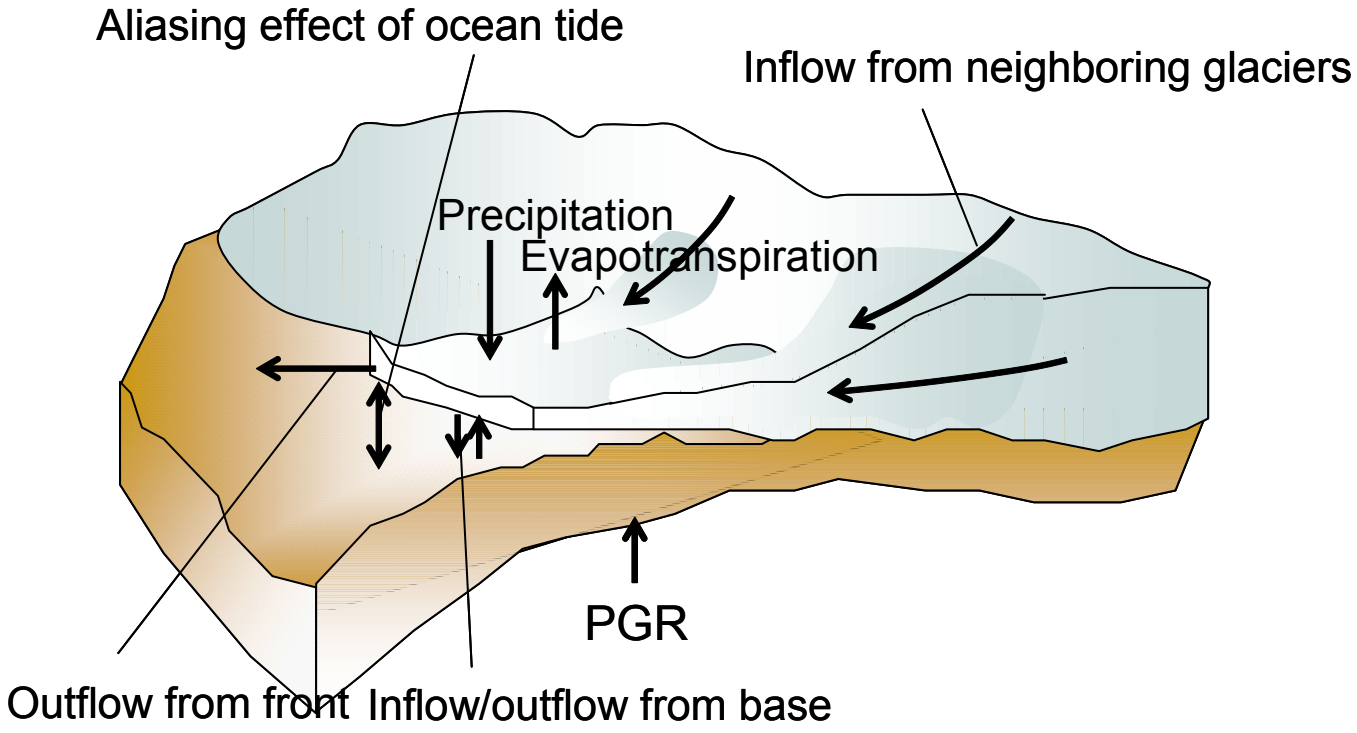

Fig. 4.5. Considerable interannual mass trend sources over FRIS.

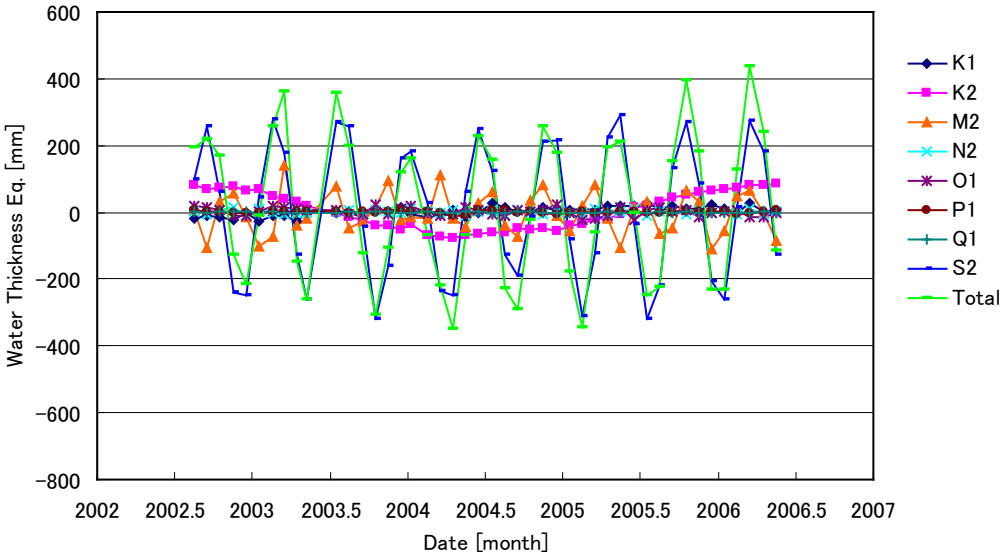

Fig. 4.6. Aliasing error of ocean tide over FRIS.

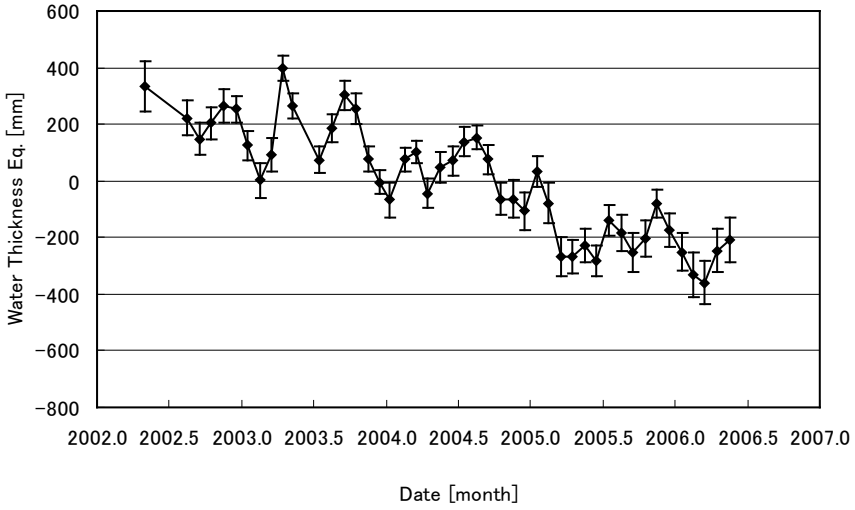

Fig. 4.7. Recovered mass variation over the PIG by UTCSR RL01.

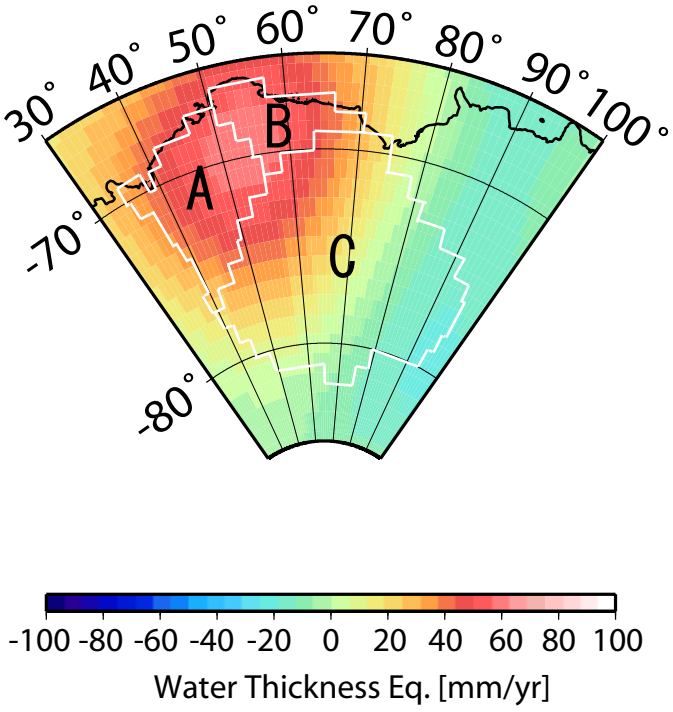

Fig. 4.8. Divisions of the basins in Enderby Land used in this study.

(a)

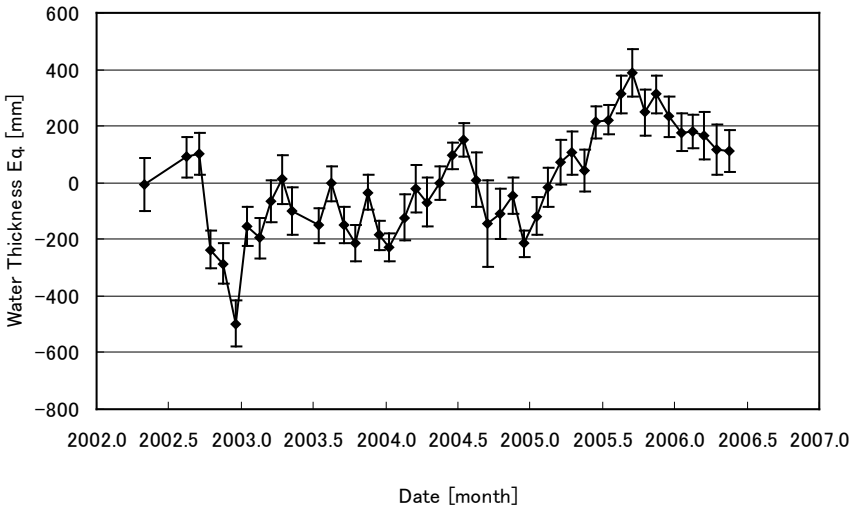

(b)

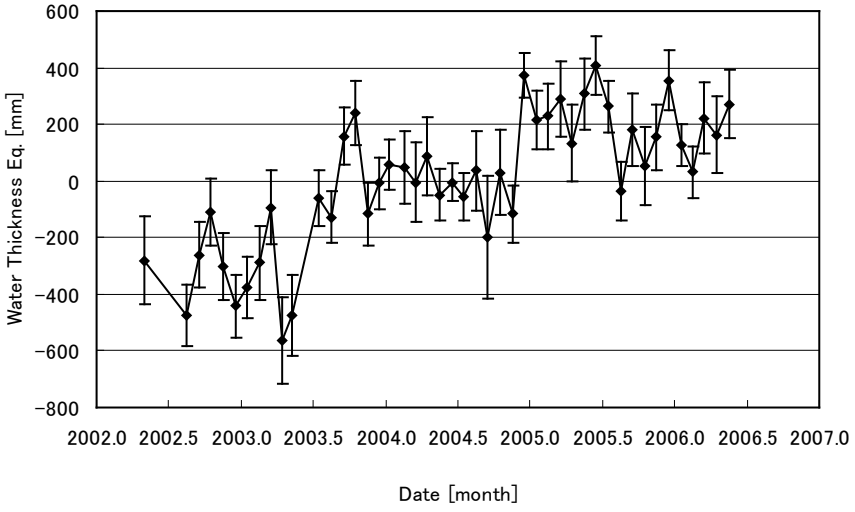

(c)

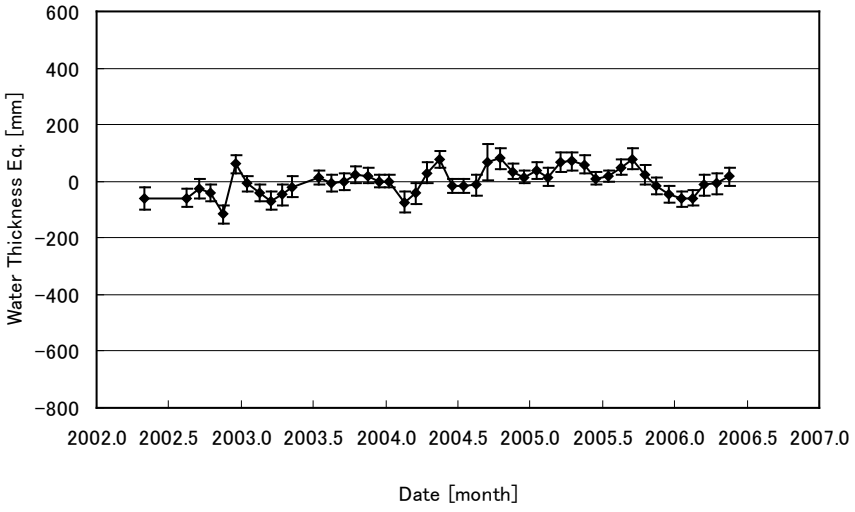

Fig. 4.9. Estimated GRACE regional mass trend in Enderby Land. (a), (b) and (c) show the results in the areas A, B and C shown in Figure 4.7, respectively.

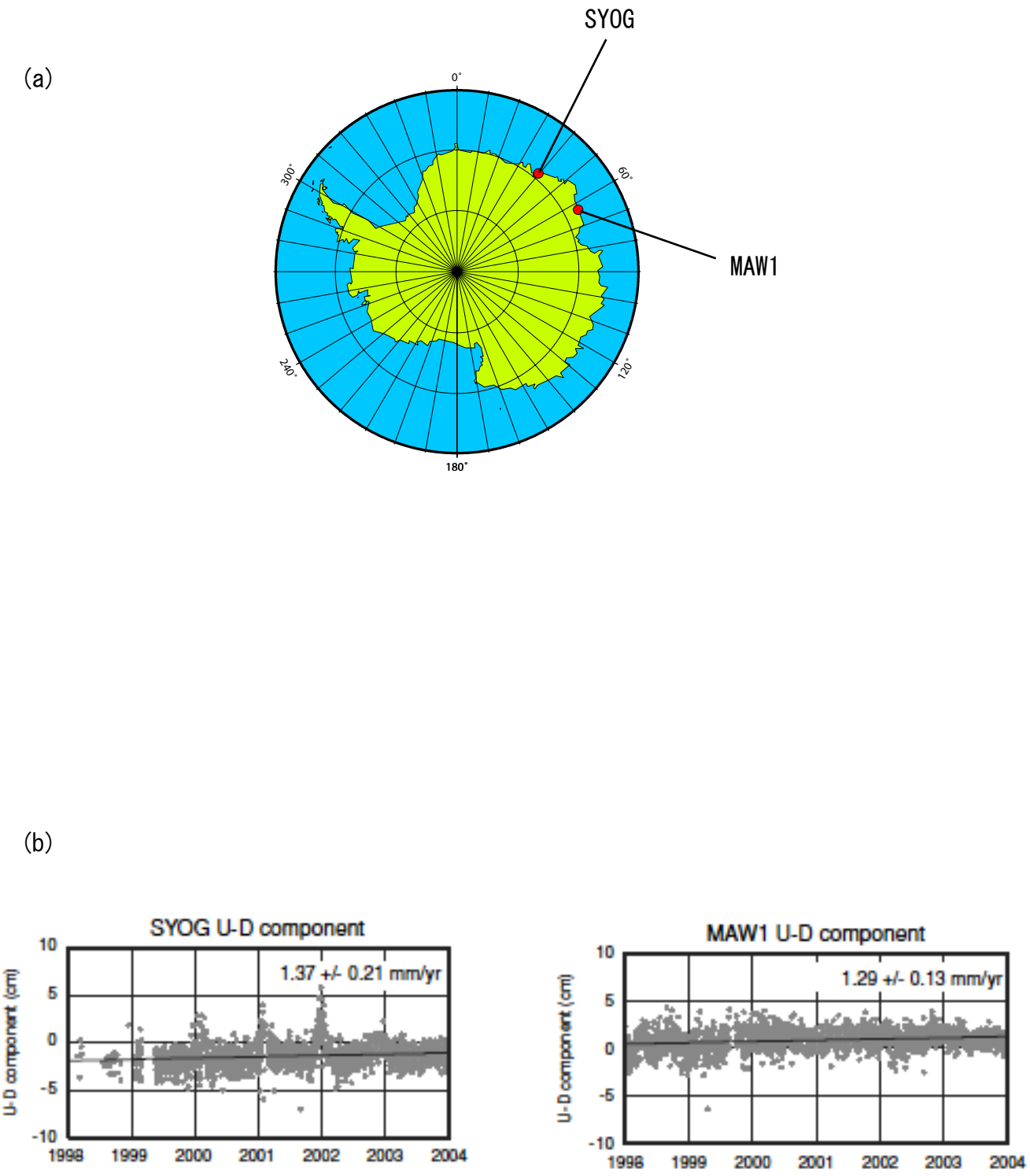

Fig. 4.10. (a) Locations of IGS station of SYOG and MAW1. (b) Vertical uplifts of SYOG and MAW1 (Ohzono et al., 2006)

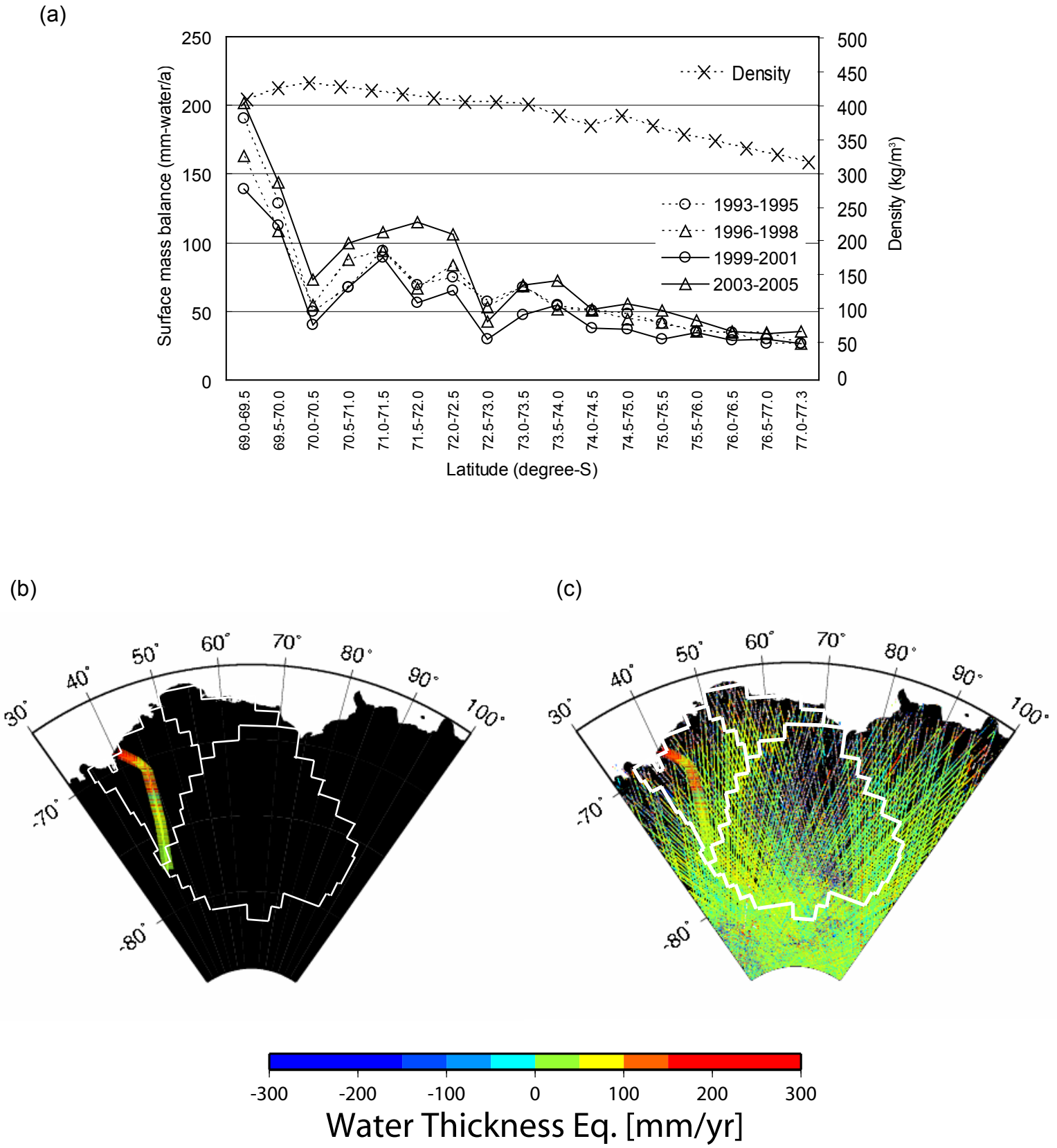

Fig. 4.11. (a) Interannual surface mass trend for the period from 1993 to 2005, estimated by the snow stake method. The snow densities along the traverse route are also plotted. (b) The spatial variations of the trend for the period from 2003 to 2005. (c)The mass trend estimated from ICESat data. The mass trend derived from the snow stake measurement is superimposed.

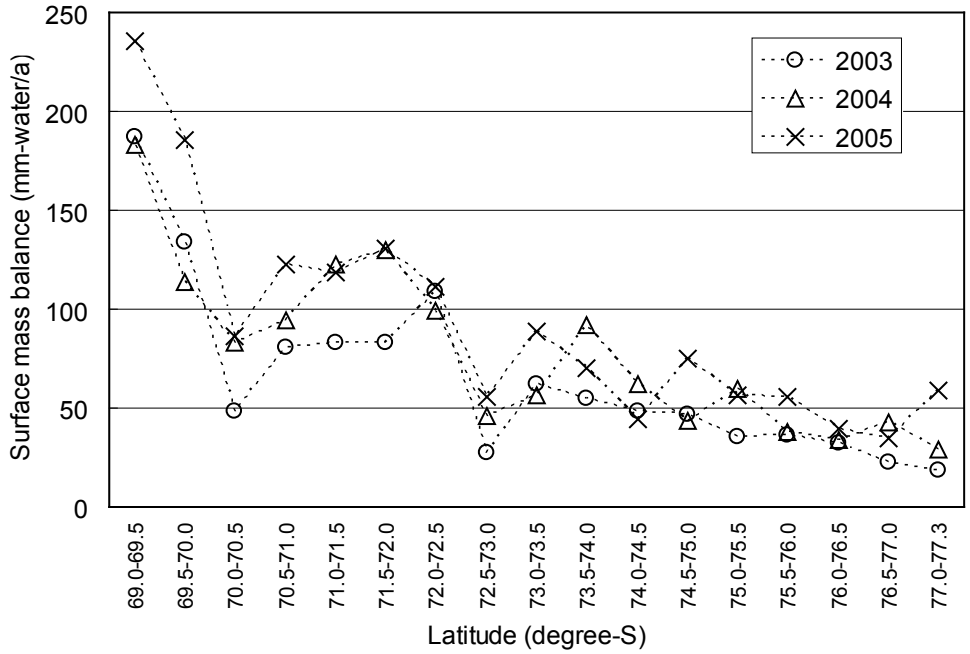

Fig. 4.12. Interannual surface mass trend for the period from 2003 to 2005, estimated by the snow stake method.

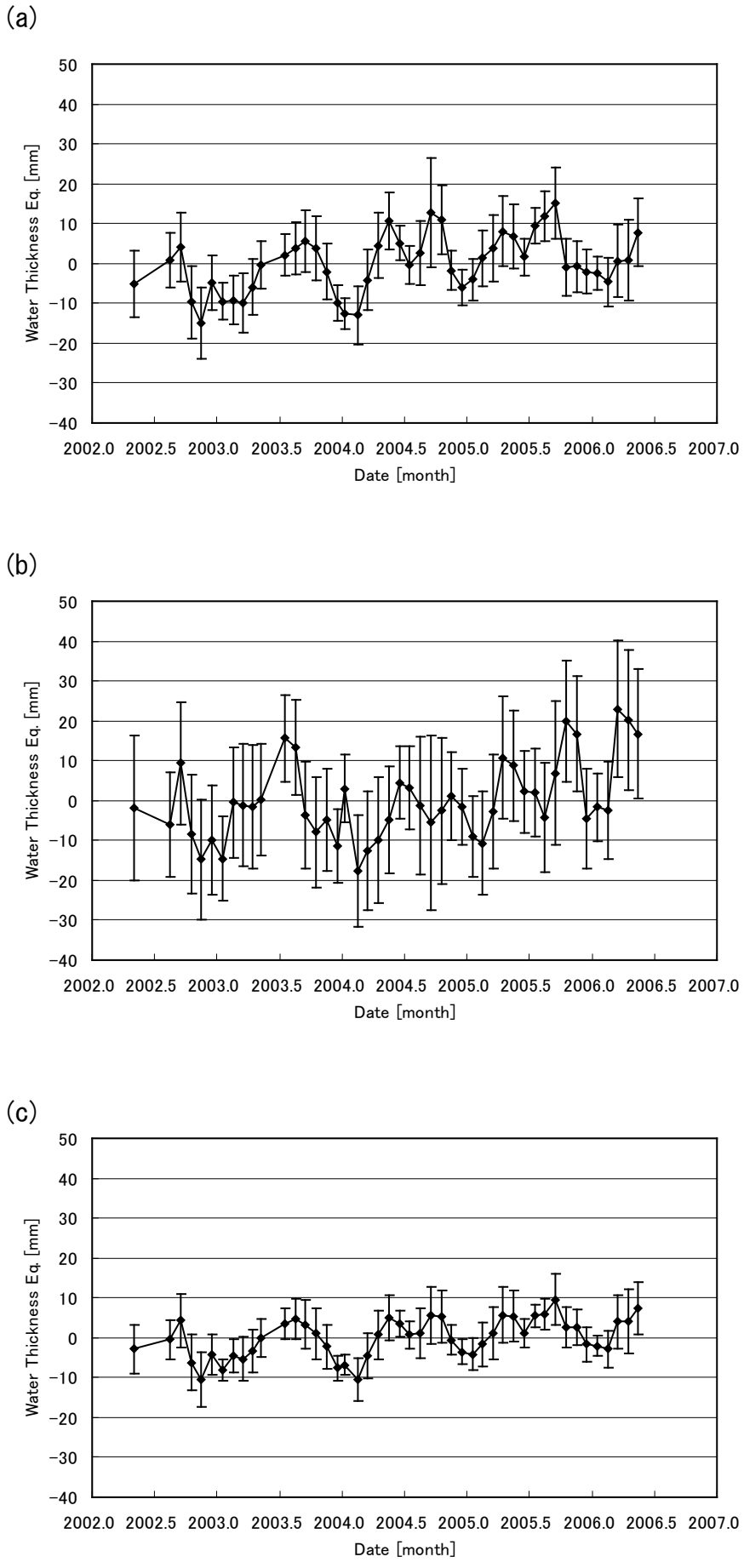

Fig. 4.13. Recovered mass variation over East (a), West (b) and the whole area (c) of Antarctica by UTCSR RL01

5. Conclusion

The regional scale mass variations in the Indochina Peninsula and in Antarctica were recovered and discussed in this study. The results show that GRACE monthly gravity field solutions can be used for the study of the landwater or the ice sheet mass variation in spatial scale larger than at least about several hundred km with reliable precision though the recovery also depends on the shape of the region.

The result in the Indochina Peninsula shows that the mass variation recovered from GRACE data is useful to separate regional signal with local signal in ground gravimetry data. It means that the regional mass recovery also contributes to estimate the local scale mass variation more precisely.

In the application for the study of ice sheet mass variation in Antarctica, GRACE data gives important information of large (continental or sub-continental) scale mass variation. However, the precise estimation, it is very important to discuss regional scale mass variation by combing with other observed or model data sets, because ice sheet mass variation should be separated from other sources which also cause mass change. The results also contribute to improve the knowledge of large scale ice sheet mass variation, and as a result, of global scale sea level change.

Thus, GRACE can recover regional mass variation with reliable precision and the result also can be available for the study of larger or smaller scale mass variation, which is closely related with each other.

Although the errors of the now released GRACE data sets are large, the result is still gives important information of the terrestrial mass variation. For example, as shown in Ch. 3, GRACE data gives a constraint for the landwater model, especially, in phase. On the other hand, at present, it is difficult to discuss the signal amplitude recovered by GRACE data precisely. One of the reason is that the difference of the amplitude released by 3 data centers. It causes about 20 % of uncertainty in addition to the uncertainties caused from other error sources.

To decrease such uncertainties, it is important to improve the data processing method as well as correction models used in the processing. Using longer period observed data, the GRACE static gravity field will be more reliable. Further, GOCE satellite, which is planned to launch in 2007, will give important constraints to the short wavelength static gravity field, and the information will be used for the improvement of the background static gravity field model. Thus, the uncertainty will relatively decrease and more precise discussion will be possible near future.

Acknowledgements

I would like to express my gratitude to Associate Prof. Yoichi Fukuda for his supervision of this work.

I would also like to express my gratitude to Dr. Toshimichi Otsubo, Dr. Toshihiro Kubo-oka, Dr. Toshiyuki Nakaegawa, Dr. Jun Nishijima, Dr. Koichiro Doi, Dr. Koji Matsumoto, Dr. Jun'ichi Okuno, Dr. Takao Kameda, Dr. Makoto Taniguchi, Dr. Kaoru Ichikawa, Dr. Naoki Hirose, Dr. Shigeru Aoki and Dr. Masao Nakada for their helpful support.

I would like to thank Prof. Shuzo Takemoto, Lecturer Kunio Fujimori, and Assistant Prof. Toshihiro Higashi. I would also like to thank all the graduate students of my laboratory that I have had the pleasure to work with.

References

Bettadpur, S. (2003), *UTCSR Level-2 Processing standards document for level-2 product release 0001, rev 1.0*, GRACE 327-742 (CSR-GR-03-03), Center for Space Research, The University of Texas at Austin, Austin.

Bettadpur, S. (2005), *UTCSR Level-2 Processing standards document for level-2 product release 0002, draft*, GRACE 327-742 (CSR-GR-03-03), Center for Space Research, The University of Texas at Austin, Austin.

Bettadpur, S. (2006a), *Product specification document, rev. 4.3*, GRACE 327-720 (CSR-GR-03-02), Center for Space Research, The University of Texas at Austin, Austin.

Bettadpur, S. (2006b), *Level-2 gravity field product user handbook, rev. 2.1*, GRACE 327-734 (CSR-GR-03-01), Center for Space Research, The University of Texas at Austin, Austin.

Bettadpur, S., F. Flechtner, and R. Schmidt (2006), *Usage guidelines for GFZ RL03 and JPL RL02 GRACE gravity fields & atmosphere/ocean background models*, GRACE Technical Note #04, http://podaac.jpl.nasa.gov/grace/documentation.html.

Case, K., G. Kruizinga and S.C. Wu (2004), *GRACE level 1B data product user handbook*, JPL D-22027, Jet Propulsion Laboratory, Pasadena.

Chambers, D.P., J. Wahr, and R.S. Nerem (2004), Preliminary observations of global ocean mass variations with GRACE, *Geophys. Res. Lett.*, *31*, L13310, doi:10.1029/2004GL020461.

Chambers, D.P. (2006), Evaluation of new GRACE time-variable gravity data over the ocean, *Geophys. Res. Lett.*, *33*, L17603, doi:10.1029/2006GL027296.

Chen, J.L., C.R. Wilson, J.S. Famiglietti, and M. Rodell (2005a), Spatial sensitivity of the Gravity Recovery and Climate Experiment (GRACE) time-variable gravity observations, *J. Geophys. Res. 110*, B08408, doi:10.1029/2004JB003536.

Chen, J.L., M. Rodell, C.R. Wilson, and J.S. Famiglietti (2005b), Low degree spherical harmonic influences on Gravity Recovery and Climate Experiment (GRACE) water storage estimates, *Geophys. Res. Lett.*, *32*, L14405, doi:10.1029/2005GL022964.

Chen, J., C.R. Wilson, and B.D. Tapley (2006a), Satellite gravity measurements confirm accelerated melting of Greenland ice sheet, *Science*, *313*, 1958-1960, doi: 10.1126/science.1129007.

Chen, J.L., C.R. Wilson, D.D. Blankenship, and B.D. Tapley (2006b), Antarctic mass rates from GRACE, *Geophys. Res. Lett.*, *33*, L11502, doi: 10.1029/2006GL026369.

Cheng, M., and J. Ries (2006), *Monthly estimates of C_{20} from 5 SLR satellites*, GRACE Technical Note #05, http://podaac.jpl.nasa.gov/grace/documentation.html.

Church, J.A., J.M. Gregory, P. Huybrechts, M. Kuhn, K. Lambeck, M.T. Nhuan, D. Qin, and P.L. Woodworth (2001), Sea level changes, in Houghton, J.T. *et al*. (Eds.) (2001), *Climate change*

2001: The scientific basis, contribution of working group I to the third assessment report of the intergovernmental panel on climate change, Cambridge University Press, Cambridge, pp. 639-694.

Davis, C.H., Y. Ki, J.R. McConnell, M.M. Frey, and E. Hanna (2005), Snowfall-driven growth in East Antarctic ice sheet mitigates recent sea-level rise, *Science*, *308*, 1898-1901, doi:10.1126/science.1110662.

Drijfhout, S., C. Heinze, M. Latif, and E. Maier-Reimer (1996), Mean circulation and internal variability in an ocean primitive equation model, *J. Phys. Oceanogr.*, *26*, 559-580.

Drinkwater, M.R., R. Floberghagen, R. Haagmans, D. Muzi, and A. Popescu, GOCE: ESA's first earth explorer core mission, in Beutler, G.B., M. Drinkwater, R. Rummel, and R. von Steiger (Eds.) (2003), *Earth gravity field from space - from sensors to earth sciences*, the Space Sciences Series of ISSI, *18*, Kluwer Academic Publishers, Dordrecht, pp. 419-432.

European Space Agency (1999), *The four candidate earth explorer core missions-gravity field and steady-state ocean circulation mission*, ESA SP-1233 (1), ESA Publications Division, Noordwijk.

Famiglietti, J., J. Chen, M. Rodell, K. Seo, T. Syed, and C. Wilson (2004), Terrestrial water storage variations from GRACE, presented at IAG International Symposium, Gravity, Geoid and Space Missions – GGSM2004, 2004, Porto.

Flechtner, F. (2003), *GFZ level-2 Processing standards document for level-2 product release 0001, rev. 1.0*, GRACE 327-743 (GR-GFZ-STD-001), GeoForschungszentrium Potsdam, Wessling.

Flechtner, F. (2005a), *GFZ level-2 processing standards document for level-2 product release 0002, rev. 1.0*, GRACE 327-743 (GR-GFZ-STD-001), GeoForschungszentrium Potsdam, Wessling.

Flechtner, F. (2005b), *GFZ level-2 processing standards document for level-2 product release 0003, rev. 1.1*, GRACE 327-743 (GR-GFZ-STD-001), GeoForschungszentrium Potsdam, Wessling.

Flechtner, F. (2005c), *AOD1B product description document, rev. 2.1*, GRACE 327-750 (GR-GFZ-AOD-0001), GeoForschungszentrium Potsdam, Wessling.

Förste, C., F. Flechtner, R. Schmidt, U. Meyer, R. Stubenvoll, F. Barthelmes, R. König, K.H. Neumayer, M. Rothacher, C. Reigber, R. Biancale, S. Bruinsma, J.-M. Lemoine., and J.C. Raimondo (2005), A new high resolution global gravity field model derived from combination of GRACE and CHAMP mission and altimetry/gravimetry surface gravity data, poster presented at EGU General Assembly 2005, 2005, Vienna.

Förste, C., F. Flechtner, R. Schmidt, R. König, U. Meyer, R. Stubenvoll, M. Rothacher, F. Barthelmes, K.H. Neumayer, R. Biancale, S. Bruinsma, and J.-M. Lemoine (2006), A mean global gravity field model from the combination of satellite mission and altimetry/gravimetry surface gravity data, poster presented at EGU General Assembly 2006, 2006, Vienna.

Fukumori, I., R. Raghunath, L. Fu, and Y. Chao (1999), Assimilation of TOPEX/POSEIDON data

into a global ocean circulation model: How good are the results? *J. Geophys. Res.*, *104* (C11), 25647, doi:10.1029/1999JC900193.

GeoForschungsZentrum, Potsdam (2003), http://www.gfz-potsdam.de/pb1/op/grace/results/.

GeoForschungsZentrum, Potsdam (2006), http://www.gfz-potsdam.de/pb1/op/grace/index_GRACE.html.

Furukawa, T., K. Kamiyama, and H. Maeno (1996), Snow surface features along the traverse route from the coast to Dome Fuji Station, Queen Maud Land, Antarctica, *Proc. NIPR Symp. Polar Meteorol. and Glaciol.*, *10*, 13-24.

Global Water System Project (2005), *The Global Water System Project: Science framework and implementation activities*. Earth System Science Partnership, http://www.gwsp.org.

Han, S.-C., C. Jekeli, and C.K. Shum (2004), Time-variable aliasing effects of ocean tides, atmosphere, and continental water mass on monthly mean GRACE gravity field, *J. Geophys. Res.*, *109*, B04403, doi: 10.1029/2003JB002501.

Han, S.-C., C.K. Shum, C. Jekeli, C.Y. Kuo, C. Wilson, and K.W. Seo (2005), Non-isotropic filtering of GRACE temporal gravity for geophysical signal enhancement, *Geophys. J. Int.*, *163*, 18-25, doi:10.1111/j.1365-246X.2005.02756.x.

Heiskanen, W.A., and H. Moritz (1967), *Physical Geodesy,* Freeman, San Francisco.

Hirose, N., I. Fukumori, V. Zlotnicki, and R.M. Ponte (2001), Modeling the high-frequency barotropic response of the ocean to atmospheric disturbances: Sensitivity to forcing, topography, and friction, *J. Geophys. Res.*, *106*(C12), 30987-30996, doi:10.1029/2000JC000763.

Hosaka, M, D. Nohara, T. Nakaegawa, and S. Yukimoto (2006), MRI global river flow model using TRIP, *J. Meteor. Soc. Jpn.*, to be submitted.

International Centre for Global Earth Model (2006), Table of available global gravity field models, http://icgem.gfz-potsdam.de/ICGEM/ICGEM.html.

Ivins, E., and T.S. James (2005), Antarctic glaciological isostatic adjustment: A new assessment, *Antarct. Sci.*, *17*, 541-553, doi: 10.1017/S0954102005002968.

Joughin I., and L. Padman (2003), Melting and freezing beneath Filchner-Ronne Ice Shelf, Antarctica, *Geophys. Res. Lett.*, *30* (9), 1477, doi:10.1029/2003GL016941.

Joughin I., and J.L. Bamber (2005), Thickening of the ice stream catchments feeding the Filchner-Ronne Ice Shelf, Antarctica, *Geophys. Res. Lett.*, *32*, L17503, doi:10.1029/2005GL023844.

Kanzow, T., F. Flechtner, A. Chave, R. Schmidt, P. Schwitzer, and U. Send (2005), Seasonal variation of ocean bottom pressure derived from Gravity Recovery and Climate Experiment (GRACE): Local variation and global patterns, *J. Geophys. Res.*, *110*, C09001, doi:10.1029/2004JC002772.

King M. A., and L. Padman (2005), Accuracy assessment of ocean tide models around Antarctica,

Geophys. Res. Lett., *32*, L23608, doi:10.1029/2005GL023901.

Klokočník, J., J. Kostelecký, and R.H. Gooding (2003), On fine orbit selection for particular geodetic and oceanographic missions involving passage through resonances, *J. Geod.*, *77*, 30-40, doi:10.1007/s00190-002-0276-3.

Knudsen, P. (2003), Ocean tides in GRACE monthly averaged gravity fields, *Space Science Reviews*, 108, 261-270, doi:10.1023/A:1026215124036.

Lemoine, F.G., S.C. Kenyon, J.K. Factor, R.G. Trimmer, N.K. Pavlis, D.S. Chinn, C.M. Cox, S.M. Klosko, S.B. Luthcke, M.H. Torrence, Y.M. Wang, R.G. Williamson, E.C. Pavlis, R.H. Rapp, and T.R. Olson (1998), *The development of the joint NASA GSFC and the National IMagery and Mapping Agency (NIMA) geopotential model EGM96*, NASA Technical Paper NASA/TP1998206861, Goddard Space Flight Center, Greenbelt, USA.

Mayer-Gürr, T., A. Eicker, and K.H. Ilk (2006), ITG-GRACE02s: a GRACE gravity field derived from short arcs of the satellite's orbit, Proceedings of the First Symposium of International Gravity Field Service, 2006, Istanbul.

Milly P.C.D., and A.B. Shmakin (2002), Global modelling of land water and energy balances Part I: The land dynamics (LaD) model. *J. Hydromet.*, *3*, 283–299, doi:10.1175/1525-7541(2002)003<0283:GMOLWA>2.0.CO;2.

Nakada, M., R. Kimura, J. Okuno, K. Moriwaki, H. Miura, and H. Maemoku (2000), Late Pleistcene and Holocene melting history of the Antarctic ice sheet derived from sea-level variations, *Mar. Geol.*, *167*, 85-103, doi:10.1016/s0025-3227(00)00018-9.

Nakaegawa, T., and M. Sugi (2001), Impact of soil moisture movement schemes in a SVATS on global climate of AGCM. In Soil–Vegetation–Atmosphere Transfer Schemes and Large–Scale Hydrological Models, in Dolman, H., J. Pomeroy, T. Oki, and A. Hall (Eds.) *IAHS Publication No. 270*, IAHS Press: Wallingford, pp. 47-52.

National Institute of Polar Research (1997), A*ntarctica: East Queen Maud Land - Enderby Land Glaciological Folio*, National Institute of Polar Research, Tokyo.

National Research Council (1997), *Satellite gravity and the geosphere-contributions to the study of the solid earth and its fluid envelope*, National Academy Press, Washington, D.C.

Nishio, F. (1978), Density of surface snow along routes S, H and Z, JARE Data Rep., 148 (Glaciology 17), 59p.

Nohara, D., A. Kitoh, M. Hosaka, and T. Oki (2006), Impact of climate change on river discharge projected by multimodel ensemble, *J. Hydromet.*, *7*, 1076-1089, doi:10.1175/JHM531.1.

Ponte, R. (1993), Variability in a homogeneous global ocean forced by barometric pressure, *Dyn. Atmos. Oceans*, *18*, 209-234.

Ohzono, M., T. Tabei, K. Doi, K. Shibuya, and T. Sagiya (2006), Crustal movement of Antarctica and Syowa Station based on GPS measurements, *Earth Planets Space*, *58*, 795-804.

Padman, L., H. A. Fricker, R. Coleman, S. Howard, and L. Erofeeva (2002), A new tide model for the Antarctic ice shelves and seas, *Ann. Glaciol.*, *34*, 247–254.

Peltier, W.R. (2004), Global glacial isostasy and the surface of the ice-age Earth: The ICE-5G (VM2) model and GRACE, *Annu. Rev. Earth Planet. Sci.*, *32*, 111-149, doi:10.1146/annurev.earth.32.082503.144359.

Ramillien, G., A. Lombard, and A. Cazenave (2006), Ice sheets mass balance from GRACE and contribution to the sea level, presented at VI Hotine-Marussi Symposium, 2006, Wuhan.

Reigber, C., H. Lühr, and P. Schwintzer (2002), CHAMP mission status, *Adv. Space Res.*, *30*, 129-134, doi:10.1016/s0273-1177(02)0276-4.

Reigber, C., R. Schmidt, F. Flechtner, R. König (2003), U. Meyer, K.H. Neumayer, P. Schwintzer, and S.Y. Zhu, First EIGEN gravity field model based on GRACE mission data only, (in preparation for *Geophys. Res. Lett.*).

Reigber, C., R. Schmidt, F. Flechtner, R. König,U. Meyer, K.H. Neumayer, P. Schwintzer, and S.Y. Zhu (2005), An Earth gravity field model complete to degree and order 150 from GRACE: EIGEN-GRACE02S, *J. Geodyn.*, *39*, 1-10, doi:10.1016/j.jog.2004.07.001.

Reigber, C., P. Schwintzer, R. Stubenvoll, R. Schmidt, F. Flechtner, U. Meyer, R. König, H. Neumayer, C. Förste, F. Barthelmes, S.Y. Zhu, G. Balmino, R. Biancale, J.-M. Lemoine, H. Meixner, and J.C. Raimondo (2006), *A high resolution global gravity field model combining CHAMP and GRACE satellite mission and surface data: EIGEN-CG01C*, Scientific Technical Report STR06/07, GeoForschungsZentrum Potsdam, Wessling.

Research Institute for Humanity and Nature (2005), Research Project 2-4, Human Impacts on Urban Subsurface Environments, http://www.chikyu.ac.jp/USE/.

Rignot, E., and S.S. Jacobs (2002), Rapid bottom melting widespread near Antarctic ice sheet grounding lines, *Science*, *296*, 2020-2023, doi:10.1126/science.1070942.

Rignot, E. and R.H. Thomas (2002), Mass balance of polar ice sheets, *Science*, *297*, 1502-1506, doi:10.1126/science.1073888.

Rodell, M., P. R. Houser, U. Jambor, J. Gottschalck, K. Mitchell, C.-J. Meng, K. Arsenault, B. Cosgrove, J. Radakovich, M. Bosilovich, J. K. Entin, J. P. Walker, D. Lohmann, and D. Toll (2004), The Global Land Data Assimilation System, *Bull. Amer. Meteor. Soc.*, *85*, 381-394, doi:10.1175/BAMS-85-3-381.

Sato, N., P.J. Sellers, D.A. Randell, E.K. Schneider, J. Shukla, J.L. Kinter III, Y.-T. Hou, and E. Albertazzi (1989), Effects of implementing the simple biosphere model (SiB) in a general circulation model, *J. Atmos. Sci.*, *46*, 2757-2782.

Schwintzer, P., C. Reigber, A. Bode, Z. Kang, S.Y. Zhu, F.H. Massmann, J.C. Raimondo, R. Biancale, G. Balmino, J.M. Lemonie, B. Moynot, J.C. Marty, F. Barlier, and Y. Boudon (1998), Long-wavelength global gravity field models: GRIM4-S4, GRIM-C4, *J. Geod.*, *71*, 189-208.

Sellers, P.J., Y. Mintz, Y.C. Sud, and A. Dalcher (1986), Simple Biosphere model (SiB) for use within general circulation model, *J. Atmos. Sci.*, *43*, 505-531.

Stammer, D., C. Wunsch, R. Giering, C. Eckert, P. Heimbach, J. Marotzke, A. Adcroft, C.N. Hill, and J. Marshall (2003), Volume, heat, and freshwater transports of the global ocean circulation 1993-2000, estimated from a general circulation model constrained by World Ocean Circulation Experiment (WOCE) data, *J. Geophys. Res., 108* (C1), 3007, doi: 10.1029/2001JC001115.

Swenson, S., and J. Wahr (2002), Methods for inferring regional surface-mass anomalies from Gravity Recovery and Climate Experiment (GRACE) measurements of time-variable gravity, *J. Geophys. Res.*, *107* (B9), 2193, doi:10.1029/2001JB000576.

Swenson, S., J. Wahr, and P.C.D. Milly (2003), Estimated accuracies of regional water storage variations inferred from the Gravity Recovery and Climate Experiment (GRACE), *Water Resour. Res.*, *39*, 1223, doi:10.1029/2002WR001808.

Swenson, S, and J. Wahr (2006), Post-processing removal of correlated errors in GRACE data, *Geophys. Res. Lett.*, *33*, L08402, doi:10.1029/2005GL025285.

Takanezawa, T., K. Matsumoto, M. Ooe, and I. Naito(2001), Effects of the long-period ocean tide on Earth rotation, gravity and crustal deformation predicted by global barotropic model-periods from Mtm to Sa-, *J. Geod. Soc. Japan*, *47*, 545-550.

Tapley, B.D., D.P. Chambers, S. Bettadpur, and J.C. Ries (2003), Large scale circulation from the GRACE GGM01 geoid, *Geophys. Res. Lett.*, *30* (22), 2163, doi:10.1029/2003GL018622.

Tapley, B.D., S. Bettadpur, M. Watkins, and C. Reigber (2004a), The Gravity Recovery and Climate Experiment: Mission overview and early results, *Geophys. Res. Lett.*, *31*, L09607, doi:10.1029/2004GL019920.

Tapley, B.D., S. Bettadpur, J.C. Ries (2004b), P.F. Thompson, and M.M. Watkins, GRACE measurements of mass variability in the Earth system, *Science*, *203*, 503-505, doi:10.1126/science.203.4380.503.

Tapley, B., J. Ries. S. Bettadpur, D. Chambers, M. Cheng, F. Condi, B. Gunter, Z. Kang, P. Nagel, R. Pastor, T. Pekker, S. Poole, and F. Wang (2005), GGM02-an improved Earth gravity field model from GRACE, *J. Geod.*, *79*, 467-478, doi:10.1007/s00190-005-0480-z.

Thomas, J.B. (1999), *An analysis of gravity-field estimation based on intersatellite dual-1-way biased ranging*, JPL Publication 98-15, Jet Propulsion Laboratory, Pasadena.

Thomas, M. (2002), Ocean induced variations of Earth's rotation – Results from a simultaneous model of global circulation and tides, Ph.D.diss., University of Hamburg, Germany.

Tokuhiro, T. (2000), Offline experiment and improvement of land surface model, SiB, Technical report of seasonal forecast for JMA, Climate and Ocean Meteorology Department, JMA.

Torge, W. (2001), *Geodesy – 3rd completely revised and extended edition,* Walter de Gruyter, Berlin.

UTCSR (Center for Space Research, The University of Texas at Austin) (2003),

http://www.csr.utexas.edu/grace/gravity/.

Velicogna I., and J. Wahr (2005), Greenland mass balance from GRACE, *Geophys. Res. Lett.*, *32*, L18505, doi:10.1029/2005GL023955.

Velicogna, I. (2005), Monitoring ice sheets mass variations from GRACE, presented at 2005 GRACE Science Team Meeting, 2005, Austin.

Velicogna, I., and J. Wahr (2006a), Measurements of time-variable gravity show mass loss in Antarctica, *Science*, *311*, 1754-1756, doi:10.1126/science.1123785.

Velicogna, I., and J. Wahr (2006b), Acceleration of Greenland ice mass loss in spring 2004, *Nature*, *443*, 329-331, doi:10.1038/nature05168.

Wagner, C., D. Mcado, J. Klokocnik, and J. Kostelecky (2006), Degradation of geopotential recovery from short repeat cycle orbits: Application to GRACE monthly fields, *J. Geod.*, *80*, 94-103, doi:10.1007/s00190-006-0036-x.

Wahr, J. (1985), Deformation induced by polar motion, *J. Geophys. Res.*, *90*, B11, 9363-9368.

Wahr, J., M. Molenaar, and F. Bryan (1998), Time variability of the Earth's gravity field: Hydrological and oceanic effects and their possible detection using GRACE, *J. Geophys. Res.*, *103* (B12), 30205, doi:10.1029/98JB02844.

Wahr, J., S. Swenson, V. Zlotnicki, and I. Velicogna (2004), Time-variable gravity from GRACE: First results, *Geophys. Res. Lett.*, *31*, L11501, doi:10.1029/2004GL019779.

Watkins, M.M. (2003), *GRACE JPL level-2 processing standards document for level-2 product release 01*, GRACE 327-744 (v 1.0), Jet Propulsion Laboratory, Pasadena.

Watkins, M.M. (2005), *GRACE JPL level-2 processing standards document for level-2 product release 02*, GRACE 327-744 (v 2.0), Jet Propulsion Laboratory, Pasadena.

Wolff, J.O., E. Maier-Reimer, and S. Legutke (1996), *The Hamburg Ocean Primitive Equation model HOPE*, Technical Report No. 13, DKRZ, Hamburg.

Wünsch, J., P. Schwintzer, and S. Petrović (2005), *Comparison of two different ocean tide models especially with respect to the GRACE satellite mission*, Science Technical Report STR05/08, GeoForshungsZentrum, Potsdam, Wessling.

Yamagishi, H. (2006), Report of the wintering party of the 45th JARE Antarctic Research Expedition, 2004-2005 –Activities at Syowa Station and the coastal area-, *Antarct. Rec.*, *50*, 1-67.

Yamamoto, K., T. Otsubo, T. Kubo-oka, and Y. Fukuda (2005), A simulation study of effects of GRACE orbit decay on the gravity field recovery, *Earth Planets Space*, *57*, 291-295.

Yamamoto, K., Y. Fukuda, T. Nakaegawa, and J. Nishijima (2006a), Landwater variation of 4 major river basins in the Indochina peninsula revealed by GRACE, *Earth Planets Space*, in press.

Yamamoto, K, Y. Fukuda, and K. Doi (2006b), An interpretation of the GRACE revealed mass trend in Enderby Land, Antarctica, *Geophys. Res. Lett.*, submitted.

Yasunari, T., A. Higuchi, J. Asanuma, and K. Nakamura (Eds.) (2003), *GAME Phase I summary*

reports, GAME publication No. 37, GAME International Project Office and GAME National Project Office, http://www.suiri.tsukuba.ac.jp/~game/summarycd2003/index.html.

Zwally, H.J., B. Schutz, W. Abdalati, J. Abshire, C. Bentley, A. Brenner, J. Bufton, J. Dezio, D. Hancock, D. Harding, T. Herring, B. Minster, K. Quinn, S. Palm, J. Spinhirne, and R. Thomas (2002), ICESat's laser measurements of polar ice, atmosphere, ocean and land, *J. Geodyn.*, *34*, 405-445, doi:10.1016/S0264-3707(02)00042-X.

Zwally, H.J., R. Schutz, C. Bentley, J. Bufton, T. Harring, J. Minster, J. Spinhirne, and R. Thomas (2006), GLAS/ICESat L2 Antarctic and Greenland Ice Sheet Altimetry Data (GLA12) V5.2 (Release 26), Boulder, CO: National Snow and Ice Data Center., Digital media.